Acceptor materials for organic solar cells

Acceptor Materials for Organic Solar Cells

PROEFSCHRIFT

ter verkrijging van de graad van doctor aan de
Technische Universiteit Eindhoven, op gezag van de
rector magnificus, prof.dr.ir. C.J. van Duijn, voor een
commissie aangewezen door het College voor
Promoties in het openbaar te verdedigen
op dinsdag 10 november 2011 om 16.00 uur

door

Marie-France Sophie Edmonde Falzon

geboren te Montreuil-sous-bois, Frankrijk

Dit proefschrift is goedgekeurd door de promotor:

prof.dr.ir. R.A.J. Janssen

Copromotor:
dr.ir. M.M. Wienk

Cover design: Marie-France Falzon, Katja Petkau
Printing: Gildeprint Drukkerijen, Enschede

A catalogue record is available from the Eindhoven University of Technology Library.

ISBN: 978-90-386-2860-8

This work was supported by the European Commission within the 6th Framework Programme. Project SolarNtype (No MRTN-CT-2006-035533) and by the Organext Interreg IV-A project.

A André.

Table of contents

Chapter 1

Introduction

1.1 Introduction

The impact of human activity on the environment and the growing energy need of the population are two problems that are now widely admitted by the general public. However, the awareness about these issues has evolved slowly. From the creation of the Club of Rome in 1968, that wanted to draw the world leaders' attention on the limits of economic growth with respect to the limited and finite resources, through the Stockholm Conference in 1972, where the environment is defined as part of the Patrimony, the concept of sustainable development has found its definition only in 1987 in the Brundtland Report. "Sustainable development is development that meets the needs of the present without compromising the ability of future generations to meet their own needs".[1] The attribution of the Nobel Prize of Chemistry in 1995 to Crutzen, Molina and Rowland for their work on the formation and depletion of ozone[2-4] highlights even more the risks of an uncontrolled growth. Finally, in 2000, the United Nations published its eight ´Millennium Development Goals´. The objective number seven is to ensure sustainable development by – among other approaches – promoting renewable energies.[5]

Unlike the fossil energies, energies produced by water, wind, geothermal energy, biomass or Sun are endless and produce very little to no CO_2 emissions. The incident power of the Sun that reaches earth surface is 174 PW, much more than the 15 TW of worldwide power consumption.[6-8] This makes solar energy the most promising source of green energy, especially as it can be directly converted into electricity using photovoltaic modules.

1.2 History of solar cells

The photovoltaic effect has been discovered by Becquerel[9,10] in 1839 when he observed that conductance through an electrolytic cell was rising upon illumination. However, it is only in 1877 that the first working solar cell was fabricated. For this purpose, Charles Fritts coated selenium with a thin layer of gold,[11] resulting in a 1% power conversion efficiency device. It was not until the mid 50's that the solar cell performance was pushed to higher efficiencies. Fuller discovered that upon doping (*i.e.* upon introduction of atoms with different valence electron number), he could transform silicon from an average to a superior conductor of current. Using these results, Pearson and Chapin developed a solar cell offering 6% efficiency.[12] The first step of fabrication was the introduction of a small amount of arsenic into the silicon. Having one valence electron more than silicon, doping with arsenic produces negatively charged silicon (or n-doped silicon). Then, boron was introduced only in a very thin layer close to the surface. Boron has one valence electron less than silicon and produces positively charged silicon (or p-doped silicon) when used as dopant.[13] The first p-n junction solar cell was thereby fabricated. Nowadays, the highest power conversion efficiency reported for silicon solar cells sunlight is 25%.[14]

However, a major drawback of this technology is the high materials and production costs. Because silicon is a weak absorber, wafers with thicknesses of 200-300 μm are required to obtain sufficient optical density for sunlight. Silicon wafers are cut from monocrystalline silicon ingots prepared in a Czochralski process. In order to reduce the amount of material needed and thereby the fabrication cost, research started to focus on thin-film solar cells utilizing good absorber materials. Amorphous silicon (a-Si), cadmium telluride (CdTe) and copper indium gallium (di)selenide (CIGS) are semiconductors used in thin-film solar cells and display efficiencies of 10.5, 12.5 and 16.7%, respectively.[14] Layers of only 5-8 μm of the semi-conductors are sufficient to absorb 90% of the light. Although the use of thin-film technology reduces fabrication cost, the performance remains lower than that of crystalline silicon solar cells. High-efficiency inorganic solar cells can be obtained by stacking multiple thin films, each one absorbing a different part of the solar spectrum. To date, the most efficient device uses a gallium arsenide (GaAs)/germanium (Ge)/gallium indium phosphide ($GaInP_2$) triple configuration and reaches 32% power conversion efficiency.[14]

1.3 Organic solar cells

Within the perspective of cost reduction and large scale production, organic materials have gained interest of research. The discovery of the conductivity of π-conjugated polymers in 1977 by Shirakawa, MacDiarmid and Heeger[15] has enabled the use of conjugated polymers in solar cells and more generally in organic electronics. While inorganic semiconductors produce free electrons and holes upon illumination at room temperature, light absorption in organic semiconductors results in the formation of a tightly bound charge pair called an exciton. The low dielectric constant of organic materials results in a strong Coulombic interaction between the electron and the hole. The binding energy is typically around 0.3 to 0.4 eV,[16] which is much larger than thermal energy (0.025 eV) and makes the charge separation quite difficult. As a direct consequence, earlier organic solar cells were exhibiting rather poor performance around 0.3% power conversion efficiency.[17] The breakthrough came in 1986 when Tang introduced a heterojunction[18] by evaporating two materials on top of each other in a so-called bilayer architecture. The crucial step is the introduction of a second material with different electron affinity and ionisation potential. The resulting electric field across the interface is the driving force for exciton dissociation. The electron is transferred into the material having the lowest reduction potential – also called acceptor material - while the hole remains in the material with the highest ionisation potential – also called donor material. However, efficiencies remained below 1%. The main cause is the rather short lifetime of excitons. They can diffuse 10 to 20 nm[19-21] before they decay while the typical thickness of a bilayer solar cell should be ~100 nm to absorb all light. Hence, only the excitons formed close to the interface can be dissociated and contribute to the current. The others will decay before they can reach the junction and are then lost. A step forward in terms of efficiency has been made after Sariciftci *et al*. reported evidence for fast photoinduced electron transfer from conducting polymers onto buckminster fullerenes.[22–24] In his work, Sariciftci formulated the idea that forming an interpenetrating network by mixing the donor and acceptor compounds in situ would be ideal. By blending the two materials, the active layer results in a bicontinuous network in which the interface is distributed all over the bulk, allowing for quantitative exciton dissociation. The first bulk heterojunction solar cells were manufactured simultaneously in 1995 by Halls[25] and Yu[26]. Further improvement has been achieved by Shaheen *et al*. in 2001,[27] showing that the processing solvent dramatically affects the power conversion efficiency of a solar cell.

1.4 Fabrication and characterization of solar cells

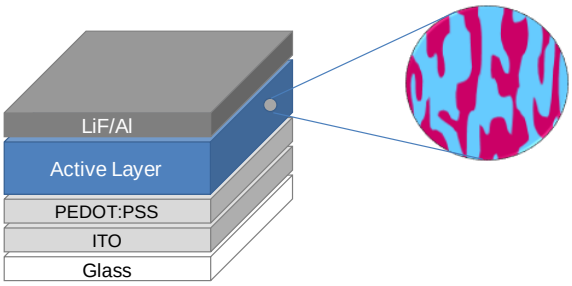

Figure 1.1: Bulk heterojunction solar cell layout. The zoom in shows the distribution of the materials interfaces over the bulk.

The architecture of an organic solar cell is shown in Figure 1.1. The device is built on an indium tin oxide (ITO) patterned glass substrate. ITO is a transparent conductive electrode with a high work-function, suitable for hole collection. In order to smoothen the surface of this electrode, a thin layer of poly(3,4-ethylenedioxythiophene):poly(styrenesulfonate) (PEDOT:PSS) is spin-cast. PEDOT:PSS has an even higher work-function than ITO and helps in a better hole collection. The active layer is then applied, followed by the evaporation of the top electrode. This reflecting electrode usually consists of an aluminium contact. Between the active layer and the aluminium, an interface layer consisting of lithium fluoride or a low work-function metal is placed in order to improve the electron collection.

To study the performance of a solar cell, the current density-voltage characteristic (*J-V* curve) in the dark and under illumination is measured. Figure 1.2 shows a typical *J-V* characteristic as an example. In the dark, the solar cell behaves like a diode and the current can go through the device only in forward bias. Under illumination, the curve is shifted downwards. The difference between the current measured in the dark and under illumination is the photocurrent that has been generated by the solar cell. Along the *J-V* curve under illumination, the power density at the maximum power point (P_{MPP}) can be found where the product of current density and voltage is maximal. A solar cell is characterized by three parameters: the open-circuit voltage (V_{oc}), the short-circuit current density (J_{sc}) and the fill factor (FF). The V_{oc} which is the maximum photovoltage that the device can supply is defined by the voltage where the current under illumination is zero.

The J_{sc} is defined as the maximum current density flowing through the device at zero applied voltage. The FF defines the quality of the *J-V* curve under illumination and is representative of how easily the charges can be extracted in the device.

$$FF = \frac{P_{MPP}}{J_{sc} . V_{oc}}$$

The power conversion efficiency of the device is defined by the ratio between the maximum output power and the power of the incident light.

$$\eta = \frac{FF . J_{sc} . V_{oc}}{P_{light}}$$

It is important to note that V_{oc}, J_{sc}, FF and, hence, η all depend on the illumination conditions and are typically measured at standardized conditions (25 °C and air mass 1.5 global (AM1.5G) solar spectrum). To date, the best material combination for bulk heterojunction organic solar cells is a blend of a π-conjugated polymer used as donor material[28–34] and a fullerene derivative, [6,6]-phenyl-C_{61}-butyric acid methyl ester[35] (PCBM), used as acceptor material. The highest power conversion efficiency reached with published materials so far is 7.4%,[36] and for undisclosed materials reports with efficiencies of 8.3% from Konarka Technologies and 9.2% of Mitsubishi Chemical exist.[37]

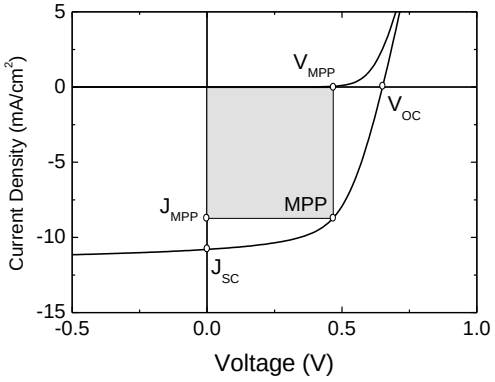

Figure 1.2: Typical *J-V* characteristics of a solar cell.

1.5 Motivation of this thesis

To date, fullerene derivatives [60]PCBM and [70]PCBM are the most efficient acceptor materials for organic solar cells. However, fullerenes absorb mainly in the ultra-violet and present a poor absorption coefficient in the visible, where the spectral irradiance of the Sun is the strongest. In polymer/fullerene blends, the light is mostly absorbed by the polymer. Following this observation, the use of a second polymer – acting this time as the acceptor material – to enhance the absorption in the active layer seems to be a sensible approach in order to improve the current produced by the solar cell. The aim of this thesis is to explore new conjugated acceptor materials and to establish design rules for such materials.

In the next paragraphs photophysical and electronic properties of conjugated materials and donor/acceptor combinations relevant to organic solar cells are presented, followed by a short overview of the state of the art in polymer acceptor materials.

1.6 Properties of excited states in polymers

In the ground state, a conjugated molecule or polymer contains in its highest occupied molecular orbital (HOMO) two electrons with paired (antiparallel) electron spins. This state is called the singlet ground state (S_0, Figure 1.3). Upon excitation by a photon, an electron can be promoted from the HOMO to the lowest unoccupied molecular orbital (LUMO). When the spin of this electron remains antiparallel to the spin of the electron left in the HOMO, the first singlet excited state is produced (S_1). With time this singlet excited state may convert into the first triplet excited state (T_1) when the spin is reversed. This phenomenon is known as intersystem crossing (ISC) and can occur depending on the degree of overlap of the vibrational levels of the singlet and triplet excited states via spin-orbit coupling or hyperfine interaction between electrons and nuclei.[38,39] According to quantum mechanics, the triplet excited T_1 state is lower than the corresponding singlet excited S_1 state by the exchange energy. Escaping from ISC the S_1 state may return to the ground state radiatively (fluorescence) or via thermal decay. Because fluorescence is a spin-allowed transition, the lifetime of the S_1 state is usually short, typically in the nanosecond regime or less. The triplet excited T_1 state is generally not formed directly from the singlet ground state S_0 because the S_0 - T_1 transition is spin-forbidden. As a consequence, the lifetime of the T_1 state is long, typically in the micro-millisecond regime. Decay from T_1 to S_0 may occur radiatively (phosphorescence) or thermally.

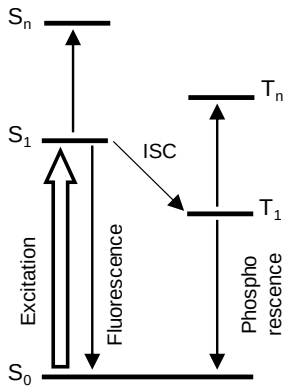

Figure 1.3: Possible optical transitions between the different excited states of a polymer.

1.7 Properties of charged polymers

As described above, after absorption of light in a blend of donor/acceptor materials, a charge transfer process can occur at the interface of the two materials. Subsequently, the charges are further separated into free charges leaving a hole in the donor material. This oxidation affects the electronic structure of the material by creating two new energy levels in the gap of the conjugated polymer.[40,41] This gives rise to four new optical transitions as depicted in Figure 1.4. According to the Fesser-Bishop-Campbell model,[42,43] only P1 and P2 transitions are allowed while the P3 and P4 transitions are not. Consequently the absorption spectra of charged polymers show two bands: one at low energy corresponding to the P1 transition and one at higher energy corresponding to the P2 transition.

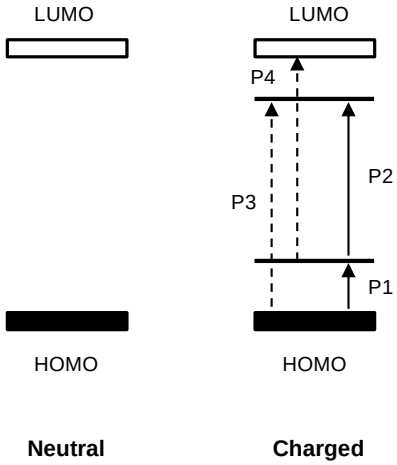

Figure 1.4: Electronic structure of a neutral (left) and oxidized (right) conjugated polymer.

1.8 Photophysical processes involved in organic solar cells

It is possible to distinguish four different photophysical processes in donor/acceptor organic solar cells between light absorption and current generation: exciton generation and migration to the interface, exciton dissociation (or charge transfer), charge dissociation and charge transport and collection at the electrodes. Figure 1.5 illustrates these different processes.

1. Exciton generation and migration

Upon illumination, both the donor and acceptor materials can be excited. An electron is then promoted to the LUMO, leaving a hole behind in the HOMO. The electron and hole are not present as free charges; they form a Coulombically bound pair called exciton. Only the photons with energy higher than the optical band gap (*i.e.* the HOMO-LUMO energy difference) can excite the material and create an exciton. Thus, it is important that the band gap of the materials is small enough such that a large part of the solar spectrum can be absorbed. As mentioned above, the dissociation of this exciton can only occur at the interface of the two materials. The exciton has to be able to reach the interface within its lifetime. Ideally, the phase separation in the active layer should not be larger than the exciton diffusion length which is approximately between 10 to 20 nm.

2. Exciton dissociation (or charge transfer)

It is believed that the exciton binding energy in conjugated materials is 0.3-0.4 eV.[44–48] At a donor/acceptor interface the exciton binding energy of the pure materials is, however, irrelevant and the only important question is whether the lowest excitonic S_1 state of the donor and acceptor has an energy that is higher than the charge-transfer (CT) state that can be produced. Veldman *et al.* have demonstrated that for charge transfer to occur it is sufficient that the CT state has an energy about 0.1 eV or more below that of the lowest S_1 state.[49] The difference between the HOMO of the donor and the LUMO of the acceptor relates, but is not equal, to the energy of the CT state. As a rule of thumb, the donor and acceptor materials should be designed in such a way that both LUMO-LUMO *and* HOMO-HOMO offsets are larger than 0.35 eV to allow electron transfer from the donor to the acceptor and hole transfer from the acceptor to the donor material.

3. Charge dissociation

Once the electron has been transferred to the acceptor, the CT state is formed. The formation of this CT state is a crucial step between exciton dissociation and free charge formation. It is important to note that at this stage, the charges are still bound by a Coulombic interaction. However, since the electron and the hole are located on two different materials, their separation distance is relatively large. As a consequence, the opposite charges can more easily escape from their Coulombic attraction.[49] The internal electric field arising from the difference in work-function of the collecting electrodes represents an additional driving force for charge separation. The CT state can dissociate into free charges and so contribute to the photocurrent, or it can recombine. In the latter case, the charges are lost and do not contribute to the photocurrent. Two different recombination paths can be considered. The CT state can decay to the ground state[50] or to the triplet state of either the donor or acceptor material.[51–55] Recombination to a triplet state can only happen after intersystem crossing of the CT state[56] and when the triplet state energy of at least one of the materials is lower than that of the CT state by about 0.1 eV or more.[49]

4. Charge transport

Once the charges are freed, they have to travel to the appropriate electrode (ITO contact for the holes and aluminium contact for the electrons) in order to contribute to the current. The first requirement is that the morphology of the materials blend should allow a pathway for the charges to reach the electrodes. Second, the materials have to possess a rather high mobility to efficiently transport the charges. If charge transport is slow or impeded, bimolecular charge recombination may occur which is reducing the performance. To enable charge collection without energetic losses, the hole collecting electrode should form an Ohmic contact with the HOMO energy level of the donor and likewise for the electron collecting contact and the LUMO of the acceptor.

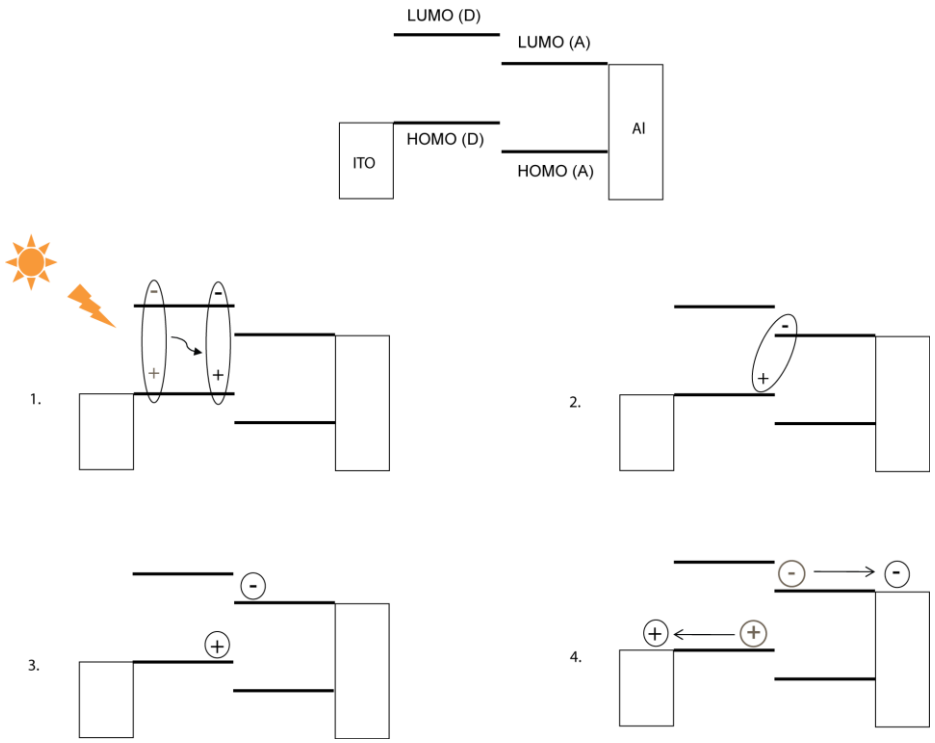

Figure 1.5: Schematic representation of the different steps during the photogeneration of free charges in a donor (D)/acceptor (A) organic solar cell.

1.9 Near steady-state photoinduced absorption

Absorption of light in organic semiconductors gives rise to several processes. Near steady-state photoinduced absorption (ss-PIA) is a versatile technique that allows us to probe the photoinduced species with lifetimes in the microsecond time domain. Photoexcitation of pristine organic materials results in the formation of singlet excited states and – if intersystem crossing occurs – to triplet excited states. In the microsecond regime the singlet states have already decayed to the ground state and ss-PIA only probes the absorption of triplet states to higher triplet states. In the PIA spectrum, a negative absorption band (photobleaching band) is observed at the absorption maximum of the excited material, due to the depletion of material in the ground state.

Photoexcitation of a donor-acceptor blend gives rise to the formation of radical cations and anions, as mentioned earlier. These radical ions exhibit two absorption bands P1 and P2 (Figure 1.2) of similar intensity that can clearly be identified by ss-PIA. The observation of two bands of same intensity in a PIA spectrum at low and higher energy, but below the optical band gap, is a clear indication of free charge formation in the blend.

1.10 Charge transport

The charge carrier mobility of the materials used in an organic solar cell is a key factor for the device performance. Measuring charge carrier mobility is not an easy task as the actual value may depend on device configuration, charge carrier density, temperature, electric field, morphology and time scale of the experiment. In general it is recommended to measure under conditions that most closely match the operating conditions of the device under consideration. For solar cells this is a sandwich configuration in which a thin film is placed between large area top and bottom contacts. Further, it is important to measure only one type of carrier (i.e. hole or electron) at a time. The space charge limited current (SCLC)[57,58] method is most appropriate for this purpose. In an organic solar cell architecture, the active layer is sandwiched between PEDOT:PSS and LiF/Al contacts. The LiF/Al electrode can inject electrons into the LUMO of the acceptor material and the PEDOT:PSS can inject holes into the HOMO of the donor polymer. If one is interested in measuring the electron mobility, it should be ensured that the current is coming from electrons only. To do so, hole injection must be prevented which can be achieved by using an electrode with a low work-function. Zinc oxide (ZnO) has a work-function similar to that of aluminium, around 4.2 eV.[59–61] The injection barrier is large enough to prevent the injection of the holes from the ZnO to the HOMO level of the polymer. According to the Mott-Gurney law for space charge limited current in a trap free intrinsic semiconductor, the current density *J* passing through scales quadratically with the voltage according to:

$$J = \frac{9}{8} \frac{\varepsilon.\mu.V^2}{L^3},$$

where ε is the dielectric constant of the material, μ the mobility, *L* the thickness of the active layer and *V* the applied voltage.

1.11 State of the art in polymer-polymer solar cells

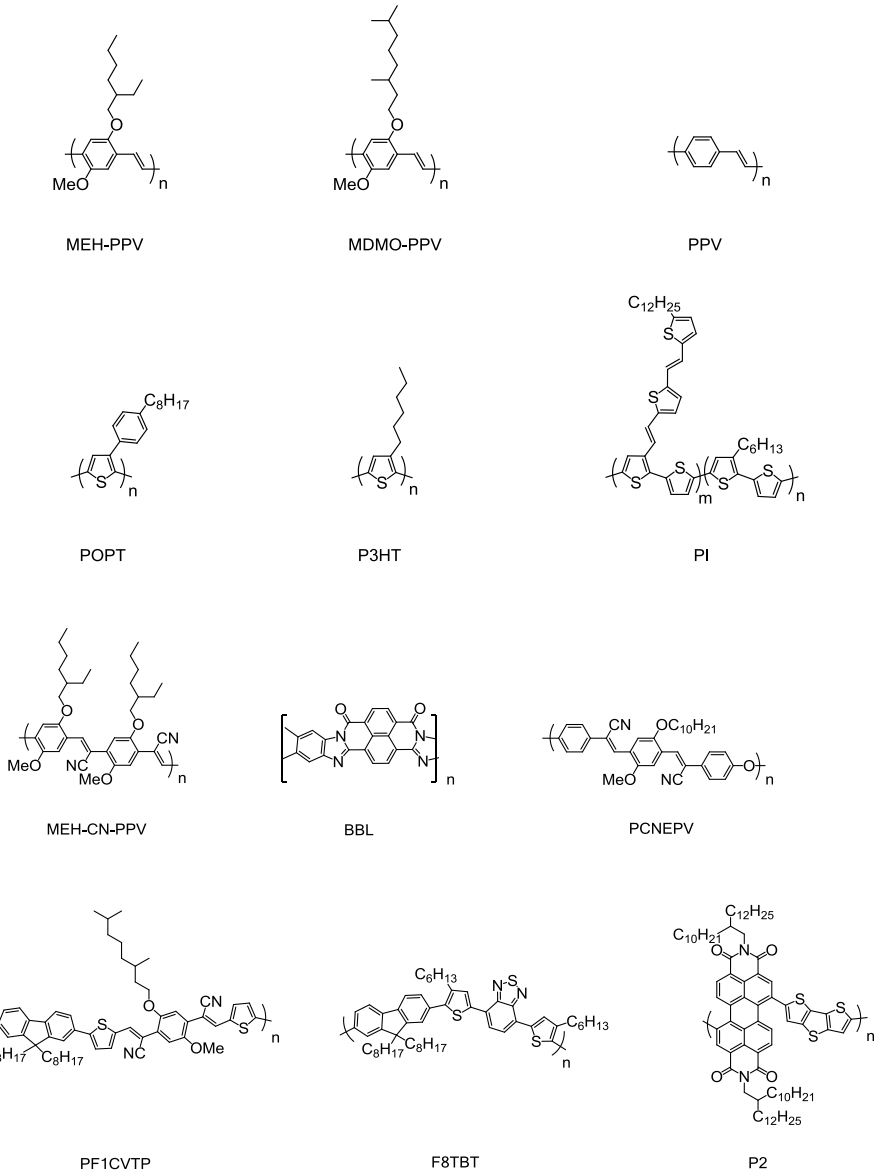

Figure 1.6: Chemical structure of polymers used in all-polymer solar cells.

The first donor polymer/acceptor polymer, i.e. all-polymer, solar cell was reported in 1995 by Yu and Heeger.[62] They used a blend of poly[2-methoxy-5-(2′-ethylhexyloxy) -1,4-phenylene vinylene], MEH-PPV (Figure 1.6), as donor and cyano-PPV, CN-PPV, as acceptor. Devices displayed performance of 0.25% at 25 mW/cm^2 light intensity. The power conversion efficiency was strongly dependent on light intensity and increased to 0.9% at microwatts intensity light. Similar measurements were performed also in 1995 by Halls *et al.*[22] using the same material combination. Three years later, Friend *et al.* published a 1.9% all-polymer solar cell.[63] The device was fabricated by lamination of two layers, one of poly[3-(4-*n*-octylphenyl)thiophene] (POPT) and one of MEH-CN-PPV. In 2000, Jenekhe *et al*.[64] published a spin-coated bilayer solar cell made of poly(*p*-phenylene vinylene) (PPV) and poly(benzimidazobenzophenanthroline ladder) (BBL) presenting a power conversion efficiency of 1.4%. In 2004, Veenstra *et al.*[65] reported a 0.75% solar cell using a blend of poly[2-methoxy-5-(3′,7′-dimethyloctyloxy)-1,4-phenylene vinylene] (MDMO-PPV) and poly[oxa-1,4-phenylene-(1-cyano-1,2-vinylene)-(2-methoxy-5-(3′,7′-dimethyloctyloxy)-1,4-phenylene)-1,2-(2-cyanovinylene)-1,4-phenylene] (PCNEPV). Two years later, Koetse *et al.*[66] used a blend of MDMO-PPV as the donor and an alternating copolymer poly{9,9-dioctylfluorene-2,7-diyl-*alt*-1,4-bis[2-(5-thienyl)-1-cyanovinyl]-2-methoxy-5-(3′,7′-dimethyloctyloxy)benzene} (PF1CVTP) as the acceptor. The device exhibited a power conversion efficiency of 1.5%. The best all-polymer solar cell was fabricated by Friend *et al.* in 2007 by using a blend of poly(3-hexylthiophene) (P3HT) and poly{(9,9-dioctylfluorene)-2,7-diyl-*alt*-[4,7-bis(3-hexylthien-5-yl)-2,1,3-benzothiadiazole]-2′,2″-diyl} (F8TBT)[67–70] with an efficiency of 1.8%. The same year Zhan *et al.*[71] presented the performance of a copolymer of perylene diimide and bis(dithienothiophene) P2 as acceptor in combination with P1, a polythiophene derivative substituted by a tris(thienylenevinylene) conjugated side chain as donor. The device exhibited an efficiency of 1% which was further improved to 1.5% in 2009.[72]

1.12 Outline of the thesis

The starting point of the work described in this thesis is the idea to use the electron-deficient units commonly employed in modern small band gap donor polymers as building blocks for novel acceptor type polymers. Chapter 2 presents three of such polymers and based on the results obtained, design rules for successful acceptor polymers are defined. Chapter 3 and 4 describe the synthesis, electronic and photovoltaic properties of a range of new n-type polymers. The operation of the solar cells is analyzed and processes limiting the performance are identified. Chapter 5 describes two indigo-based dyes presenting much deeper LUMO levels than the polymers synthesized in Chapters 3 and 4, to have a greater driving force for electron transfer. Finally, Chapter 6 presents the synthesis and application of small band gap polymers based on diketopyrrolopyrrole and pyrrole. These materials possess high hole mobility and show efficiency of 3% in bulk heterojunction solar cells.

References

(1) World Commission on Environment and Development. *Our common future*; Oxford University Press: Oxford, New York, **1987**.
(2) Molina, M. J.; Rowland, F. S. *Nature* **1974**, *249*, 810.
(3) Fishman, J.; Ramanathan, V.; Crutzen, P. J.; Liu, S. C. *Nature* **1979**, *282*, 818.
(4) Abbatt, J. P. D.; Molina, M. J. *Annu. Rev. Energy. Environ.* **1993**, *18*, 1.
(5) United Nations General Assembly, *resolution 2 session 55* United Nations Millennium Development Goals.
(6) International Energy Agency, *World Energy Outlook 2010*; OECD/IEA: Paris, **2010**.
(7) Fröhlich, C.; Lean, J. *The Astron. Astrophys. Rev.* **2004**, *12*, 273.
(8) Fröhlich, C.; Lean, J. *Geophys. Res. Lett.* **1998**, *25*, 4377.
(9) Académie des sciences *C. R. Acad. Sci.*; Gauthier-Villars: Paris, 1835.
(10) Williams, R. *J. Chem. Phys.* **1960**, *32*, 1505.
(11) Petrova-Koch, V. In *High-Efficient Low-Cost Photovoltaics*; Petrova-Koch, V.; Hezel, R.; Goetzberger, A., Eds.; Springer Berlin Heidelberg: Berlin, Heidelberg, 2009; Vol. 140, pp. 1-5.
(12) Chapin, D. M.; Fuller, C. S.; Pearson, G. L. *J. Appl. Phys.* **1954**, *25*, 676.
(13) Perlin, J. Silicon Solar Cell Turns 50 **2004**.
(14) Green, M. A.; Emery, K.; Hishikawa, Y.; Warta, W. *Progress in Photovoltaics: Research and Applications* **2011**, *19*, 84.
(15) Chiang, C. K.; Fincher, C. R.; Park, Y. W.; Heeger, A. J.; Shirakawa, H.; Louis, E. J.; Gau, S. C.; MacDiarmid, A. G. *Phys. Rev. Lett.* **1977**, *39*, 1098.
(16) Arkhipov, V. I.; Bässler, H. *physica status solidi (a)* **2004**, *201*, 1152.
(17) Chamberlain, G. A. *Solar Cells* **1983**, *8*, 47.
(18) Tang, C. W. *Appl. Phys. Lett.* **1986**, *48*, 183.
(19) Haugeneder, A.; Neges, M.; Kallinger, C.; Spirkl, W.; Lemmer, U.; Feldmann, J.; Scherf, U.; Harth, E.; Gügel, A.; Müllen, K. *Phys. Rev. B* **1999**, *59*, 15346.
(20) Theander, M.; Yartsev, A.; Zigmantas, D.; Sundström, V.; Mammo, W.; Andersson, M. R.; Inganäs, O. *Phys. Rev. B* **2000**, *61*, 12957.
(21) Markov, D. E.; Amsterdam, E.; Blom, P. W. M.; Sieval, A. B.; Hummelen, J. C. *J. Phys. Chem. A* **2005**, *109*, 5266.
(22) Sariciftci, N. S.; Smilowitz, L.; Heeger, A. J.; Wudl, F. *Science* **1992**, *258*, 1474.
(23) Sariciftci, N. S.; Heeger, A. J. U.S. Patent: 5331183 **1994**.
(24) Sariciftci, N. S.; Heeger, A. J. U.S. Patent: 5454880 **1995**.
(25) Halls, J. J. M.; Walsh, C. A.; Greenham, N. C.; Marseglia, E. A.; Friend, R. H.; Moratti, S. C.; Holmes, A. B. *Nature* **1995**, *376*, 498.
(26) Yu, G.; Gao, J.; Hummelen, J. C.; Wudl, F.; Heeger, A. J. *Science* **1995**, *270*, 1789.
(27) Shaheen, S. E.; Brabec, C. J.; Sariciftci, N. S.; Padinger, F.; Fromherz, T.; Hummelen, J. C. *Appl. Phys. Lett.* **2001**, *78*, 841.
(28) Svensson, M.; Zhang, F.; Veenstra, S. C.; Verhees, W. J. H.; Hummelen, J. C.; Kroon, J. M.; Inganäs, O.; Andersson, M. R. *Adv. Mater.* **2003**, *15*, 988.
(29) Wang, X.; Perzon, E.; Oswald, F.; Langa, F.; Admassie, S.; Andersson, M. R.; Inganäs, O. *Adv. Funct. Mater.* **2005**, *15*, 1665.
(30) Mühlbacher, D.; Scharber, M.; Morana, M.; Zhu, Z.; Waller, D.; Gaudiana, R.; Brabec, C. *Adv. Mater.* **2006**, *18*, 2884.
(31) Hou, J.; Chen, H.-Y.; Zhang, S.; Li, G.; Yang, Y. *J. Am. Chem. Soc.* **2008**, *130*, 16144.
(32) Wienk, M. M.; Turbiez, M.; Gilot, J.; Janssen, R. A. J. *Adv. Mater.* **2008**, *20*, 2556.
(33) Blouin, N.; Michaud, A.; Gendron, D.; Wakim, S.; Blair, E.; Neagu-Plesu, R.; Belletete, M.; Durocher, G.; Tao, Y.; Leclerc, M. *J. Am. Chem. Soc.* **2008**, *130*, 732.
(34) Zhou, E.; Nakamura, M.; Nishizawa, T.; Zhang, Y.; Wei, Q.; Tajima, K.; Yang, C.; Hashimoto, K. *Macromolecules* **2008**, *41*, 8302.

(35) Hummelen, J. C.; Knight, B. W.; LePeq, F.; Wudl, F.; Yao, J.; Wilkins, C. L. *J. Org. Chem.* **1995**, *60*, 532.
(36) Liang, Y.; Xu, Z.; Xia, J.; Tsai, S.-T.; Wu, Y.; Li, G.; Ray, C.; Yu, L. *Adv. Mater.* **2010**, *22*, E135.
(37) Service, R. F. *Science* **2011**, *332*, 293.
(38) McQuarrie, D.; Simon, J. *Physical Chemistry, a Molecular Approach*; University Science Book: Sausalito, **1997**.
(39) Skoog, D.; Holler, F.; Nieman, T. *Principles of Instrumental Analysis*; Saunders College Pub: Philadelphia, **1998**.
(40) Cornil, J.; Beljonne, D.; Brédas, J. L. *J. Chem. Phys.* **1995**, *103*, 834.
(41) Cornil, J.; Beljonne, D.; Brédas, J. L. *J. Chem. Phys.* **1995**, *103*, 842.
(42) Fesser, K.; Bishop, A. R.; Campbell, D. K. *Phys. Rev. B* **1983**, *27*, 4804.
(43) Cornil, J.; Brédas, J. *Adv. Mater.* **1995**, *7*, 295.
(44) Barth, S.; Bässler, H. *Phys. Rev. Lett.* **1997**, *79*, 4445.
(45) Halls, J. J. M.; Cornil, J.; dos Santos, D. A.; Silbey, R.; Hwang, D.-H.; Holmes, A. B.; Brédas, J. L.; Friend, R. H. *Phys. Rev. B* **1999**, *60*, 5721.
(46) Brédas, J.-L.; Beljonne, D.; Coropceanu, V.; Cornil, J. *Chem. Rev.* **2004**, *104*, 4971.
(47) Koster, L. J. A.; Mihailetchi, V. D.; Blom, P. W. M. *Appl. Phys. Lett.* **2006**, *88*, 093511.
(48) Scharber, M. C.; Mühlbacher, D.; Koppe, M.; Denk, P.; Waldauf, C.; Heeger, A. J.; Brabec, C. J. *Adv. Mater.* **2006**, *18*, 789.
(49) Peumans, P.; Forrest, S. R. *Chem. Phys. Lett.* **2004**, *398*, 27.
(50) Mihailetchi, V. D.; Koster, L. J. A.; Hummelen, J. C.; Blom, P. W. M. *Phys. Rev. Lett.* **2004**, *93*, 216601.
(51) Ford, T. A.; Avilov, I.; Beljonne, D.; Greenham, N. C. *Phys. Rev. B* **2005**, *71*, 125212.
(52) Veldman, D.; Offermans, T.; Sweelssen, J.; Koetse, M. M.; Meskers, S. C. J.; Janssen, R. A. J. *Thin Solid Films* **2006**, *511-512*, 333.
(53) Westenhoff, S.; Howard, I. A.; Hodgkiss, J. M.; Kirov, K. R.; Bronstein, H. A.; Williams, C. K.; Greenham, N. C.; Friend, R. H. *J. am. Chem. Soc.* **2008**, *130*, 13653.
(54) Veldman, D.; Meskers, S. C. J.; Janssen, R. A. J. *Adv. Funct. Mater.* **2009**, *19*, 1939.
(55) Di Nuzzo, D.; Aguirre, A.; Shahid, M.; Gevaerts, V. S.; Meskers, S. C. J.; Janssen, R. A. J. *Adv. Mater.* **2010**, *22*, 4321.
(56) Veldman, D.; Chopin, S. M. A.; Meskers, S. C. J.; Janssen, R. A. J. *J. Phys. Chem. A* **2008**, *112*, 8617.
(57) Lampert, M. A. *Phys. Rev.* **1956**, *103*, 1648.
(58) Murgatroyd, P. N. *J. Phys. D: Appl. Phys.* **1970**, *3*, 151.
(59) Waldauf, C.; Morana, M.; Denk, P.; Schilinsky, P.; Coakley, K.; Choulis, S. A.; Brabec, C. J. *Appl. Phys. Lett.* **2006**, *89*, 233517.
(60) White, M. S.; Olson, D. C.; Shaheen, S. E.; Kopidakis, N.; Ginley, D. S. *Appl. Phys. Lett.* **2006**, *89*, 143517.
(61) Wang, J.-C.; Weng, W.-T.; Tsai, M.-Y.; Lee, M.-K.; Horng, S.-F.; Perng, T.-P.; Kei, C.-C.; Yu, C.-C.; Meng, H.-F. *J. Mater. Chem.* **2010**, *20*, 862.
(62) Yu, G.; Heeger, A. J. *J. Appl. Phys.* **1995**, *78*, 4510.
(63) Granstrom, M.; Petritsch, K.; Arias, A. C.; Lux, A.; Andersson, M. R.; Friend, R. H. *Nature* **1998**, *395*, 257.
(64) Jenekhe, S. A.; Yi, S. *Appl. Phys. Lett.* **2000**, *77*, 2635.
(65) Veenstra, S. C.; Verhees, W. J. H.; Kroon, J. M.; Koetse, M. M.; Sweelssen, J.; Bastiaansen, J. J. A. M.; Schoo, H. F. M.; Yang, X.; Alexeev, A.; Loos, J.; Schubert, U. S.; Wienk, M. M. *Chem. Mater.* **2004**, *16*, 2503.
(66) Koetse, M. M.; Sweelssen, J.; Hoekerd, K. T.; Schoo, H. F. M.; Veenstra, S. C.; Kroon, J. M.; Yang, X.; Loos, J. *Appl. Phys. Lett.* **2006**, *88*, 083504.
(67) McNeill, C. R.; Abrusci, A.; Zaumseil, J.; Wilson, R.; McKiernan, M. J.; Burroughes, J. H.; Halls, J. J. M.; Greenham, N. C.; Friend, R. H. *Appl. Phys. Lett.* **2007**, *90*, 193506.

(68) McNeill, C. R.; Halls, J. J. M.; Wilson, R.; Whiting, G. L.; Berkebile, S.; Ramsey, M. G.; Friend, R. H.; Greenham, N. C. *Adv. Funct. Mater.* **2008**, *18*, 2309.
(69) McNeill, C. R.; Abrusci, A.; Hwang, I.; Ruderer, M. A.; Müller-Buschbaum, P.; Greenham, N. C. *Adv. Funct. Mater.* **2009**, *19*, 3103.
(70) McNeill, C. R.; Hwang, I.; Greenham, N. C. *J. Appl. Phys.* **2009**, *106*, 024507-8.
(71) Tan, Z.; Zhou, E.; Zhan, X.; Wang, X.; Li, Y.; Barlow, S.; Marder, S. R. *Appl. Phys. Lett.* **2008**, *93*, 073309.
(72) Zhan, X.; Tan, Z.; Zhou, E.; Li, Y.; Misra, R.; Grant, A.; Domercq, B.; Zhang, X.-H.; An, Z.; Zhang, X.; Barlow, S.; Kippelen, B.; Marder, S. R. *J. Mater. Chem.* **2009**, *19*, 5794.

Chapter 2

Conjugated copolymers of electron-deficient aromatic heterocycles

Abstract. The aim of this chapter is to establish design rules for designing and synthesizing acceptor polymers in organic solar cells. The design explored in this chapter is based on the conjugating well-known electron-deficient aromatic heterocycles such as quinoxaline, benzothiadiazole and thienopyrazine. Three polymers using different combinations of these units have been synthesized and characterized. The electrochemical properties of the different materials reveal, however, that none of them can be used as acceptor polymer but by correlating the frontier orbital energies to the chemical structure, a new perspective towards the design of acceptor polymers could be established.

2.1 Introduction

Renewable energy is one of the most important challenges of the 21st century and its technologies represent a large interest for industries at present. Photovoltaics is one of the technologies able to provide an answer to the sustainable energy issue. An attractive approach to low-cost photovoltaics is organic solar cells. In the 90's, two materials were developed to be used as donor materials in organic solar cells: poly[2-methoxy-5-(3',7'-dimethyloctyloxy)-1,4-phenylene vinylene] (MDMO-PPV) and poly(3-hexylthiophene) (P3HT). When blended with [6,6]-phenyl-C_{61}-butyric acid methyl ester ([60]PCBM) these materials had efficiencies between 2.5 and 5%.[1-3] To improve these efficiencies, research has mainly focused on the development of new donor polymers. The reduction of the optical band gap in order to maximize the overlap with the solar spectrum was the main challenge. One way to achieve this goal was to alternate electron-rich and electron-deficient units along the polymer chain.[4,5] This design has lead to polymers presenting lower reduction potentials compared to that of MDMO-PPV or P3HT.[6]

As research has mainly focused on the quest of new donor material, relatively few efforts have been made to develop new acceptor materials. Several acceptor polymers designed for application in solar cells employ cyano groups to induce acceptor type behaviour and this has resulted in cells with a power conversion efficiency up to 1.7%.[7-15] Another strategy has been to incorporate perylene bisimides in the main chain[16-19] or as pendant groups,[20,21] which has provided a similar performance of about 1.5%. Also electron-deficient, nitrogen heterocycles have been proposed, alternating with vinylene in e.g. poly(pyridopyrazine vinylene)[22] or poly(quinoxaline vinylene).[23] Jenekhe and co-workers have advanced the use of acceptor poly(benzimidazobenzophenanthroline)[24,25] ladder polymers in bilayer cell configurations.

A successful acceptor polymer should display HOMO and LUMO levels that are correctly positioned with respect to the donor material used. In this work we consider P3HT as the donor. Its properties and processability are now known and its performance in solar cells makes it a good donor material.[26-28] P3HT has its LUMO at -3.15 eV and its HOMO at -5.05 eV.[29] To enable efficient electron transfer at the donor-acceptor interface a minimal offset between the two LUMO and the two HOMO levels of $\Delta E \approx 0.35$ eV is mandatory. The complementary acceptor polymer for P3HT would thus have its LUMO level below -3.5 eV and its HOMO level below -5.4 eV.

The purpose of this chapter is to establish design rules for the synthesis of acceptor polymers based on the recent advances in small band gap donor polymers. These small band gap p-type polymers often exist of alternating electron-rich and electron-deficient units. For the latter quinoxaline, thienopyrazine and benzothiadiazole are widely used. Their sp^2-hybridized nitrogen atoms provide electron-withdrawing character and lead to a lowering of the LUMO energy level. One can then think that a strategy to a successful acceptor polymer would be to homo- or co-polymerize these or similar units.

Here, we present the synthesis and optical properties of (co)polymers **I**, **II** and **III** using different combination of quinoxaline, benzothiadiazole and thienopyrazine units (Figure 2.1). Cyclic voltammetry will give us an estimation of the frontier orbital energies of the materials. From these results, it was possible to assess the viability of copolymerizing electron-deficient heterocycles for successful acceptor polymers and established refined design rules for such materials.

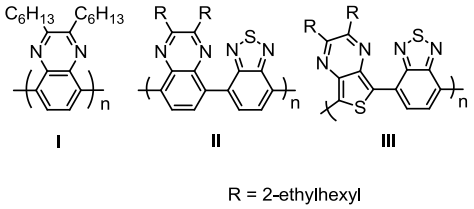

Figure 2.1: Chemical structures of (co)polymers **I**, **II** and **III.**

2.2 Results and discussion

Synthesis. Scheme 2.1 shows the synthetic pathway for monomers **3-9** used in the polymerization of **I-III**. Diketones **1a-b** were prepared according to a literature procedure by reacting oxalyl chloride with the corresponding alkylmagnesium bromide,[30] which is prepared at low temperature. Thienopyrazine **3b** was obtained by condensation of **1b** with the commercially available diamine **2**. Bromination of **3b** with *N*-bromosuccinimide (NBS) yielded monomer **4b** which is of limited stability. Benzothiadiazole **5** was brominated with bromine and after recrystallization gave compound **6** which was then used for two different reactions. First, **6** was reduced with $NaBH_4$ giving the diamine **7**. The subsequent condensation with **1a** and **1b** yielded 5,8-dibromoquinoxalines **8a** and **8b**, respectively. Second, **6** was converted into the bisboronic ester of the benzothiadiazole to yield monomer **9**.[31]

As shown in Scheme 2.2, monomer **8a** was homopolymerized using a Yamamoto coupling. The polymerization was carried out for 40 h in dry toluene using bis(cyclooctadiene)nickel(0) and bipyridine. After work-up, fractionation with methanol, acetone, hexane and chloroform, polymer **I** was obtained as a yellow film in 65% yield. Momomers **4b** and **8b** were copolymerized with **9** using a Suzuki cross-coupling. The polymerization was carried out for 72 h in dry toluene, with aqueous K_2CO_3 as the base, Aliquat 336 as the phase transfer agent and tetrakis(triphenylphosphine)palladium(0) as catalyst. After work-up, fractionation with methanol, acetone, hexane and chloroform polymers **II** and **III** were isolated as a brown solid in 55% yield and as a blue powder in 60%, respectively.

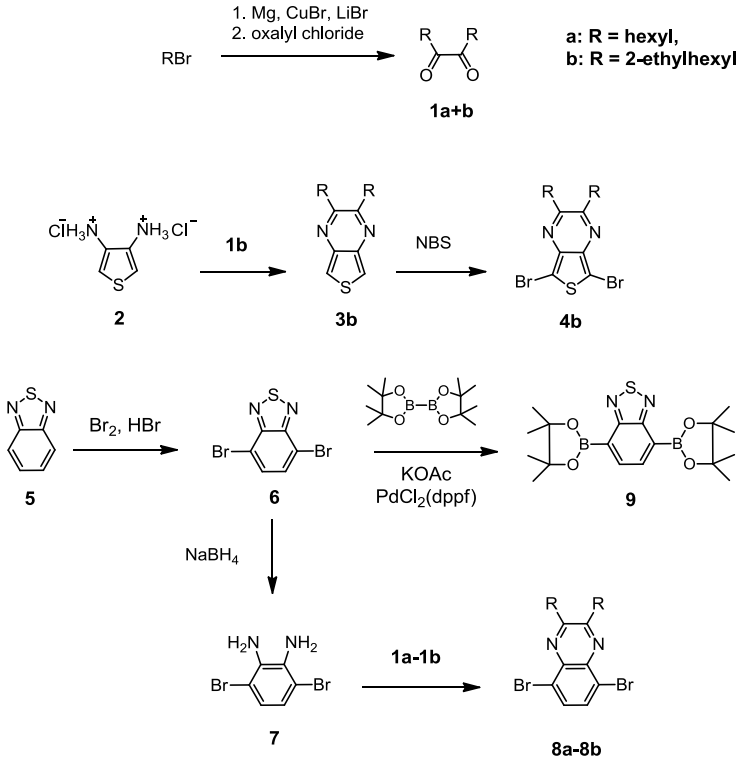

Scheme 2.1: Synthetic route to monomers **4**, **8** and **9**.

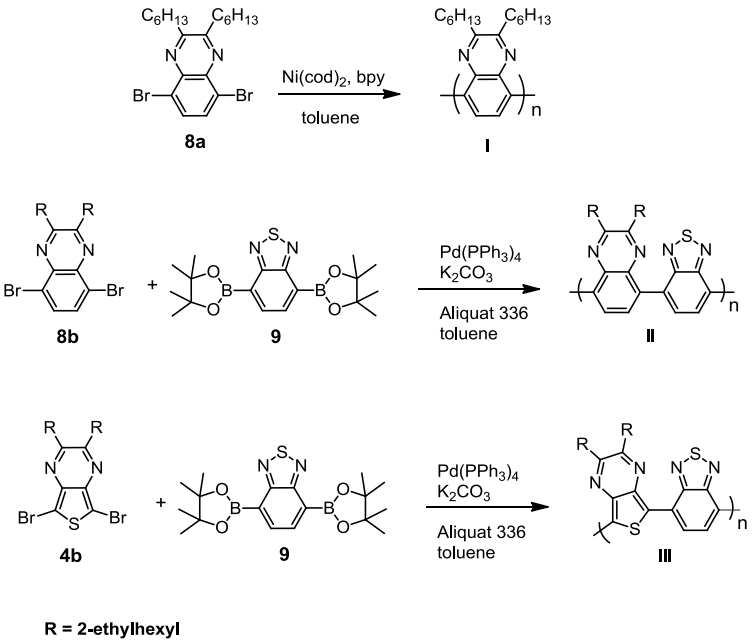

Scheme 2.2: Synthesis polymers **I**, **II** and **III**.

Optical properties. The UV-vis absorption spectra of the polymers were measured in chloroform solution (Figure 2.2). The maximum absorption wavelengths (λ_{max}) of **I** and **II** are significantly lower than that of **III**. The optical band gap –estimated from the onset of absorption– is at 2.88 and 2.44 eV for **I** and **II**, respectively. The 90 nm red-shift going from homopolymer **I** to alternating copolymer **II** can be explained by the introduction of the benzothiadiazole moieties, which are somewhat stronger electron-deficient units compared to the quinoxalines. **III** shows a large bathochromic shift of 560 nm compared to **II**; the optical band gap is estimated at 1.15 eV. Thienopyrazine is both a better donor and a better acceptor than quinoxaline or benzothiadiazole, which results in strong reduction of the band gap.[32,33] Additionally, **III** consists of alternating of 5- and 6-membered rings along the chain which will reduce the interring dihedral angle and increase conjugation. In contrast, connected 6-membered rings form the main chain of **I** and **II**, which are well known to enhance the intercycle torsion because the presence of consecutive phenyl rings, lead to steric hindrance between the ortho-hydrogens thus hampering coplanarity of the backbone. The bandwidth is decreased and the direct consequence is an increase of the band gap of the polymer.[5]

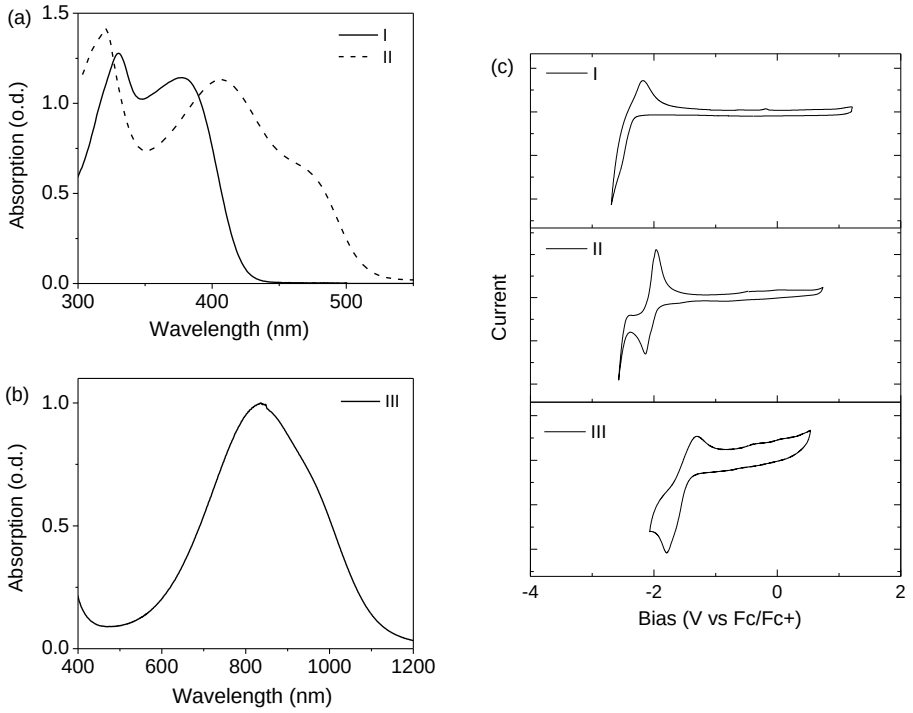

Figure 2.2: Normalized absorption spectra of polymers **I** and **II** (a) and **III** (b) in $CHCl_3$. Cyclic voltammograms of polymers **I**, **II and III** in 0.1 M of $TBAPF_6$ in ODCB at 25 °C (c).

The electrochemical properties of the polymers were determined in solution in ODBC using $TBAPF_6$ as supporting electrolyte (0.1 M). For these polymers, cyclic voltammograms exhibit only the reduction peaks (Figure 2.2c). The reduction potential decreases from **I** to **III** (Table 2.1). As expected, replacing quinoxaline unit by a benzothiadiazole unit leads to a lower LUMO level (-2. 91 for **I** and -3.32 eV for **II**), but has almost no influence on the HOMO level (-5.79 and -5.75 eV). The thienopyrazine unit, which is both a better donor and a better acceptor, in polymer **III** further lowers the LUMO level by about 0.5 eV to -3.81 eV and raises the HOMO level up to -5.00 eV. The HOMO-LUMO offset of **III** is very small, around 1.15 eV. Conjugated polymers can be considered in terms of two limiting mesomeric forms – the aromatic structure and the quinoid structure – (Figure 2.3) the latter being energetically not favourable. It has been suggested that introduction of thienopyrazine units stabilizes the quinoidal form of the polymer in which six π electrons are in the 6-membered ring fused on top of the thiophene core.[34]

Brédas demonstrated that as the quinoid contributions to the geometry become larger, the top of the HOMO band shifts up in energy and the bottom of the LUMO band shifts down in energy by a similar amount, explaining why thienopyrazine-based polymers often present a high lying HOMO level.[35] More recent calculations on alternating thiophene-thienopyrazine oligomers, however, show that the reduction of the band gap in these systems can be attributed to the pronounced donor and acceptor character of thienopyrazine units, only with some admixing of quinoid character to the ground state.[33]

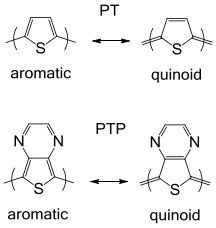

Figure 2.3: Aromatic and quinoidal resonance structure of polythiophene and polythienopyrazine.

Looking at Table I it is clear that none of the three polymers fulfils the requirements (LUMO ≤ -3.5 eV and HOMO ≤ -5.4 eV) to be an acceptor polymer with respect to P3HT. In principle, it would be possible to combine poly(9,9′-dioctylfluorene-*co*-bis-*N*,*N*′-(4-butylphenyl)-bis-*N*,*N*′-phenyl-1,4-phenylene-diamine) (PFB) as a donor material with **I** or **II** as acceptor. PFB displays a LUMO at -2.3 eV and a HOMO at -5.1 eV and a band gap of 2.8 eV.[36] However, the use of wide band gap polymer-polymer combinations as (PFB:**I** or PFB:**II)** in bulk heterojunction solar cells can not lead to an efficient solar energy conversion because the materials absorb only in the UV region and would lead to very low photocurrents.

Table 2.1: Optical and electrochemical properties of polymers in solution.

Polymer	λ_{onset} (nm)	E_g (eV)	E_{red} (V)[a]	HOMO (eV)[b]	LUMO (eV)[c]
I	430	2.88	-2.34	-5.79	-2.91
II	510	2.43	-1.93	-5.75	-3.32
III	1040	1.19	-1.44	-5.00	-3.81

[a] Versus Fc/Fc^+. [b] Estimated from the LUMO energy and the optical band gap.
[c] Determined using a work-function value of -5.23 eV for Fc/Fc^+.[29]

Electron mobility. Electron-mobility measurements have been carried out on polymer **III** in a bottom gate - bottom contact field-effect transistor. The high LUMO energy levels of **I** and **II** preclude such measurements because electrons in the LUMO become trapped at the SiO_2 gate dielectric. Typically the LUMO energy has to be below -3.5 eV to use a SiO_2 gate dielectric. Figure 2.4 shows the transfer curve of **III.** The electron mobility is about 10^{-4} cm^2/Vs. Despite the relatively high electron mobility, which is crucial for acceptor materials in solar cell, the low oxidation potential of **III** prevents its use as an acceptor polymer in combination with almost any conjugated donor polymer known to date.

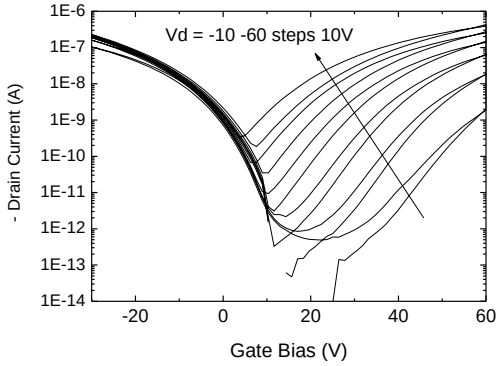

Figure 2.4: N-type transfer characteristic of polymer **III**.

2.3 Conclusions

Polymers **I** and **II** possess high oxidation potentials with HOMO energies of -5.8 eV, but their reduction potentials are too high to allow electron transfer from any suitable donor polymer. Polymer **III** exhibits relatively high electron mobility and a low lying LUMO energy level which are two essential properties for acceptor materials. Unfortunately, the HOMO level energy is much too high to allow hole transfer to any donor material.

The quinoxaline and benzothiadiazole-based polymers present a large optical band gap due to the twisting of the phenyl rings along the chain. The introduction of thiophene rings into the backbone may alleviate the twisting and the band gap issues at the same time. Indeed, a way to decrease the band gap of a polymer is to increase the double bond character between the units.[5] This can be done by an alternating sequence of a strong electron-rich and a strong electron-poor unit in the polymer chain. The bond length

alternation is then reduced due to the stabilization of charges between electron-rich and electron-poor units.

2.4 Experimental section

Materials and methods. Polymerization reactions were conducted under an argon atmosphere. Commercial chemicals were used as received. ^{1}H NMR and ^{13}C NMR spectra were recorded at 400 MHz on a VARIAN mercury spectrometer with $CDCl_3$ as the solvent and tetramethylsilane (TMS) as the internal standard. The peaks are given in ppm, relative to TMS (0 ppm). Molecular weights were determined with GPC on a Shimadzu LC-10AD using a Polymer Laboratories Resipore column (length 300 mm, diameter 7.5 mm), a Shimadzu SPD-M20A photodiode array detector from 250-700 nm and ODCB as the eluent with a flow rate of 1 mg/min. (T = 348 K). Polystyrene standards were used.

UV-vis-nearIR optical absorption spectra were recorded on a Perkin-Elmer Lambda 900 spectrophotometer. Cyclic voltammetry was conducted under an inert atmosphere with a scan rate of 0.1 V/s, using 1 M tetrabutylammonium hexafluorophosphate in ODCB as the electrolyte. The working electrode was a platinum disk and the counter electrode was a silver rod electrode. A silver wire coated with silver chloride (Ag/AgCl) was used as a quasi reference electrode in combination with Fc/Fc^{+} as an internal standard. Atomic force microscopy (AFM) was measured using a Veeco MultiMode with a Nanoscope III controller, in tapping mode. The used probes were PPP-NCH-50 from Nanosensors. Field-effect transistors were fabricated using heavily doped silicon wafers as the common gate electrode with a 200 nm thermally oxidized SiO_2 layer as the gate dielectric. Using conventional photolithography, gold source and drain electrodes were defined in a bottom contact device configuration with channel width and length of 10000 μm and 10 μm, respectively. A 10 nm layer of titanium was used, acting as an adhesion layer for the gold on SiO_2. The SiO_2 layer was exposed to the vapor of the primer hexamethyldisilazane for 60 min. prior to semiconductor deposition in order to passivate the surface of the dielectric. Films of polymer **III** were spun from a chloroform solution at 1000 rpm for 30 s. Freshly prepared devices were annealed in a dynamic vacuum of 10^{-5} mbar at 140 °C for 2 h to remove traces of solvent. All electrical measurements were performed in vacuum using an HP 4155C semiconductor parameter analyzer.

General procedure for α-diones (**1a-b**). In a first flask, the alkyl bromide (152 mmol) was added dropwise to a refluxing suspension of iodine-activated magnesium (4.0 g, 165 mmol) in Et_2O (120 mL). In a separate flask, LiBr (25.5 g, 293 mmol) and CuBr (21.1 g, 0.146 mol) were stirred vigorously in THF (410 mL) to form a green suspension. This mixture was then cooled to -90 °C and the Grignard reagent was slowly added to the LiBr/CuBr suspension. The mixture was stirred for 20 min. at -90 °C and oxalyl chloride (7.77 g, 61.0 mmol) was added slowly via syringe to maintain a temperature below -70 °C. The mixture was stirred at -90 to -95 °C for 1 h, allowed to warm to room temperature and quenched with saturated aqueous NH_4Cl. The organic layer was separated and the aqueous layer extracted repeatedly with ethyl acetate. The combined organic layers were thoroughly washed with NH_4Cl, dried over anhydrous Na_2SO_4, concentrated by rotary evaporation and the residue separated on a silica column using a 95:5 petroleum ether/ethyl acetate mixture. The desired product eluted as the first band.

Tetradecane-7,8-dione (**1a**). The compound was obtained as a yellow solid (10 g, 77%)**,** ^{1}H NMR (400 MHz, $CDCl_3$) δ: 0.86 (t, *J* = 7.2 Hz, 6H), 1.24 (m, 12H), 1.56 (p, *J* = 7.2 Hz, 4H), 2.72 (t, *J* = 7.2 Hz, 4H), ^{13}C NMR (100 MHz, $CDCl_3$) δ: 200.4, 36.3, 31.7, 29.0, 23.2, 22.7, 14.2.

5,10-Diethyltetradecane-7,8-dione (1b). The compound was obtained as a yellow liquid (8.2 g, 48 %). ^{1}H NMR (400 MHz, $CDCl_3$) δ: 2.65 (d, 4H, *J* = 6.6 Hz), 1.86 (m, 2H), 1.45-1.10 (m, 16H), 0.95-0.75 (m, 12H). ^{13}C NMR (100 MHz, $CDCl_3$) δ: 200.6, 40.3, 35.0, 33.3, 28.9, 26.5, 22.9, 14.0, 10.8.

2,3-Bis(2'-ethylhexyl)thieno[3,4-*b*]pyrazine (**3b**). Compounds **2** (1.4 g, 7.5 mmol) and **1b** (2.1 g, 7.5 mmol) were reacted after neutralisation of **2** with Et_3N (2 mL) in ethanol (20 mL) to yield a red-orange solution which was stirred for 3 h and then concentrated by rotary evaporation without heating to give a solid residue. The residue was washed repeatedly with petroleum ether, the combined petroleum ether washes were dried with anhydrous Na_2SO_4 and then concentrated by rotary evaporation to give a light tan product. The product was purified further by column chromatography with 5% (v/v) ethyl acetate/hexane to give **3b** as light tan needles in a yield of 73% (1.97 g). ^{1}H NMR (400 MHz, $CDCl_3$) δ: 0.88 (t, *J* = 7.5 Hz, 6H), 1.26 (m, 24H), 1.36 (p, *J* = 7.5 Hz, 4H), 1.46 (p, *J* = 7.5 Hz, 4H), 1.78 (p, *J* = 7.5 Hz, 4H), 2.88 (t, *J* = 7.5 Hz, 4H), 7.80 (s, 2H); ^{13}C NMR

(100 MHz, $CDCl_3$) δ: 156.7, 141.9, 116.1, 36.0, 32.2, 30.0, 29.9, 29.8, 29.7, 29.6, 28.7, 22.9, 14.4.

5,7-Dibromo-2,3-bis(2'-ethylhexyl)thieno[3,4-*b*]pyrazine (**4b**). To a solution of **3b** (865 mg, 2.4 mmol) in chloroform/acetic acid (1:1, 60 mL) was added NBS (897 mg, 5 mmol) in the dark and stirred overnight under argon. Then, water (60 mL) was added to the mixture, the organic layer was separated and washed a first time with a KOH solution and then with water. The combined organic layers were dried over Na_2SO_4 and concentrated by rotary evaporation without heating to give a solid residue. The product was further purified by chromatography using hexane/dichloromethane (1:1) to give **4b** as a greenish yellow solid in 50% yield (622 mg). ^{1}H NMR (400 MHz, $CDCl_3$) δ: 0.96 (m, 12 H), 1.20-1.50 (m, 16 H), 1.94-2.05 (m, 2 H), 2.83 (d, J = 6.9 Hz, 4 H). ^{13}C NMR (100 MHz, $CDCl_3$) δ: 157.9, 139.1, 103.1, 39.5, 37.9, 32.7, 28.8, 26.0, 23.0, 14.1, 10.9.

4,7-Dibromobenzo-2,1,3-thiadiazole (**6**). A solution of 2,1,3-benzothiadiazole **5** (10.0 g, 73.4 mmol) in aq. HBr (48%, 70 mL) was heated to reflux, and Br_2 (12 mL, 233.6 mmol) was added dropwise over 1 h. After complete addition of Br_2, the mixture was further stirred at reflux during 2 h. The precipitate was filtered hot and washed abundantly with water and acetone. The solid compound was taken up in dichloromethane, the filtrate dried over Na_2SO_4 and after concentration the residue was recrystallized from EtOH to give **6** as white needles (17.7 g, 85%). ^{1}H NMR (400 MHz, $CDCl_3$) δ: 7.71 (s, 2H). ^{13}C NMR (100 MHz, $CDCl_3$) δ: 153.1, 132.4, 113.9.

3,6-Dibromobenzene-1,2-diamine (**7**). To a suspension of **6** (5.0 g, 17 mmol) in EtOH cooled at 0 °C, $NaBH_4$ (11.4 g, 300 mmol) was added portionwise and the mixture was stirred at room temperature for 20 h. The mixture was concentrated and extracted twice with Et_2O. The organic phases were washed with brine until the phase was colorless and then dried over Na_2SO_4. Evaporation of the solvent gave **7** as a white solid (3.8 g, 78%). ^{1}H NMR (400 MHz, $CDCl_3$) δ: 3.89 (br. s, 4 H); 6.84 (s, 2H). ^{13}C NMR (100 MHz, $CDCl_3$) δ: 133.8, 123.3, 109.7.

5,8-Dibromo-2,3-dihexylquinoxaline (**8a**). A solution of **7** (3.0 g, 11.3 mmol) and tetradecane-7,8-dione **1a** (2.55 g, 11.3 mmol) in EtOH was heated to reflux for 3 h. The reaction mixture was allowed to cool to room temperature and filtered. The precipitate was washed with ethanol and dried in vacuum to give **8a** as a white powder (5.1 g, 75%). ^{1}H NMR (400 MHz, $CDCl_3$) δ: 7.80 (s, 2H), 3.06 (t, *J* = 7.25 Hz, 4H), 1.91 (q, *J* = 6.39 Hz, 4H), 1.42 (m, 4H), 1.34 (m, 8H), 0.90 (t, *J* = 7.65 Hz, 6H). ^{13}C NMR (100 MHz, $CDCl_3$) δ: 158.22, 139.23, 131.92, 123.32, 34.75, 31.74, 29.18, 27.71, 22.63, 14.11.

5,8-Dibromo-2,3-bis(2'ethylhexyl)quinoxaline (8b). A solution of **7** (3.0 g, 11.3 mmol) and 5,10-diethyl-tetradecane-7,8-dione **1b** (3.19 g, 11.3 mmol) in EtOH was heated to reflux for 3 h. After removal of the solvent by evaporation, the residue was dissolved in ethyl acetate and extracted with water. The organic extract was dried over Na_2SO_4 and the solvent was evaporated under reduced pressure. The residue was subjected to column chromatography (95:5 heptane/AcOEt; R_f = 0.29) to obtain **8b** as a yellowish oil (1.2 g, 65%). ^{1}H NMR (400 MHz, $CDCl_3$) δ: 7.81 (s, 2H), 3.0 (d, *J* = 7.05 Hz, 4H), 2.12 (m, 2H), 1.45−1.35 (m, 20H), 0.94 (t, *J* = 7.3 Hz, 6H), 0.87 (m, 8H). ^{13}C NMR (100 MHz, $CDCl_3$) δ: 158.11, 138.99, 131.86, 123.40, 38.82, 38.06, 32.82, 28.88, 26.06, 23.06, 14.13, 10.93. MALDI-TOF MS (*MW* = 512.36): m/z = 512.12 [M^+].

2,1,3-Benzothiadiazole-4,7-bis(boronic acid pinacol ester) (**9**). To a solution of 4,7-dibromo-2,1,3-benzothiadiazole (1 g, 3.41 mmol) in dried 1,4-dioxane (10 mL), bis(pinacolato)diboron (2 g, 7.8 mmol), [1,1'-bis(diphenylphosphino)ferrocene] palladium(II) dichloride ($PdCl_2$(dppf)) (500 mg, 0.6 mmol) and KOAc (2 g, 20 mmol) were added at room temperature and the mixture was stirred overnight at 80 °C. The reaction was quenched by addition of water and extracted with ethyl acetate (30 mL × 3). The organic layers were washed with brine, dried over Na_2SO_4 and concentrated in vacuum to yield a dark red solid. The solid was purified by silica gel chromatography by 10 % ethyl acetate in hexane to give the desired compound as a yellow solid (600 mg, 46 %). ^{1}H NMR (400 MHz, $CDCl_3$) δ: 8.10 (s, 2H), 1.41 (s, 24H). ^{13}C NMR (100 MHz, $CDCl_3$) δ: 157.55, 138.11, 84.91, 25.3. MALDI-TOF MS (*MW* = 388.1): m/z = 388.0 [M^+].

Polymer I. A solution of bis(cyclooctadiene)nickel(0) ($Ni(cod)_2$) (298.2 mg, 1.09 mol) and bipyridine (192 mg, 1.21 mol) in dry toluene (6 mL) was heated at 85 °C and **4a** (150 mg, 330 mmol) was added with extra dry toluene (6 mL). After 40 h at 85 °C, 100 mL of MeOH/acetone/0.1M HCl (1:1:1) was added and the mixture was vigorously stirred for 3 h. An extraction with dichloromethane was done, followed by EDTA and water washings. The organic phases were concentrated and the polymer was fractionated with a Soxhlet extractor. Polymer **I** was obtained as a yellow solid in 70% yield (70 mg). GPC(PS): M_n = 200 kg/mol, PDI = 2.5. ^{1}H (400 MHz, $CDCl_3$) δ: 8.18 (br, 1H), 2.81 (br, 2H), 1.56 (br, 2H), 1.22 (m, 4H), 0.84 (br, 3H).

Polymer II. To a solution of **5** (150 mg, 0.44 mmol) and **4b** (254 mg, 0.44 mmol) in degassed toluene (6 mL) were added 3 droplets of Aliquat 336 and $Pd(PPh_3)_4$. The solution was stirred and K_2CO_3 (3 mL, 2 M in water) was added. The 2 phases were heated at reflux for 80 h. Then, methanol (100 mL) was added, the precipitate was collected and fractionated with a Soxhlet extractor. Polymer **II** was obtained as a brown solid in 65% yield (123 mg). GPC(PS): M_n = 8.2 kg/mol, PDI = 1.9. ^{1}H (400 MHz, $CDCl_3$) δ: 8.23 (br, 2H), 2.79 (br, 2H), 1.55 (br, 2H), 1.22 (m, 9H), 0.86 (br, 3H).

Polymer III. Compounds **5** (136 mg, 0.35 mmol) and **3b** (200 mg, 0.35 mmol) were reacted according to the procedure described above for polymer **II** to offer polymer **III** as blue crystals in 88% yield (170 mg). GPC(PS): M_n = 5.3 kg/mol, PDI = 2.2. ^{1}H (400 MHz, $CDCl_3$) δ: 8.83 (br, 1H), 3.2 (br, 2H), 1.8-0.6 (m, 15H).

References

(1) Wienk, M. M.; Kroon, J. M.; Verhees, W. J. H.; Knol, J.; Hummelen, J. C.; van Hal, P. A.; Janssen, R. A. J. *Angew. Chem. Int. Ed.* **2003**, *42*, 3371.

(2) Shaheen, S. E.; Brabec, C. J.; Sariciftci, N. S.; Padinger, F.; Fromherz, T.; Hummelen, J. C. *Appl. Phys. Lett.* **2001**, *78*, 841.

(3) Li, G.; Shrotriya, V.; Huang, J.; Yao, Y.; Moriarty, T.; Emery, K.; Yang, Y. *Nat. Mater.* **2005**, *4*, 864.

(4) Roncali, J. *Chem. Rev.* **1997**, *97*, 173.

(5) van Mullekom, H. A. M.; Vekemans, J. A. J. M.; Havinga, E. E.; Meijer, E. W. *Mater. Sci. Eng.: R: Reports* **2001**, *32*, 1.

(6) Kroon, R.; Lenes, M.; Hummelen, J.; Blom, P.; De Boer, B. *Polym. Rev.* **2008**, *48*, 531.

(7) Yu, G.; Heeger, A. J. *J. Appl. Phys.* **1995**, *78*, 4510.

(8) Halls, J. J. M.; Walsh, C. A.; Greenham, N. C.; Marseglia, E. A.; Friend, R. H. Moratti, S. C.; Holmes, A. B. *Nature* **1995**, *376*, 498.

(9) Veenstra, S. C.; Verhees, W. J. H.; Kroon, J. M.; Koetse, M. M.; Sweelssen, J. Bastiaansen, J. J. A. M.; Schoo, H. F. M.; Yang, X.; Alexeev, A.; Loos, J.; Schubert, U. S.; Wienk, M. M. *Chem. Mater.* **2004**, *16*, 2503.

(10) Kietzke, T.; Horhold, H.; Neher, D. *Chem. Mater.* **2005**, *17*, 6532.

(11) Offermans, T.; van Hal, P. A.; Meskers, S. C. J.; Koetse, M. M.; Janssen, R. A. J. *Phys. Rev. B* **2005**, *72*, 045213.

(12) Koetse, M. M.; Sweelssen, J.; Hoekerd, K. T.; Schoo, H. F. M.; Veenstra, S. C.; Kroon, J. M.; Yang, X.; Loos, J. *Appl. Phys. Lett.* **2006**, *88*, 083504.

(13) Veldman, D.; Offermans, T.; Sweelssen, J.; Koetse, M. M.; Meskers, S. C. J.; Janssen, R. A. J. *Thin Solid Films* **2006**, *511-512*, 333.

(14) Mandoc, M. M.; Veurman, W.; Koster, L. J. A.; Koetse, M. M.; Sweelssen, J.; de Boer, B.; Blom, P. W. M. *J. Appl. Phys.* **2007**, *101*, 104512.

(15) Yin, C.; Kietzke, T.; Neher, D.; Hörhold, H.-H. *Appl. Phys. Lett.* **2007**, *90*, 092117.

(16) Neuteboom, E. E.; Meskers, S. C. J.; van Hal, P. A.; van Duren, J. K. J.; Meijer, E. W.; Janssen, R. A. J.; Dupin, H.; Pourtois, G.; Cornil, J.; Lazzaroni, R.; Brédas, J.-L.; Beljonne, D. *J. Am. Chem. Soc.* **2003**, *125*, 8625.

(17) Zhan, X.; Tan, Z.; Domercq, B.; An, Z.; Zhang, X.; Barlow, S.; Li, Y.; Zhu, D.; Kippelen, B.; Marder, S. R. *J. Am. Chem. Soc.* **2007**, *129*, 7246.

(18) Hou, J.; Zhang, S.; Chen, T. L.; Yang, Y. *Chem. Commun.* **2008**, 6034.

(19) Huo, L.; Zhou, Y.; Li, Y. *Macromol. Rapid Commun.* **2008**, *29*, 1444.

(20) Neuteboom, E. E.; van Hal, P. A.; Janssen, R. A. J. *Chem. Eur. J.* **2004**, *10*, 3907.

(21) Palermo, V.; Otten, M. B. J.; Liscio, A.; Schwartz, E.; de Witte, P. A. J.; Castriciano, M. A.; Wienk, M. M.; Nolde, F.; De Luca, G.; Cornelissen, J. J. L. M.; Janssen, R. A. J.; Müllen, K.; Rowan, A. E.; Nolte, R. J. M.; Samorì, P. *J. Am. Chem. Soc.* **2008**, *130*, 14605.

(22) Zhang, F.; Jonforsen, M.; Johansson, D. M.; Andersson, M. R.; Inganäs, O. *Synth. Met.* **2003**, *138*, 555.

(23) Huo, L.; Tan, Z.; Zhou, Y.; Zhou, E.; Han, M.; Li, Y. *Macromol. Chem. Phys.* **2007**, *208*, 1294.

(24) Jenekhe, S. A.; Yi, S. *Appl. Phys. Lett.* **2000**, *77*, 2635.

(25) Alam, M. M.; Jenekhe, S. A. *Chem. Mater.* **2004**, *16*, 4647.

(26) Kim, Y.; Cook, S.; Tuladhar, S. M.; Choulis, S. A.; Nelson, J.; Durrant, J. R.; Bradley, D. D. C.; Giles, M.; McCulloch, I.; Ha, C.-S.; Ree, M. *Nat. Mater.* **2006**, *5*, 197.

(27) Ma, W.; Yang, C.; Gong, X.; Lee, K.; Heeger, A. J. *Adv. Funct. Mater.* **2005**, *15*, 1617.

(28) Mihailetchi, V. D.; Xie, H. X.; de Boer, B.; Koster, L. J. A.; Blom, P. W. M. *Adv. Funct. Mater.* **2006**, *16*, 699.

(29) Veldman, D.; Meskers, S. C. J.; Janssen, R. A. J. *Adv. Funct. Mater.* **2009**, *19*, 1939.

(30) Kenning, D. D.; Mitchell, K. A.; Calhoun, T. R.; Funfar, M. R.; Sattler, D. J.; Rasmussen, S. C. *J. Org. Chem.* **2002**, *67*, 9073.
(31) Zhang, M.; Tsao, H. N.; Pisula, W.; Yang, C.; Mishra, A. K.; Mullen, K. *J. Am. Chem. Soc.* **2007**, *129*, 3472.
(32) Kitamura, C.; Tanaka, S.; Yamashita, Y. *Chem. Mater.* **1996**, *8*, 570.
(33) Karsten, B. P.; Viani, L.; Gierschner, J.; Cornil, J.; Janssen, R. A. J. *J. Phys. Chem. A* **2009**, *113*, 10343.
(34) Brédas, J. L.; Heeger, A. J.; Wudl, F. *J. Chem. Phys.* **1986**, *85*, 4673.
(35) Bredas, J. L. *J. Chem. Phys.* **1985**, *82*, 3808.
(36) Arias, A. C.; Corcoran, N.; Banach, M.; Friend, R. H.; MacKenzie, J. D.; Huck, W. T. S. *Appl. Phys. Lett.* **2002**, *80*, 1695.

Chapter 3

Designing acceptor polymers for organic photovoltaic devices

Abstract. One of the challenges in the field of organic photovoltaics is developing alternatives to the family of fullerene derivatives that are commonly used as acceptor material but that generally lack a strong optical absorption coefficients. We describe the synthesis and optoelectronic properties of three new electron acceptor polymers that use the alternation of thiophene units and electron-deficient units as a common design theme. The acceptor polymers are combined with poly(3-hexylthiophene) as electron donor material in bulk heterojunction solar cells. The performance of the photovoltaic devices is limited by incomplete exciton dissociation and a sluggish separation of the photogenerated electrons and holes at low fields. The separation is in competition with charge recombination to the triplet state. In addition, the low electron mobility in the acceptor polymers hampers charge collection.

3.1 Introduction

Bulk heterojunction organic solar cells offer a promising approach to solar energy at low cost and large areas.[1-4] The most efficient bulk heterojunction organic solar cells use a conjugated polymer as the donor p-type material[5-7] and a C_{60} or C_{70} fullerene derivative as the acceptor n-type material.[8,9] Commonly used fullerene derivatives as [60]PCBM and [70]PCBM have good electron mobility[10] due to their semi-crystalline nature[11] and offer solubility in a range of organic solvents for easy processing, but have the disadvantage that their absorption of solar light is not very good, especially for C_{60} derivatives. Next to fullerenes and small-molecules,[12] such as perylene diimide derivatives,[13,14] polymers have attracted attention as acceptor materials.[15] Polymer acceptors offer advantages with respect to contributing more strongly to the absorption of visible or near-IR light but the progress in polymer:polymer solar cell in terms of efficiency has not kept up with that of polymer:fullerene cells.[15]

In this work, we selected P3HT as the donor material. Considering that this polymer has a LUMO level at -3.15 eV and a HOMO level at -5.05 eV,[16] a matching acceptor polymer for P3HT would then have its LUMO level below -3.5 eV and its HOMO level below -5.4 eV.

While several acceptor polymers designed for application in solar cells employ cyano groups[17-25] or perylene diimides,[26-29] our design of new acceptor polymers is based on the recent advances in small band gap p-type polymers.[5-7] These small band gap p-type polymers often exist of alternating electron-rich and electron-deficient units. For the latter quinoxaline, thienopyrazine and benzothiadiazole are widely used. Their sp^2-hybridized nitrogen atoms provide electron-withdrawing character and lead to a lowering of the LUMO energy level. One can then think that a strategy to a successful acceptor polymer would be to homo- or co-polymerize these or similar units.

In Chapter 2, two materials were synthesized: polymer **I** which is a homopolymer of quinoxaline units and polymer **II**, a copolymer of quinoxaline and benzothiadiazole moieties. Polymers **I** and **II** possess high oxidation potentials with HOMO energies of -5.8 eV, but their reduction potentials are too high to allow electron transfer from any suitable donor polymer. Their large optical band gap is mainly due to the twisting of phenyl rings along the chain.

To alleviate these constraints we designed three related polymers **PA**, **PB** and **PC** (Figure 3.1) that carry one thiophene unit for each electron-deficient unit. As a consequence five and six membered rings are alternating along the chain. The 1:1 ratio is chosen to keep the HOMO level as low as possible and by changing the acceptor from benzothiadiazole, via triazolobenzene to quinoxaline we can tune the LUMO level. Polymers **PA**, **PB** and **PC** are synthesized via a combination of Suzuki and Stille reactions and their optical and electrochemical properties are presented. The new polymers are tested as acceptor material in solar cells with P3HT as the donor and the photophysical and morphological properties of the photoactive layers have been investigated to rationalize the results.

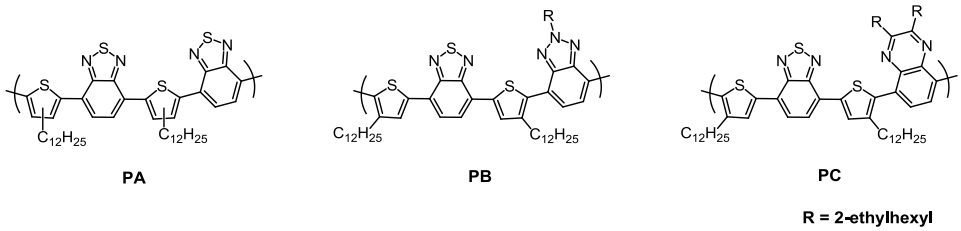

Figure 3.1: Structures of **PA**, **PB** and **PC**. All alkyl groups in these polymers are *n*-alkyl except for **PB** and **PC** where R represents a branched 2'-ethylhexyl group.

3.2 Results and discussions

Synthesis. The synthesis of **PA**, **PB** and **PC** follows the reactions depicted in Scheme 3.1 (monomers **1**, **5** and **8**) and Scheme 3.2 (polymerization). Starting from 3-dodecylthiophene, reaction with 2.0 equiv. of *N*-bromosuccinimide (NBS) in DMF afforded monomer **1**.[30] Treatment of 3-dodecylthiophene with TMEDA and *n*-buthyllithium in THF and subsequent quenching by adding 1.5 equiv. of tributyltinchloride gave 4-dodecyl-2-tributylstannylthiophene **2**.[31] Stille coupling of either **3** (synthesized in a procedure as described in ref [32]) or **6** (synthesized in a procedure as described in ref [33]) with two equivalents of **2** using bis(triphenylphosphine)palladium(II) chloride [$Pd(PPh_3)_2Cl_2$] as a catalyst gave **4** and **7**, respectively. Compounds **4** and **7** were then dibrominated using 2.05 equiv. of NBS in DMF at 45 °C for 5 h to obtain monomers **5** and **8** respectively.

As shown in Scheme 3.2, Suzuki polymerization of either **1**, **5** or **8** with 2,1,3-benzothiadiazole-4,7-bis(boronic acid pinacol ester) (**9**) using tetrakis(triphenylphosphine) palladium(0) [$Pd(PPh_3)_4$], aqueous potassium carbonate, Aliquat 336 in toluene at 110 °C for 80 h afforded polymers **PA**, **PB** and **PC** in ~60% yield. The molecular weights (M_n) of **PB** and **PC** are in the same range, 9700 g/mol and 9600 g/mol, respectively, while the value for **PA** is lower, 4500 g/mol.

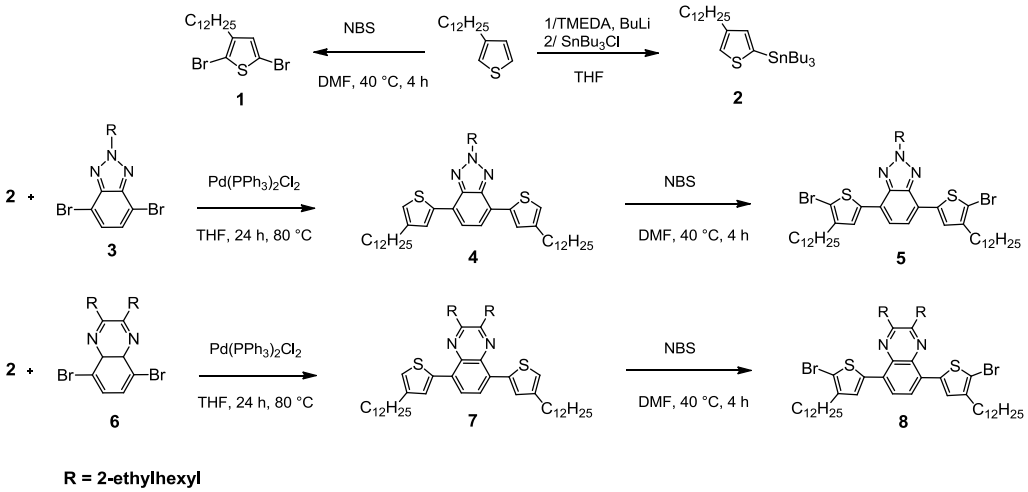

Scheme 3.1: Synthetic pathway to the monomers **1**, **5** and **8**.

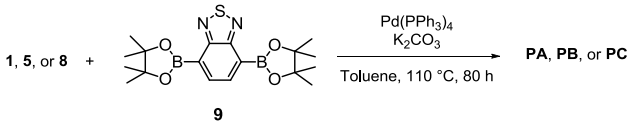

Scheme 3.2: Synthesis of the polymers **PA**, **PB** and **PC**.

Optical and electrochemical properties. The absorption spectra of the polymers dissolved in ODCB and as thin film are shown in Figure 3.2 and the results are collected in Table 3.1. The optical gaps of **PA**, **PB** and **PC** determined at the onset of absorption in ODCB are very similar at E_g^{sol} = 2.09, 2.18 and 2.18 eV. In thin films, all the onsets of absorption (E_g) are red-shifted by about 0.2 eV, indicating some aggregation.

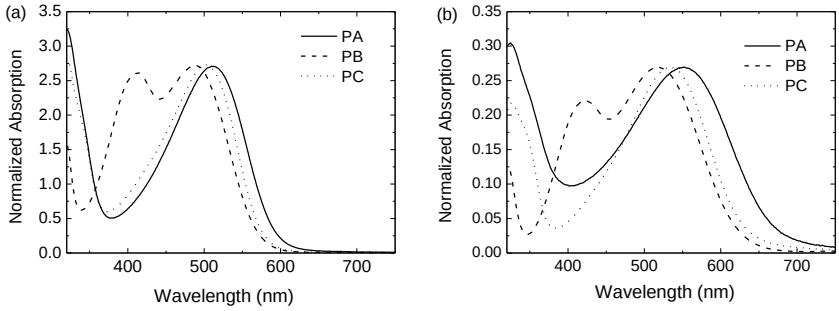

Figure 3.2: Optical absorption spectra of **PA**, **PB** and **PC**. (a) in ODCB solution. (b) in thin film.

Table 3.1: Molecular weight, optical and electrochemical properties of P3HT, **PA**, **PB** and **PC**.

	M_n (kg/mol)	PD	E_g^{sol} (eV)	E_g (eV)	E_{ox} [a] (V)	E_{red} [a] (V)	E_{cv}^{sol} (eV)	E_{HOMO}^{opt} [b] (eV)	E_{LUMO}^{opt} [b] (eV)	E_{CT} [c] (eV)	E_T [c] (eV)
P3HT	30	2.1	2.25	1.91	0.06	-2.34	2.40	-5.05	-3.14		1.32
PA	4.5	1.5	2.09	1.86	0.36	-1.67	2.03	-5.51	-3.65	1.70	1.24
PB	9.7	1.8	2.18	2.01	0.33	-1.80	2.13	-5.50	-3.49	1.85	1.36
PC	9.6	2.0	2.16	1.94	0.35	-1.84	2.19	-5.46	-3.52	1.83	1.31

[a] CV measurements in ODCB (0.1M TBAPF6) vs. Fc/Fc^+ as internal standard. [b] Calculated form equations (3.1) and (3.2). [c] For a blend with P3HT, calculated from equation (3.3). [d] Estimated from $E_T = (E_g^{sol} - 0.7)(E_g / E_g^{sol})$, see text.

Cyclic voltammetry was performed in ODCB for each polymer (Figure 3.3) and the results are collected in Table 3.1. **PA**, **PB** and **PC** all have similar oxidation potentials at ~0.35 V vs. Fc/Fc^+. Because the three polymers differ in the nature of the electron-deficient unit, the reduction potential varies and is less negative for **PA** (–1.67 V vs. Fc/Fc^+) than for **PB** (–1.80 V vs. Fc/Fc^+) and **PC** (–1.84 V vs. Fc/Fc^+), indicative of a stronger acceptor properties for **PA**. The electrochemical gap (E_{cv}^{sol}), determined as the difference between the onsets of the oxidation and reduction potentials, is in good agreement with the optical gap E_g^{sol}.

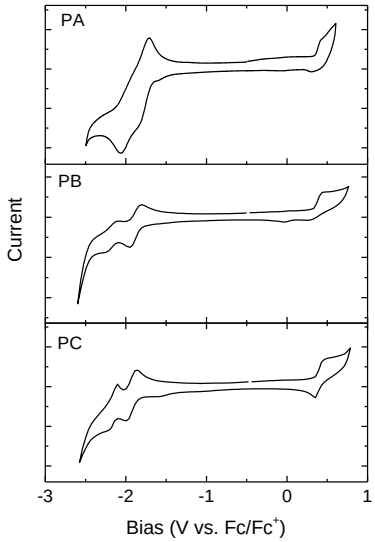

Figure 3.3: Cyclic voltammograms of **PA**, **PB** and **PC** in ODCB (0.1 M $TBAPF_6$).

The optical HOMO and LUMO energy levels versus vacuum are also given in Table 3.1. We use the experimental difference between E_{cv}^{sol} and E_g to estimate "effective" optical HOMO (E_{HOMO}^{opt}) and LUMO (E_{LUMO}^{opt}) energies of the separate materials in thin solid films following a method described recently.[16] These energies are derived from E_{ox} and E_{red} assuming that the difference $E_{cv}^{sol} - E_g$ can be equally divided over the HOMO and the LUMO and using a work function value of –5.23 eV for Fc/Fc^+:[34–36]

$$E_{HOMO}^{opt} = -5.23\,eV - e\,E_{ox} + \tfrac{1}{2}(E_{cv}^{sol} - E_g) \quad (3.1)$$

$$E_{LUMO}^{opt} = -5.23\,eV - e\,E_{red} - \tfrac{1}{2}(E_{cv}^{sol} - E_g) \quad (3.2)$$

Note that, by this definition, the "effective" HOMO-LUMO gap $|E_{HOMO}^{opt} - E_{LUMO}^{opt}|$ of a material is equal to its optical gap E_g in film and hence one could argue that these "effective" HOMO and LUMO levels incorporate the intramolecular exciton binding energy in the solid state.

At first inspection, each of the three polymers fulfils the requirements to be an efficient acceptor polymer with respect to P3HT as donor. The offsets of $E_{\mathrm{LUMO}}^{\mathrm{opt}}$ are 0.35–0.50 eV and the offsets of $E_{\mathrm{HOMO}}^{\mathrm{opt}}$ are 0.40-0.45 eV. Hence, our design of alternating copolymers with a 1:1 ratio of electron-rich and electron-deficient units along the chain has resulted in materials that seem to have the correct energy levels to be used as acceptor material in a device together with P3HT as the p-type material. A more refined estimate can be made using the expected energy of the charge transfer state (E_{CT}) in the three blends. This CT energy can be estimated from $E_{\mathrm{HOMO}}^{\mathrm{opt}}$ and $E_{\mathrm{LUMO}}^{\mathrm{opt}}$ energies via the empirical relation:[16]

$$E_{\mathrm{CT}} = |E_{\mathrm{HOMO}}^{\mathrm{opt}}(\mathrm{D}) - E_{\mathrm{LUMO}}^{\mathrm{opt}}(\mathrm{A})| + 0.29\mathrm{eV} \quad (3.3)$$

in which 0.29 eV represents a Coulomb term to account for the higher energy of the intermolecular CT exciton compared to an intramolecular exciton due to the larger electron–hole separation distance. This gives the values E_{CT} = 1.70, 1.85 and 1.83 eV for blends of P3HT with **PA**, **PB** and **PC** respectively. We note that these values are on the borderline for efficient photoinduced electron transfer, considering that the optical band gap of the blends are E_{g} = 1.86, 1.91 and 1.91 eV, respectively and that a criterion of $E_{\mathrm{g}} - E_{\mathrm{CT}} \geq 0.08$ (±0.02) eV has been established.[16] It may be further noted that while the energy of fully separated polarons is not accurately known, it would be higher than E_{CT} in a simple continuum dielectric approximation, reducing the chances of forming free charges.

Based on the $E_{\mathrm{HOMO}}^{\mathrm{opt}}$ and $E_{\mathrm{LUMO}}^{\mathrm{opt}}$ energies of the donor and acceptor materials it is possible to estimate the expected open-circuit voltage (V_{oc}) in the corresponding solar cells via the empirical relation $eV_{\mathrm{oc}} = |E_{\mathrm{HOMO}}^{\mathrm{opt}}(\mathrm{D}) - E_{\mathrm{LUMO}}^{\mathrm{pot}}(\mathrm{A})| - 0.18$ eV.[16] This leads to expected values of 1.22, 1.38 and 1.35 V for blends of P3HT with **PA**, **PB** and **PC**, respectively.

Solar cells. The polymers were applied in bulk heterojunction solar cells with P3HT as the donor material. The active layers were spin-coated from ODCB onto an indium tin oxide (ITO) covered glass substrate covered by a 50 nm film of PEDOT:PSS. LiF (1 nm) and Al (100 nm) were thermally evaporated as top electrode. A distinct photovoltaic effect has been observed for each of the three blends. We note that the use of Ca as top electrode gave very similar results. For each polymer the mixing ratio with P3HT and the layer thickness

were optimized for maximal performance. For each blend a 1:1 weight ratio was found to be optimal. Annealing was needed to improve the performance of the devices and especially to approach the expected open-circuit voltage. The effect of the annealing is shown in Figure 3.4 for the short-circuit current (J_{sc}), open-circuit voltage (V_{oc}), fill factor (FF) and power conversion efficiency (PCE) of P3HT:**PA** cells under simulated AM1.5G conditions (100 mW/cm^2). The influence of annealing on the photocurrent density was less strong than for polymer:polymer blends reported by Greenham et al.[37] where the short-circuit current improved by a factor of 10 upon annealing.

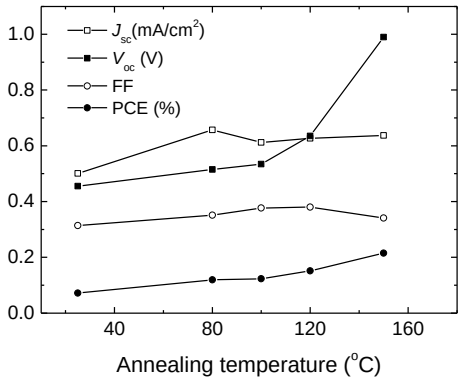

Figure 3.4: Effect of annealing on the solar cell characteristics of P3HT:**PA** devices.

Representative *J-V* curves for each blend after annealing are shown in Figure 3.5 and the characteristics of the best devices are summarized in Table 3.2. After annealing V_{oc} is ~1 V (for P3HT:**PA** device) and ~1.15 V for P3HT:**PB** and P3HT:**PC**. These values are about 0.2 V less than expected based on the analysis presented in the previous section. Also FF is low, especially for P3HT:**PB** and P3HT:**PC**. For P3HT:**PA**, FF is somewhat higher and in the range of most polymer:polymer solar cells. A low FF in polymer-polymer solar cells is often associated with trap-limited electron tansport[24] but can also result from a sluggish separation and resultant recombination of geminate photogenerated electron–hole pairs.[38] With short-circuit currents on the order of J_{sc} = 0.6–0.7 mA/cm^2, the power conversion efficiency of the cells is low (PCE = 0.18–0.23%) (Table 3.2).

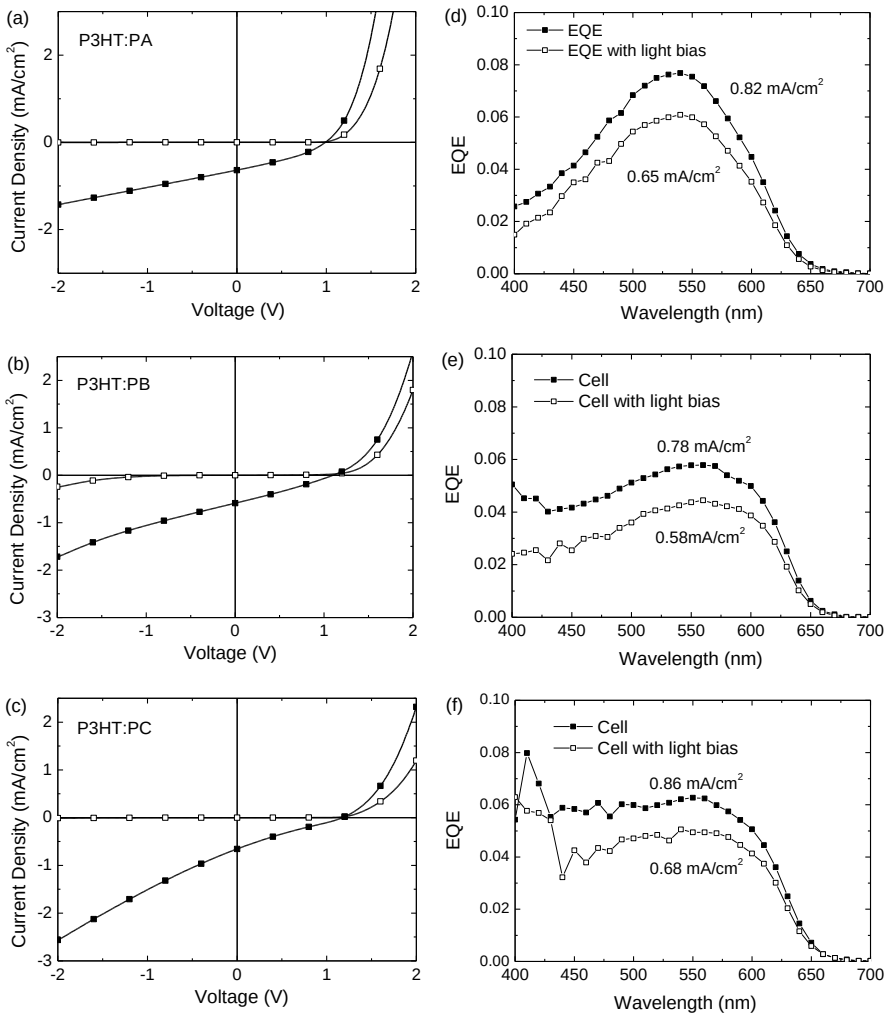

Figure 3.5: (a, b, c) Representative *J-V* curves for P3HT:**PA**, P3HT:**PB** and P3HT:**PC** solar cells in the dark (open markers) and under simulated AM1.5G conditions (closed markers). (d, e, f) EQE spectra of P3HT:**PA**, P3HT:**PB**, P3HT:**PC** solar cells under low monochromatic light intensity and with 1 Sun equivalent light bias illumination. The numbers in the panels represent the J_{sc} that is obtained with convoluting the EQE with the solar AM1.5G spectrum.

Table 3.2: Characteristics of P3HT:acceptor-polymer devices under 100 mW/cm^2 white light illumination.

	Ratio	*d* (nm)	J_{sc} (mA/cm^2)	V_{oc} (V)	FF	PCE (%)
P3HT:**PA**	1:1	40	0.65	0.99	0.35	0.23
P3HT:**PB**	1:1	35	0.58	1.10	0.28	0.18
P3HT:**PC**	1:1	35	0.68	1.15	0.23	0.18

J_{sc} and FF are obviously limiting the performance and it is important to investigate the reasons why. Several processes may cause a low photocurrent: (a) an inefficient photoinduced electron transfer or absence of long-lived free charges in the active layer; (b) an inadequate morphology for charge separation or transport. These issues are addressed in the following sections. For each of the blends there is a considerable increase of the photocurrent at reverse bias. This demonstrates that the separation or collection of photogenerated charge carriers is field dependent.

Another factor that may limit the device performance is the moderate molecular weight of the acceptor polymers. For polymer:fullerene mixtures an increase in polymer molecular weight often gives an increased solar cell performance,[39] but for polymer:polymer blends the effect of polymer molecular weight has been found to be less evident.[40]

Photophysical processes in the blends. The electron transfer efficiency has been investigated by measuring the fluorescence quenching on a blend of P3HT with 50% of acceptor-polymer after thermal treatment. As shown in Figure 3.6, the experiment reveals that the luminescence of polymers **PA**, **PB** and **PC** is quenched by ~70%. Even though quenching is not complete, the experiment reveals considerable interaction between the two components in the blend.

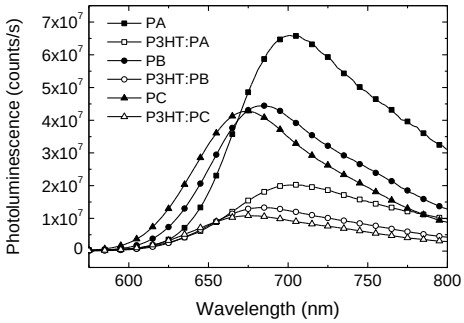

Figure 3.6: Photoluminescence spectra recorded at room temperature of **PA**, **PB** and **PC** as pristine films and in blends with P3HT.

In addition, we performed photoinduced absorption (PIA) spectroscopy to investigate charge formation and recombination in these blends. Upon photoexcitation of the blends an electron is expected to be transferred from P3HT to the acceptor polymer and the resulting charge separated state can often be observed spectroscopically. Figure 3.7 shows the PIA spectra of the pristine polymers and the photoactive blends. Pure P3HT shows a PIA signal at 1.08 and 1.25 eV and bleaching signals at 1.97 and 2.13 eV. The PIA band is attributed to the $T_n \leftarrow T_1$ absorption of the P3HT triplet state.[41,42] In pristine P3HT a weak PIA signal is observed at ~0.5 eV that is characteristic for the low-energy excitation of P3HT radical cations and emphasizes that excitation of P3HT itself leads to only few long lived charges.[43] The PIA spectra of **PA** and the P3HT:**PA** blend are shown in Figure 3.7b, together with the signal of pure P3HT. The PIA spectrum of **PA** shows a single band at 1.20 eV, which we attribute to a $T_n \leftarrow T_1$ transition. The PIA spectrum of the P3HT:**PA** blend differs significantly from the spectra of pristine P3HT and **PA**. The most apparent difference is the higher intensity with a maximum at 1.22 eV. Further we note a weak, but distinct absorption between 0.4 and 0.5 eV. Similar characteristics are seen in Figure 3.7c and 3.7d. The blend PIA spectra can be understood by considering that a photoinduced

electron transfer reaction between the two components forms a charge-transfer state, which subsequently recombines to the triplet excited state on the donor or acceptor material (CT $\rightarrow$ T_1). Indeed, the PIA spectra of the blends appear to be a superposition of the $T_n \leftarrow T_1$ PIA signals of the two components, but at considerably higher signal intensity. Charge recombination to the triplet (CRT, Figure 3.8) has recently been identified for a number of donor/acceptor blends and may represent a significant loss mechanism by reducing the photocurrent.[21,23,44-48]

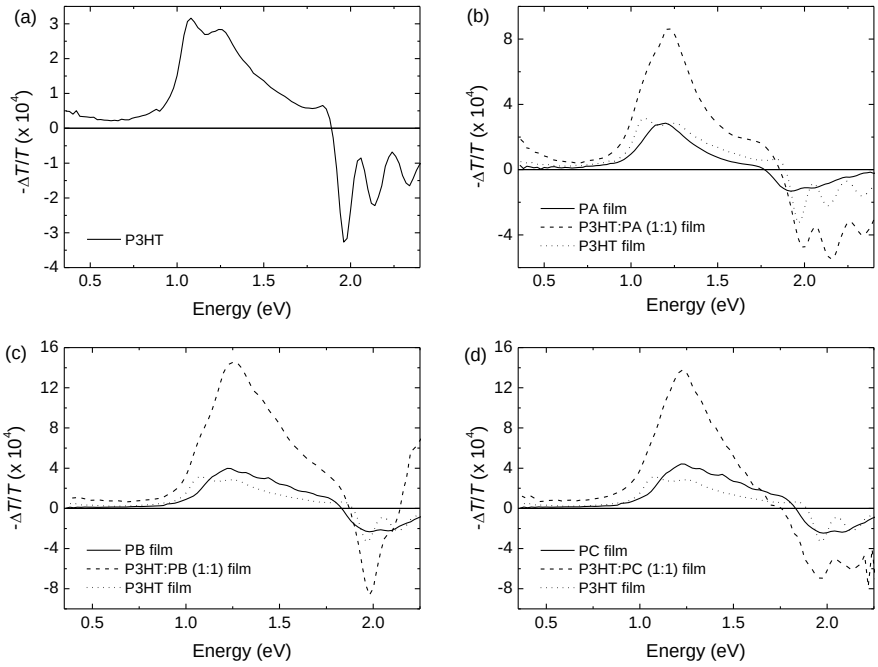

Figure 3.7: PIA spectra recorded at 80 K of (a) P3HT. (b) **PA** and P3HT:**PA**. (c) **PB** and P3HT:**PB**. (d) **PC** and P3HT:**PC**.

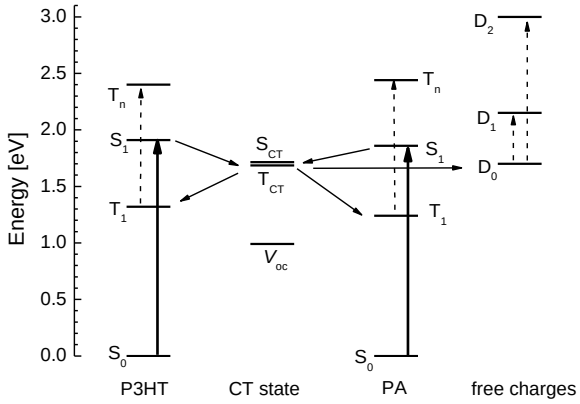

Figure 3.8: State diagram for the P3HT:**PA** blend. Dashed line arrows indicate photoinduced absorptions. Solid line arrows represent photoexcitations and following spontaneous relaxation. The charge recombination to the triplet state (CRT) is shown. Very similar diagrams apply to P3HT:**PB** and P3HT:**PC** blends.

Further support for this mechanism comes from considering the triplet energies E_T of the components in thin films. To estimate these energies we used the onsets of ground state absorption (E_g^{sol} in Table 3.1) to estimate their triplet energies in solution via the relation $E_T^{sol} = E_g^{sol} - 0.70(\pm 0.1)\,eV$ that has been proposed by Köhler and Beljonne,[49] and then correcting for possible changes when going form solution to film $E_T = E_T^{sol}(E_g / E_g^{sol})$.[16] This leads to E_T energies of 1.24-1.36 eV (Table 3.1) that are significantly below the energies of the CT states (1.70-1.85 eV) and confirm that charge recombination to the triplet state is energetically favoured (Figure 3.8). We further note that following this procedure to estimate the T_1 energy, the T_1 state of P3HT is almost degenerate with that of **PA, PB** and **PC** (Table 3.1), explaining why the PIA spectra of the blends show superposition of the $T_n \leftarrow T_1$ PIA signals of the two components.

The CRT process is a loss mechanism in the efficiency of solar cells and can rationalize in part the low photocurrent in the devices. Since E_{CT} is only slightly less that E_g in these blends, photoinduced electron-transfer is only slightly exergonic, consistent with the PL quenching experiment showing a non-complete quenching of the fluorescence of P3HT.

Morphology of the blends. The morphology of bulk heterojunction solar cells is generally crucial for the power conversion efficiency. Small acceptor-donor domains and associated intimate mixing are desirable for exciton quenching, while larger domains and percolating pathways improve charge separation and their transport to the electrodes. It is thus important to control morphology of the active layer and make sure that it does not limit the performance. To assess the morphology of the layers AFM has been performed on the layers used in the devices. As shown in Figure 3.9, the height images reveal relatively smooth films. For P3HT:**PA** the height differences (15 nm) are larger than for the P3HT:**PB** and P3HT:**PC** films (5 nm). The corresponding phase images show contrast that can be associated with two different materials phase segregated at the surface. We note that the phase contrast does not necessarily originate from pure donor and pure acceptor phases, but that each will contain some quantity of the other component. In all the three examples, the bright domains are predominant in the phase image. The size of the domains as inferred from the images varies from 10-100 nm and seems to be somewhat smaller for the P3HT:**PA** blend than for P3HT:**PB** and P3HT:**PC**. Since this largest distance is longer than the exciton diffusion length of typically less than 10 nm, the surface topology is consistent with the incomplete (~70%) quenching of the photoluminescence and this might explain (in part) the limited short-circuit current.

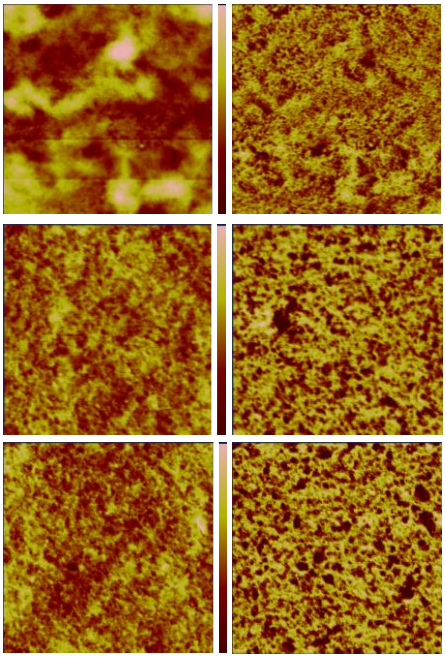

Figure 3.9: Height (left) and phase (right) AFM images of the surface of the P3HT:acceptor polymer blends (1 μm × 1 μm). Top: P3HT:**PA**, vertical scale 15 nm and 25°. Middle: P3HT:**PB** vertical scale 5 nm and 30°. Bottom P3HT:**PC**, vertical scale 5 nm and 25°.

Mobility measurements. Charge carrier mobility of the materials is a key factor for the performance of polymer solar cells. The charge carrier mobility that is measured not only depends on the material, but also on the experimental conditions such as charge carrier density and device layout. For a meaningful comparison, it is desirable to measure the mobility under experimental conditions that approach those of an operational solar cell. Because the hole mobility of P3HT in a solar cell configuration is known (μ_h = ~ 2×10^{-8} m^2/Vs),[50] we are interested in measuring the electron mobility (μ_e) of the acceptor materials. For that, the active layer was incorporated in an electron-only device where hole injection is blocked by applying low work function electrodes. In the electron-only devices we use LiF/Al as top and ZnO as bottom electrode; both provide an energy barrier of ~1 eV for hole injection into P3HT.

In Figure 3.10, the experimental dark current density of the electron-only devices for both the pristine acceptor materials and the polymer blends are shown. The applied voltage (V_{appl}) was corrected for both the built-in voltage (V_{BI}) and the voltage drop (V_{RS}) that arise respectively from the difference in work-function between the two electrodes and from the substrate series' resistance. The dark current density scales quadratically with the corrected voltage $V = V_{appl} - V_{BI} - V_{RS}$. This behaviour is characteristic of space charge limited current (SCLC) transport through the layer. The SCLC current can be approximated by:[51]

$$J_e = \frac{9}{8}\varepsilon_0\varepsilon_r\mu_e\frac{V^2}{L^3}\exp\left(0.891\gamma_e\sqrt{\frac{V}{L}}\right) \quad (3.4)$$

where J_e is the electron current density, μ_e the zero-field mobility of the electrons, γ_e the field activation factor, ε_0 the permittivity of free space, ε_r the relative permittivity of the material and L the thickness of the active layer. The experimental data (see Supplementary Material) were fitted using equation (3.4) and the results are shown by the solid line and are summarized in Table 3.3. The mobility of the pristine acceptor polymers is in the range of 10^{-11} m^2/Vs. Upon blending with P3HT, no improvement is observed. We note that the electron mobility value is 4 orders of magnitude lower than that of PCBM[10] and 3 less than the hole mobility of P3HT,[50] The large difference in hole and electron mobility and the low value of the latter are important factors that limit the solar cell performance.[52]

Table 3.3: Electron mobility of the pristine **PA**, **PB** and **PC** and their blend with P3HT.

Polymer	Pristine μ_e (m^2/Vs)	Blend with P3HT μ_e (m^2/Vs)
PA	5×10^{-11}	2×10^{-11}
PB	3.5×10^{-11}	2×10^{-11}
PC	3×10^{-11}	1.5×10^{-11}

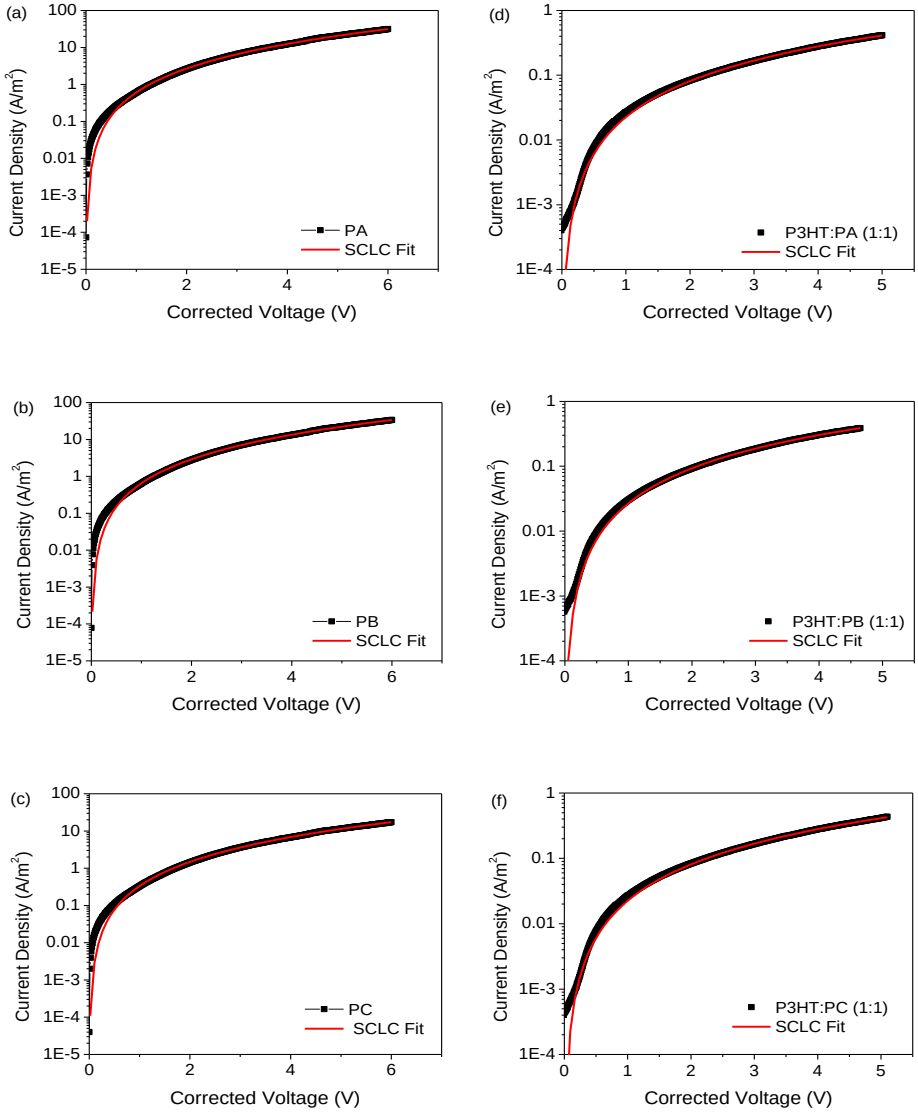

Figure 3.10: Dark current density characteristics of the electron-only device for each pristine acceptor material with a thickness of around 130 nm (left) and for each blend with a thickness of around 280 nm (right).

3.3 Conclusion

The synthesis of three copolymers composed of a 1:1 ratio electron-rich:electron-deficient units, has lead to materials that can be used as acceptor materials in bulk heterojunction solar cells together with P3HT as the donor material. A photovoltaic effect has been observed with the three polymers, leading to devices with high open-circuit voltages (0.99-1.15 V), but with current densities and fill factors that limit the efficiency to ~0.2%. The low fill factors and photocurrents are most likely related to a field-activated dissociation of photogenerated electron-hole pairs at the interface. In accordance, near steady-state photoinduced absorption revealed that charge recombination from the charge transfer state at the interfaces into the triplet excited state of the components occurs and that the yield of long lived charges is small. This mechanism accounts for the low photocurrent, especially when dissociation of the charge transfer state at the D:A interface into free charge carriers is hampered by low charge carrier mobilities.[53] The limited formation of free charge carriers may further be enhanced by the relatively small energy difference between the optical band gap energy of the polymers and that of the interface charge transfer state of (0.06-0.16 eV, Table 3.1) and the fact that phase-separation in these blends seems to occur on a scale larger than the exciton diffusion length. From this work it is clear that the design of acceptor polymers for solar cell applications that are compatible with P3HT as a donor remains a challenge. Future improvements can possibly be found by designing materials with lower HOMO and LUMO energies, higher electron mobility and improved miscibility with the donor polymer.

3.4 Experimental section

Materials and methods. Polymerization reactions were conducted under an argon atmosphere. Commercial chemicals were used as received. 3-Dodecylthiophene and 2,1,3-benzothiadiazole-4,7-bis(boronic acid pinacol ester) were obtained from Sigma-Aldrich. The P3HT used in this study had M_n = 30 kg/mol with a polydispersity of 2.1 and regioregularity higher than 98.5%. ^{1}H NMR and ^{13}C NMR spectra were recorded at 400 MHz on a VARIAN mercury spectrometer with $CDCl_3$ as the solvent and tetramethylsilane (TMS) as the internal standard. The peaks are given in ppm, relative to TMS (0 ppm). Molecular weights were determined with G**PC** on a Shimadzu LC-10AD using a Polymer Laboratories Resipore column (length 300 mm, diameter 7.5 mm), a Shimadzu SPD-M20A photodiode array detector from 250-700 nm and ODCB as the eluent with a flow rate of 1 mL/min. (T = 348 K). Polystyrene standards were used.

UV-vis-nearIR optical absorption spectra were recorded on a Perkin-Elmer Lambda 900 spectrophotometer. Cyclic voltammetry was conducted under an inert atmosphere with a scan rate of 0.1 V/s, using 1 M tetrabutylammonium hexafluorophosphate in ODCB as the electrolyte. The working electrode was a platinum disk and the counter electrode was a silver rod electrode. A silver wire coated with silver chloride (Ag/AgCl) was used as a quasi reference electrode in combination with Fc/Fc^+ as an internal standard. Atomic force microscopy (AFM) was measured using a Veeco MultiMode with a Nanoscope III controller, in tapping mode. The used probes were PPP-NCH-50 from Nanosensors.

Photovoltaic devices were made by spin coating poly(ethylenedioxythiophene): poly(styrene sulfonate) (PEDOT:PSS) (Clevios P, VP Al4083) onto pre-cleaned, patterned indium tin oxide (ITO) substrates (14 Ω per square) (Naranjo Substrates). The top electrode, consisting of LiF (1 nm) and Al (100 nm), was deposited by vacuum evaporation at ~3×10^{-7} mbar. The active area of the cells was 0.091 cm^2. *J-V* characteristics were measured under ~100 mW/cm^2 white light from a tungsten-halogen lamp filtered by a Schott GG385 UV filter and a Hoya LB120 daylight filter, using a Keithley 2400 source meter. Short-circuit currents under AM1.5G conditions were estimated from the spectral response and convolution with the solar spectrum. The spectral response was measured under simulated 1 Sun operation conditions using bias light from a 532 nm solid state laser (Edmund Optics). Monochromatic light from a 50 W tungsten halogen lamp (Philips focusline) in combination with monochromator (Oriel, Cornerstone 130) was modulated

with a mechanical chopper. The response was recorded as the voltage over a 50 Ω resistance, using a lock-in amplifier (Stanford Research Systems SR830). A calibrated Si cell was used as reference. The device was kept behind a quartz window in a nitrogen filled container. The thickness of the active layers in the photovoltaic devices was measured on a Veeco Dektak150 profilometer.

Electron-only devices were fabricated by replacing the PEDOT:PSS layer by a ZnO layer. A 10 mg/mL solution of ZnO nanoparticles in acetone was spin-coated at 1500 rpm to obtain a 20 nm closed-layer. *J-V* characteristics were measured in the dark using a Keithley 2400 source meter.

Photoinduced absorption (PIA) spectra were recorded by exciting with a mechanically modulated Ar-ion (496.5 nm) pump beam and monitoring the resulting change in transmission of a tungsten-halogen probe light through the sample (ΔT) with a phase-sensitive lock-in amplifier after dispersion by a grating monochromator and detection, using Si, InGaAs and cooled InSb detectors. The pump power incident on the sample was typically 25 mW with a beam diameter of 2 mm. The PIA ($\Delta T/T$) was corrected for the photoluminescence, which was recorded in a separate experiment. Photoinduced absorption spectra and photoluminescence spectra were recorded with the pump beam in a direction almost parallel to the direction of the probe beam. Temperature (80 K) of the samples was controlled by using an Oxford Optistat continuous flow cryostat.

4,7-Dibromo-2-(2'-ethylhexyl)benzotriazole (3). 4,7-Dibromo-1,2,3-benzotriazole[32] (1.2 g, 4.3 mmol), potassium tert-butoxide (0.54 g, 4.8 mmol) and 2-ethylhexyl-1-iodide (1.43 g, 5.9 mmol) were dissolved in methanol (15 mL). The reaction mixture was refluxed for 12 h and monitored by TLC. After removal of the solvent by evaporation, the residue was dissolved in $CHCl_3$ and extracted with water. The organic layer was dried over Na_2SO_4 and the solvent was evaporated under reduced pressure. The residue was subjected to column chromatography (3:2 chloroform:hexane; R_f, 0.29) to obtain **3** as a colorless oil (3.7 g, 31%). ^{1}H (400 MHz, $CDCl_3$, δ): 7.43 (s, 2H), 4.68 (d, J = 7.30 Hz, 2H), 2.30 (m, 1H), 1.33−1.25 (m, 9H), 0.91 (t, J = 7.25 Hz, 3H), 0.86 (m, 3H). ^{13}C NMR (400 MHz, $CDCl_3$, δ): 143.6, 129.4, 109.9, 60.8, 40.2, 30.2, 28.2, 23.7, 22.8, 13.9, 10.3. MALDI-TOF MS (*MW* = 389.13): m/z = 388.99 amu [M^+].

4,7-Bis(4-dodecylthien-2-yl)-2-(2'-ethylhexyl)benzotriazole (4). 4-Dodecyl-2-tributyl stannylthiophene (**2**)[31] (1.28 g, 2.36 mmol, 2.3 eq), dibromo compound **3** (0.40 g, 1.028 mmol) and $Pd(PPh_3)_4$ (10.6 mg, 9.2×10^{-3} mmol) were dissolved in dry and degassed toluene. The mixture was heated at 85 °C for 60 h in the dark. Water was added, the organic phase was separated and the aqueous layer was extracted with chloroform. The combined organic layers were washed with brine and subsequently dried over Na_2SO_4. After removal of the solvent under reduced pressure, the residue was purified by column chromatography on silica gel with petroleum ether/dichloromethane (6:1) as eluent to afford **4** as a yellow solid in a yield of 47% (0.532 g). ^{1}H (400 MHz, $CDCl_3$) δ: 7.92 (s, 2H), 7.58 (s, 2H), 6.96 (s, 2H), 4.77 (d, J = 6.9 Hz, 2H), 2.68 (t, J = 7.28 Hz, 4H), 2.26 (m, 1H), 1.71 (m, 4H), 1.45−1.26 (m, 44H), 1.02 (t, J = 7.46 Hz, 3H), 0.89 (m, 9H). ^{13}C NMR (400 MHz, $CDCl_3$) δ: 144.3, 141.9, 139.6, 128.3, 123.6, 122.3, 120.2, 59.4, 40.4, 29.7, 29.6, 29.4, 28.5, 26.8, 22.9, 22.7, 17.3, 14.1, 10.6. MALDI-TOF MS (*MW*= 732.22 g/mol): *m*/*z* = 731.48 amu [M^+].

4,7-Bis(5-bromo-4-dodecylthien-2-yl)-2-(2'-ethylhexyl)benzotriazole (5). *N*-bromo succinimide (NBS) (0.116 g, 0.652 mmol, 2.05 eq.) was added portionwise to a solution of **4** (0.233 g, 0.318 mmol) in DMF (15 mL). After complete addition, the mixture was stirred for 5 h at 45 °C and then CH_2Cl_2 (20 mL) was added. The solution was washed with brine and subsequently dried over Na_2SO_4. After removal of the solvent under reduced pressure, the residue was purified by column chromatography on silica gel with heptane as eluent to afford **5** as a red solid in a yield of 80% (0.226 g). ^{1}H (400 MHz, $CDCl_3$) δ: 7.72 (s, 2H), 7.46 (s, 2H), 4.75 (d, J = 5.4 Hz, 2H), 2.62 (t, J = 7.18 Hz, 4H), 2.20 (m, 1H), 1.65 (m, 4H), 1.38−1.26 (m, 44H), 1.02 (t, J = 7.46 Hz, 3H), 0.90 (m, 9H). ^{13}C NMR (400 MHz, $CDCl_3$) δ: 143.0, 141.6, 139.2, 127.5, 122.9, 121.9, 110.0, 59.4, 40.4, 29.7, 29.5, 28.5, 22.9, 22.7, 14.1, 10.6. MALDI-TOF MS (*MW* = 890.01 g/mol): *m*/*z* = 889.32 amu [M^+].

5,8-Bis(4-dodecylthien-2-yl)-2,3-bis(2'-ethylhexyl)quinoxaline (7). 4-Dodecyl-2-tributyl stannylthiophene (**2**)[31] (1.45 g, 2.69 mmol, 2.3 eq), dibromo compound **6**[33] (0.6 g, 1.17 mmol) and $Pd(PPh_3)_4$ (10.6 mg, 9.2×10^{-3} mmol) were dissolved in dry and degassed toluene. The mixture was heated at 85 °C for 60 h under dark. Water was added, the organic phase was separated and the aqueous layer was extracted with chloroform. The combined organic layers were washed with brine and subsequently dried over Na_2SO_4. After removal of the solvent under reduced pressure, the residue was purified by column

chromatography on silica gel with petroleum ether/dichloromethane (6:1) as eluent to afford **7** as an orange solid in a yield of 62% (0.620 g). ^{1}H (400 MHz, $CDCl_3$) δ: 8.01 (s, 2H), 7.71 (s, 2H), 7.06 (s, 2H), 3.01 (d, J = 7.20 Hz, 4H), 2.65 (t, J = 7.80 Hz, 4H), 2.30 (m, 2H), 1.68 (m, 4H), 1.39−1.25 (m, 46H), 0.93 (t, J = 7.0 Hz, 6H), 0.86 (m, 18H). ^{13}C NMR (400 MHz, $CDCl_3$) δ: 155.4, 142.7, 138.8, 137.2, 130.8, 125.8, 123.1, 39.3, 38.4, 29.7, 29.5, 28.9, 25.9, 23.1, 22.7, 14.1, 10.9. MALDI-TOF MS (*MW* = 855.46 g/mol): *m*/*z* = 854.64 amu [M^+].

5,8-Bis(5-bromo-4-dodecylthien-2-yl)-2,3-bis(2'-ethylhexyl)quinoxaline (8). *N*-bromosuccinimide (NBS) (0.091 g, 0.511 mmol, 2.05 eq.) was added portionwise to a solution of **7** (0.213 g, 0.249 mmol) in DMF (15 mL). After complete addition, the mixture was stirred for 5 h at 45 °C and then CH_2Cl_2 (20 mL) was added. The solution was washed with brine and subsequently dried over Na_2SO_4. After removal of the solvent under reduced pressure, the residue was purified by column chromatography on silica gel with heptane as eluent to afford **8** as a red solid in a yield of 85% (0.215 g). ^{1}H (400 MHz, $CDCl_3$) δ: 7.98 (s, 2H), 7.48 (s, 2H), 3.02 (d, J = 6.5 Hz, 4H), 2.60 (t, J = 7.30 Hz, 4H), 2.30 (m, 2H), 1.65 (m, 4H), 1.42−1.27 (m, 46H), 0.89 (t, J = 7.4 Hz, 6H), 0.87 (m, 18H). ^{13}C NMR (400 MHz, $CDCl_3$) δ: 155.4, 142.7, 138.8, 137.2, 130.8, 125.8, 123.1, 39.3, 38.4, 29.7, 29.5, 28.9, 25.9, 23.1, 22.7, 14.1, 10.9. MALDI-TOF MS (*MW* = 1013.25 g/mol): *m*/*z* = 1012.47 amu [M^+].

Polymer PA. To a solution of **9** (150 mg, 0.44 mmol) and **1** (254 mg, 0.44 mmol) in degassed toluene (6 mL) were added 3 droplets of Aliquat 336 and $Pd(PPh_3)_4$. The solution was stirred and K_2CO_3 (3 mL, 2 M in water) was added. The two phase system was heated at reflux for 80 h. Methanol (100 mL) was then added, the precipitate was collected and fractionated with a Soxhlet extractor to afford gave 100 mg of a deep purple solid (62 %). GPC(PS): M_n = 4.5 kg/mol, PDI = 1.5. ^{1}H (400 MHz, $CDCl_3$) δ: 8.18 (br, 1H), 7.97 (br, 1H), 7.76 (br, 1H), 2.79 (br, 2H), 1.75 (br, 2H), 1.24 (br, 18H), 0.86 (br, 3H).

Polymer PB. Monomers **9** (58.9 mg, 0.17 mmol) and **5** (155 mg, 0.17 mmol) were reacted according to the procedure described above and gave 80 mg of a deep red solid (55 %). GPC(PS): M_n = 9.7 kg/mol, PDI = 1.8. ^{1}H (400 MHz, $CDCl_3$) δ: 8.19 (br, 2H), 7.94 (br, 2H), 7.78 (br, 2H), 3.05 (br, 4H), 2.80 (br, 4H), 2.40 (br, 2H), 1.77 (br, 4H), 1.30 (m, 52H), 0.88 (m, 12H), 0.75 (t, J = 7.18 Hz, 6H).

Polymer PC. Monomers **9** (38.8 mg, 0.115 mmol) and **8** (113 mg, 0.115 mmol) were reacted according to the procedure described above and gave 70 mg of a deep red solid (60 %). GPC(PS): M_n = 9.6 kg/mol, PDI = 2.0. ^{1}H (400 MHz, $CDCl_3$) δ: 8.16 (br, 2H), 2.78 (br, 2H), 7.72 (br, 2H), 4.82 (br, 2H), 2.80 (br, 4H), 2.30 (m, 1H), 1.76 (br, 4H), 1.35 (m, 44H), 1.04 (t, J = 7.42, 9H).

References

(1) Brabec, C. J.; Durrant, J. R. *MRS Bull.* **2008**, *33*, 670.
(2) Janssen, R. A. J.; Hummelen, J. C.; Sariciftci, N. S. *MRS Bull.* **2005**, *30*, 33.
(3) Thompson, B. C. ; Fréchet, J. M. J. *Angew. Chem., Int. Ed.* **2008**, *47*, 58.
(4) Dennler, G.; Scharber, M. C.; Brabec, C. J. *Adv. Mater.* **2009**, *21*, 1323.
(5) Boudreault, P. L. T.; Najari, A.; Leclerc, M. *Chem. Mater*., **2011**, *23*, 456.
(6) Liang, Y. ; Yu, L. *Acc. Chem. Res*. **2010**, *43*, 1227.
(7) Chen, J.; Cao, Y. *Acc. Chem. Res*. **2010**, *43*, 1709.
(8) Yu, G.; Gao, J.; Hummelen, J. C.; Wudl, F.; Heeger, A. J. *Science* **1995**, *270*, 1789.
(9) Wienk, M. M.; Kroon, J. M.; Verhees, W. J. H.; J. Knol, Hummelen, J. C.; van Hal, P. A.; Janssen, R. A. J. *Angew. Chem., Int. Ed.* **2003**, *42*, 3371.
(10) Mihailetchi, V. D.; van Duren, J. K. J.; Blom, P. W. M.; Hummelen, J. C.; Janssen, R. A. J.; Kroon, J. M.; Rispens, M. T.; Verhees, W. J. H.; Wienk, M. M. *Adv. Funct. Mater*. **2003**, *13*, 43.
(11) Yang, X.; van Duren, J. K. J.; Rispens, M. T.; Hummelen, J. C.; Janssen, R. A. J.; Michels, M. A. J.; Loos, J. *Adv. Mater.* **2004**, *16*, 802.
(12) Brunetti, F. G.; Gong, X.; Tong, M.; Heeger, A. J.; Wudl, F. *Angew. Chem., Int. Ed.* **2010**, *49*, 532.
(13) Dittmer, J. J.; Marseglia, E. A.; Friend, R. H. *Adv. Mater*. **2000**, *12*, 1270.
(14) Schmidt-Mende, L.; Fechtenkotter, A.; Müllen, K.; Moons, E.; Friend, R. H.; MacKenzie, J. D. *Science* **2001**, *293*, 1119.
(15) McNeill, C. R.; Greenham, N. C. *Adv. Mater.* **2009**, *21*, 3840.
(16) Veldman, D.; Meskers, S. C. J.; Janssen, R. A. J. *Adv. Funct. Mater.* **2009**, *19*, 1939.
(17) Yu, G.; Heeger, A. J. *J. Appl. Phys.* **1995**, *78*, 4510.
(18) Halls, J. J. M.; Walsh, C. A.; Greenham, N. C.; Marseglia, E. A.; Friend, R. H.; Moratti, S. C.; ; Holmes, A. B. *Nature* **1995**, *376*, 498.
(19) Veenstra, S. C.; Verhees, W. J. H.; Kroon, J. M.; Koetse, M. M.; Sweelssen, J.; Bastiaansen, J. J. A. M.; Schoo, H. F. M.; Yang, X.; Alexeev, A.; Loos, J.; Schubert, U. S.; Wienk, M. M. *Chem. Mater*. **2004**, 16, 2503.
(20) Kietzke, T.; Hörhold, H.-H.; Neher. D. *Chem. Mater.* **2005,** *17*, 6532.
(21) Offermans, T.; van Hal, P. A.; Meskers, S. C. J.; Koetse, M. M.; Janssen, R. A. J. *Phys. Rev. B* **2005**, *72*, 045213.
(22) Koetse, M. M.; Sweelssen, J.; Hoekerd, K.; Schoo, H. F. M.; Veenstra, S. C.; Kroon, J. M.; Yang, X.; Loos, J. *Appl. Phys. Lett.* **2006**, *88*, 083504.
(23) Veldman, D.; Offermans, T.; Sweelssen, J.; Koetse, M. M.; Meskers, S. C. J.; Janssen, R. A. J. *Thin Solid Films* **2006**, *511–512*, 333.
(24) Mandoc, M. M.; Veurman, W.; Koster, L. J. A.; Koetse, M. M.; Sweelssen, J.; de Boer, B.; Blom, P. W. M. *J. Appl. Phys.* **2007**, *101*, 104512.
(25) Yin, C.; Kietzke, T.; Neher, D.; Hörhold, H.-H. *Appl. Phys. Lett.* **2007**, *90*, 092117.
(26) Neuteboom, E. E.; Meskers, S. C. J.; van Hal, P. A.; van Duren, J. K. J.; Meijer, E. W.; Janssen, R. A. J.; Dupin, H.; Pourtois, G.; Cornil, J.; Lazzaroni, R.; Brédas, J.-L.; Beljonne, D. *J. Am. Chem. Soc.* **2003**, *125*, 8625.
(27) Zhan, X.; Tan, Z.; Domercq, B.; An, Z.; Zhang, X.; Barlow, S.; Li, Y.; Zhu, D.; Kippelen, B.; Marder, S. R. *J. Am. Chem. Soc***. 2007**, 129, 7246.
(28) Hou, J.; Zhang, S.; Chen, T. L.; Yang, Y. *Chem. Commun.* **2008**, 6034.
(29) Huo, L.; Zhou, Y.; Li, Y. *Macromol. Rapid Commun.* **2008**, *29*, 1444.
(30) Bäuerle, P.; Pfau, F.; Schlupp, H.; Würthner, F.; Gaudl, K. U.; Balparda Caro, M.; Fischer, P. *J. Chem. Soc., Perkin Trans 2* **1993**, 489.
(31) Zoombelt, A. P.; Gilot, J.; Wienk, M. M.; Janssen, R. A. J. *Chem. Mater.* **2009**, *21*, 1663.
(32) Balan, A.; Gunbas, G.; Durmus, A.; Toppare L., *Chem. Mater.* **2008**, *20*, 7510–7513

(33) Chen, C.-H.; Hsieh, C.-H.; Dubosc, M.; Cheng, Y.-J.; Hsu, C.-S. *Macromolecules*, **2010**, 43, 697.
(34) Using a potential value of 4.6±0.2 eV for NHE versus vacuum (ref. [35]) and 0.63 eV (ref. [36]) for Fc/Fc+ versus NHE.
(35) Bockris, J. O. M.; Khan, S. U. M. *Surface Electrochemistry. A Molecular Level Approach*, Kluwer Academic/Plenum Publishers, New York **1993**.
(36) Pavlishchuk, V. V.; Addison, A. W. *Inorg. Chim. Acta* **2000**, *298*, 97.
(37) McNeill, C. R.; Halls, J. J. M.; Wilson, R.; Whiting, G. L.; Berkebile, S.; Ramsey, M. G.; Friend, R. H.; Greenham, N. C. *Adv. Funct. Mater.* **2008**, *18*, 2309.
(38) Lenes, M.; Morana, M.; Brabec, C. J.; Blom, P. W. M. *Adv. Funct. Mater*. **2009**, *19*, 1106.
(39) Bijleveld, J. C.; Zoombelt, A. P.; Mathijssen, S. G. J.; Wienk, M. M.; Turbiez, M.; de Leeuw, D. M.; Janssen, R. A. J. *J. Am. Chem. Soc.* **2009**, *131*, 16616.
(40). Friedel, B.; McNeill, C. R.; Greenham, N. C. *Chem. Mater.* **2010**, *22*, 3389.
(41) See supporting information of ref [16].
(42) Christiaans, M. P. T.; Langeveld-Voss, B. M. W.; Janssen, R. A. J. *Synth. Met.* **1999**, *101*, 177.
(43) Sheng, C.-X.; Tong, M.; Singh, S.; Vardeny Z. V., *Phys. Rev. B* **2007**, *75*, 085206.
(44) Scharber, M. C.; Schultz, N. A.; Sariciftci, N. S.; Brabec, C. J. *Phys. Rev. B* **2003**, *67*, 085202.
(45) Ford, T. A.; Avilov, I.; Beljonne, D.; Greenham, N. C. *Phys. Rev. B* **2005**, *71*, 125212.
(46) Ohkita, H.; Cook, S.; Astuti, Y.; Duffy, W.; Heeney, M.; Tierney, S.; McCulloch, I.; Bradley, D. D. C.; Durrant, J. R. *Chem. Commun.* **2006**, 3939.
(47) Ford, T. A.; Ohkita, H.; Cook, S.; Durrant, J. R.; Greenham, N. C. *Chem. Phys. Lett.* **2008**, *454*, 237.
(48) Schuppel, R.; Schmidt, K.; Uhrich, C.; Schulze, K.; Wynands, D.; Brédas, J. L.; Brier, E.; Reinold, E.; Bu, H.-B.; Bäuerle, P.; Mannig, B.; Pfeiffer, M.; Leo, K. *Phys. Rev. B* **2008**, *77*, 085311.
(49) Kohler, A.; Beljonne, D. *Adv. Funct. Mater*. **2004**, *14*, 11.
(50) Mihailetchi, V. D.; Xie, H.; de Boer, B.; Koster, L. J. A.; Blom, P. W. M. *Adv. Funct. Mater*. **2006**, *16*, 699.
(51) Murgatroyd, P. N. *J. Phys. D* **1970**, *3*, 151.
(52) Mihailetchi, V. D.; Wildeman, J.; Blom, P. W. M. *Phys. Rev. Lett.* **2005**, *94*, 12660.
(53) Veldman, D.; Ipek, O.; Meskers, S. C. J.; Sweelssen, J.; Koetse, M. M.; Veenstra, S. C.; Kroon, J. M.; van Bavel, S. S.; Loos, J.; Janssen, R. A. J. *J. Am. Chem. Soc.* **2008**, *130*, 7721.

Chapter 4

Diketopyrrolopyrrole-based acceptor polymers for photovoltaic application

Abstract. Developing new acceptor materials as alternative to fullerene acceptors remains a challenge in the field of organic photovoltaics. We report on the synthesis and optoelectronic properties of three acceptor polymers bearing diketopyrrolopyrrole units in the main chain (**PA**, **PB** and **PC**). Their performance as acceptor material in bulk heterojunction solar cells using P3HT as the donor material has been tested. The solar cells show relatively high open-circuit voltages (≥ 0.9 V) but low fill factors and short-circuit current densities limit the photovoltaic device performance. Formation of free charge carriers and low electron mobility are identified as the major obstacles. In blends of P3HT with **PA** or **PB** charge formation is limited, while for the P3HT:**PC** blend photogenerated charges recombine into the **PC** triplet state before they can separate, unless assisted by a reverse electric field.

4.1 Introduction

In the last decade, materials research in the field of polymer solar cells has mainly focused on the developing new electron donor polymers.[1-6] The highest published efficiency has reached 7.4% for blends of a conjugated polymer as electron donor with a fullerene derivative ([6,6]-phenyl C_{71}-butyric acid methyl ester) as electron acceptor.[7,8] In these systems, the light is mainly absorbed by the polymer and less by the fullerene. A promising alternative for organic solar cells would then be to use a blend of two π-conjugated polymers that both contribute significantly to the absorption of light. In such a blend the optical properties of the two materials can be tuned in order to absorb complementary parts of the solar spectrum and efficiently collect photons. While this idea has existed from the start of polymer solar cell research, progress in terms of efficiency has been limited.[9-11]

Organic and polymer solar cells operate by creating excitons after absorbing a photon in one of the materials. These excitons have to dissociate at the interface between the electron donor and electron acceptor materials to form charges. The free energy for exciton dissociation is given by the difference in exciton energy, or optical gap (E_g) and the energy of the charge transfer (CT) state at the interface (E_{CT}). These energies are related to the HOMO and LUMO levels of the two semiconductors and it has been established experimentally that –as a rule of thumb– the offset of the energies of the two HOMO *and* the two LUMO levels should *both* be at least ~0.35 eV to ensure electron transfer from donor to acceptor (Figure 4.1).[12-14] The formation of the charge separated state is –in first approximation– independent of whether the donor or acceptor is in the excited state.

In this work we consider poly(3-hexylthiophene) (P3HT) as the donor. P3HT is known as an efficient p-type polymer[15,16] characterized by a LUMO level at –3.15 eV and a HOMO level at –5.05 eV.[17] The complementary acceptor polymer should therefore have its LUMO level below –3.5 eV and its HOMO level below –5.4 eV to create the offsets of >0.35 eV with the corresponding levels of P3HT that ensure efficient charge formation. In addition to energy level requirements, a successful acceptor polymer should also have good electron mobility. In recent years, a number of polymers based on diketopyrrolopyrrole (DPP) units have been developed that display low LUMO energy levels, high extinction coefficients and high electron mobilities in field-effect transistors.[18-20] It is thus of interest to explore these DPP-based polymers for use as acceptor material in polymer:polymer blends for solar cells. In this chapter we describe the synthesis of three DPP-based polymers and their acceptor properties (Scheme 4.1). The new polymers were tested in

bulk-heterojunctions with P3HT. Their electron mobility was measured and the photophysical and morphological properties of the photoactive layers have been investigated in detail. To rationalize the results and device performance, we focus on the role and influence of the interfacial charge transfer state.

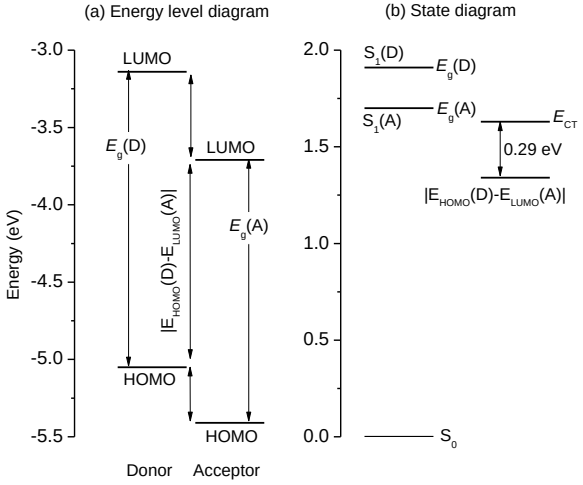

Figure 4.1: (a) Orbital energy level diagram and (b) corresponding state diagram for the donor and acceptor energy levels in an organic solar cell. The diagram pertains to the P3HT:**PC** blend, but analogous diagrams apply for P3HT:**PA** and P3HT:**PB** as well.

4.2 Results and discussion

Synthesis. In Scheme 4.1 the synthesis of polymers **PA**, **PB** and **PC** is described. The polymerization involves a Suzuki cross-coupling using a mixture of Pd and PPh_3 as catalyst, aqueous K_2CO_3 as base and Aliquat 336 as phase transfer agent in toluene. All three polymers were obtained in ~ 60% yield. For **PA** and **PB**, 3,6-bis(4-bromophenyl)-2,5-bis(2'-hexyldecyl)pyrrolo[3,4-c]pyrrole-1,4(*2H*,*5H*)-dione was polymerized with commercially available 4,7-bis(4,4,5,5-tetramethyl-1,3,2-dioxaborolan-2-yl)-2,1,3-benzothiadiazole or 2,5-bis[4,4,5,5-tetramethyl-1,3,2-dioxaborolan-2-yle]thiophene. For **PC**, 3,6-bis(5-bromo-2-thienyl)-2,5-bis(2'-butyloctyl)pyrrolo[3,4-c]pyrrole-1,4(*2H*,*5H*)-dione was reacted with 2,7-bis(4,4,5,5-tetramethyl-1,3,2-dioxaborolan-2-yl)-9,9-dioctylfluorene.[20] The molecular weights (M_n) of **PA**, **PB** and **PC** are roughly in the same range: 16.6, 11.8 and 10.5 kg/mol respectively.

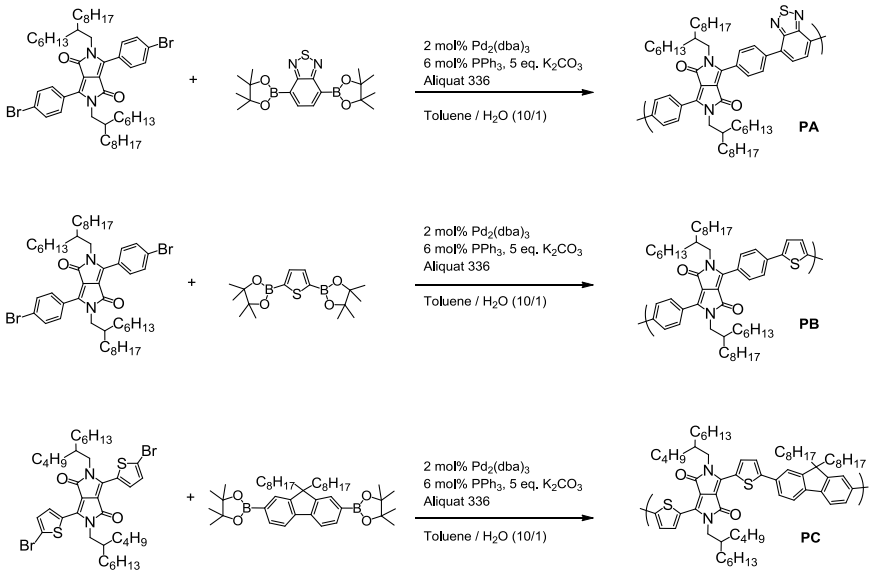

Scheme 4.1: Synthesis of the polymers **PA**, **PB** and **PC**.

Opto-electrical properties. The optical absorption spectra of the polymers dissolved in *o*-dichlorobenzene (ODCB) and in thin films are shown in Figure 4.2 together with cyclic voltammograms that were recorded for polymers in ODCB. The results are collected in Table 4.1. The optical gap in solution –defined as the onset of absorption– decreases from **PA**, via **PB** to **PC** (2.1, 2.0 and 1.75 eV respectively). The oxidation potential follows the same trend (0.50, 0.40 and 0.22 V vs. Fc/Fc^{+}). The reduction potential is the same for **PA** and **PB** (–1.70 V vs. Fc/Fc^{+}) and more positive for **PC** (–1.55 V vs. Fc/Fc^{+}), indicating a stronger acceptor character in **PC**. The optical HOMO and LUMO energy levels versus vacuum as well as the energy of the charge transfer state (E_{CT}) are given in Table 4.1. They were determined from E_{ox} and E_{red} relative to the work function value of –5.23 eV for Fc/Fc^{+}[21-23] and assuming that the energy difference $e(E_{ox} - E_{red}) - E_g$ (with e the elementary charge) can be equally divided over the HOMO and the LUMO levels as explained in Ref. 17. This results in the following definitions for E_{HOMO}^{opt} and E_{LUMO}^{opt} and in an empirical relation for E_{CT} (see also Figure 4.1):[17]

$$E_{\mathrm{HOMO}}^{\mathrm{opt}} = -5.23\,\mathrm{eV} - e\,E_{\mathrm{ox}} + \tfrac{1}{2}(E_{\mathrm{cv}}^{\mathrm{sol}} - E_g) \qquad (4.1)$$

$$E_{\mathrm{LUMO}}^{\mathrm{opt}} = -5.23\,\mathrm{eV} - e\,E_{\mathrm{red}} - \tfrac{1}{2}(E_{\mathrm{cv}}^{\mathrm{sol}} - E_g) \qquad (4.2)$$

$$E_{\mathrm{CT}} = |\,E_{\mathrm{HOMO}}^{\mathrm{opt}}(\mathrm{D}) - E_{\mathrm{LUMO}}^{\mathrm{opt}}(\mathrm{A})\,| + 0.29\,\mathrm{eV} \qquad (4.3)$$

In (4.1) and (4.2) $E_{\mathrm{cv}}^{\mathrm{sol}}$ is defined as $E_{\mathrm{cv}}^{\mathrm{sol}} = e(E_{\mathrm{ox}} - E_{\mathrm{red}})$. In this approach $\left| E_{\mathrm{HOMO}}^{\mathrm{opt}} - E_{\mathrm{LUMO}}^{\mathrm{opt}} \right|$ is equal to the optical gap E_{g} in the film and hence these optical HOMO and LUMO levels incorporate the intramolecular exciton binding energy in the solid state. Each of the three polymers fulfils the requirement described in the introduction to be used as an acceptor material with respect to P3HT. The $E_{\mathrm{LUMO}}^{\mathrm{opt}}$ and $E_{\mathrm{HOMO}}^{\mathrm{opt}}$ are below –3.5 eV and –5.4 eV respectively. Furthermore, for each combination $E_{\mathrm{g}*} - E_{\mathrm{CT}} \geq 0.08$ (±0.02) eV ($E_{\mathrm{g}*}$ being the lowest of the two optical gaps: $E_{\mathrm{g}*}$ = min [E_{g}(D),E_{g}(A)]) which has previously been established as a criterion for photoinduced electron transfer to occur.[17]

Table 4.1: Molecular weights, optical and electrochemical properties and charge carrier mobilities of P3HT, **PA**, **PB** and **PC**.

	M_{n} (kg/mol)	PD	$E_{\mathrm{g}}^{\mathrm{sol}}$ (eV)	E_{g} (eV)	E_{ox} [a] (V)	E_{red} [a] (V)	$E_{\mathrm{cv}}^{\mathrm{sol}}$ (eV)	$E_{\mathrm{HOMO}}^{\mathrm{opt}}$ [b] (eV)	$E_{\mathrm{LUMO}}^{\mathrm{opt}}$ [b] (eV)	μ_{e} (m^2/Vs)	E_{CT} [c] (eV)
P3HT	30.0	2.1	2.25	1.91	0.06	-2.34	2.40	-5.05	-3.14		
PA	16.6	2.5	2.10	2.05	0.50	-1.70	2.20	-5.66	-3.61	3×10^{-11}	1.73
PB	11.8	2.0	2.00	2.00	0.40	-1.70	2.10	-5.58	-3.58	1×10^{-11}	1.76
PC	10.5	2.2	1.75	1.72	0.22	-1.55	1.77	-5.43	-3.71	5×10^{-10}	1.63

[a] CV measurements in ODCB vs. Fc/Fc^+ as internal standard. [b] Calculated form eqs. (4.1) and (4.2). [c] For a blend with P3HT, calculated from eq. (4.3).

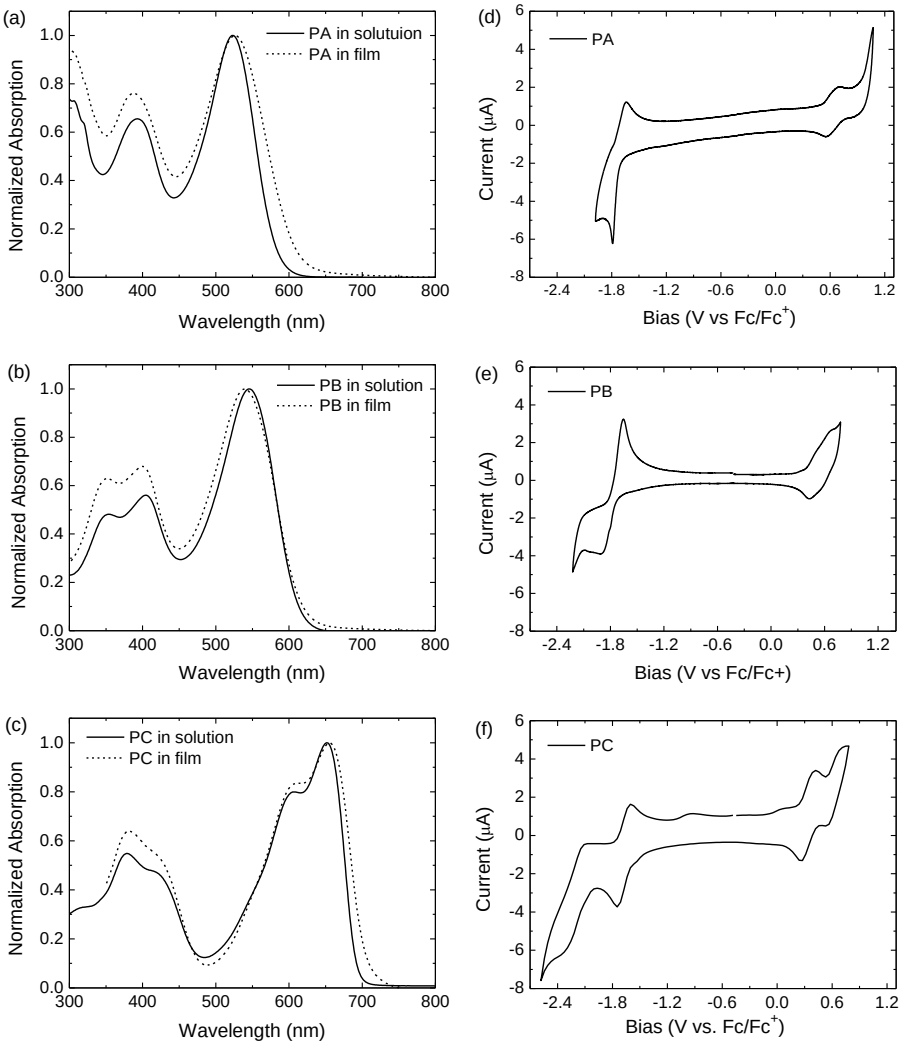

Figure 4.2: (a, b, c) Optical absorption spectra of **PA**, **PB** and **PC**. The solid line represents the absorption of the polymers in solution in ODCB. The dotted line represents the absorption of the polymers in thin films. (d, e, f) Cyclic voltammograms of **PA**, **PB** and **PC** in solution in ODCB (0.1 M $TBAPF_6$).

Mobility measurements. In determining the electron mobilities it is important to measure under conditions that are close to the solar cell operation. Therefore, we applied the materials as a thin layer in an electron-only device between a ITO/ZnO hole blocking bottom electrode and a Ca/Al electron injecting top electrode. In Figure 4.3, we have collected the experimental dark current densities of these electron-only devices. The applied voltage (V_{appl}) was corrected for the built-in voltage (V_{bi}) that arises from the difference in work-function between the two electrodes and for the voltage drop (V_{rs}) due to substrate series' resistance by setting $V = V_{appl} - V_{bi} - V_{rs}$. The experimental current densities scale quadratically with V, characteristic of space charge limited transport through the layer and the zero-field mobility μ_e of the electrons was determined by a fit of the data to the equation for space charge limited current (SCLC):[24]

$$J_e = \frac{9}{8}\varepsilon_0\varepsilon_r\mu_e\frac{V^2}{L^3}\exp\left(0.891\gamma_e\sqrt{\frac{V}{L}}\right) \qquad (4.4)$$

where J_e is the electron current density, γ_e the field activation factor, ε_0 the permittivity of free space, ε_r the relative permittivity of the material and L the thickness of the active layer. Polymer **PC** exhibits an electron mobility of $\mu_e = 5 \times 10^{-10}$ m^2/Vs, which is one order of magnitude higher than the electron mobilities measured for **PA** and **PB** ($\mu_e = 3 \times 10^{-11}$ and $\mu_e = 1 \times 10^{-11}$ m^2/Vs respectively). Upon blending the acceptor polymers with P3HT, the electron mobility changes only slightly to $\mu_e = 2 \times 10^{-11}$, 1×10^{-11} and 9×10^{-10} m^2/Vs for the P3HT:**PA**, P3HT:**PB** and P3HT:**PC** blends, respectively.

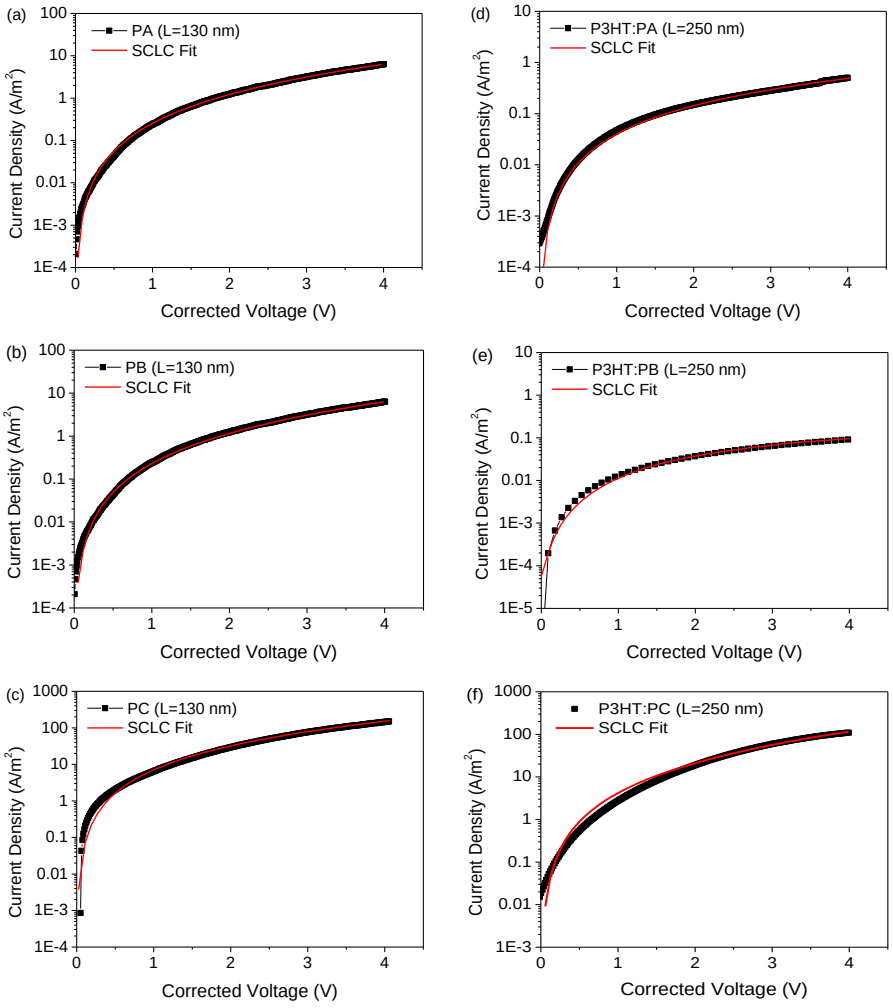

Figure 4.3: (a,b,c) Dark current density characteristics of the electron-only device of **PA**, **PB** and **PC**. Thickness is ~ 150 nm. (d,e,f) Dark current density characteristics of the electron-only device of blends P3HT:**PA**, P3HT:**PB** and P3HT:**PC**. Thickness is ~ 250 nm.

Photovoltaic devices. The polymers were applied in bulk heterojunction solar cells with P3HT as the donor material. The active layers were spin-coated from $CHCl_3$:ODCB (9:1) onto an indium tin oxide (ITO) covered glass substrate covered by a 50 nm film of PEDOT:PSS. Ca (10 nm) and Al (100 nm) were thermally evaporated as top electrode. For each polymer the ratio with P3HT and the layer thickness were optimized for maximal performance. Annealing at 120 °C was needed to improve the performance of the devices. The representative *J-V* curves and external quantum efficiency (EQE) measurements are shown in Figure 4.4. The performance and characteristics of the best devices are summarized in Table 4.2. Devices made of blends of P3HT:**PA**, P3HT:**PB** and P3HT:**PC** exhibit very similar open-circuit voltages (0.94, 0.90 and 0.90 V, respectively) and comparable fill factors (0.22, 0.27 and 0.25, respectively). The short-circuit densities differ significantly. P3HT:**PA** and P3HT:**PB** offer a very limited J_{sc} of 0.68 and 0.44 mA/cm^2 respectively. For P3HT:**PC**, the short-circuit current is much higher and reaches a value of 1.63 mA/cm^2. The overall power conversion efficiency (PCE) for P3HT:**PA**, P3HT:**PB** and P3HT:**PC** is 0.14%, 0.11% and 0.36%, respectively. The short-circuit current densities were calculated by convoluting the EQE with the solar AM 1.5G spectrum.

Table 4.2: Characteristics of P3HT:acceptor-polymer devices under 100 mW/cm^2 white light illumination.

	Ratio	*d* (nm)	J_{sc} (mA/cm^2)	V_{oc} (V)	FF	PCE (%)
P3HT:**PA**	1:1	50	0.68	0.94	0.22	0.14
P3HT:**PB**	1:1	55	0.44	0.90	0.27	0.11
P3HT:**PC**	1:1	55	1.63	0.90	0.25	0.36

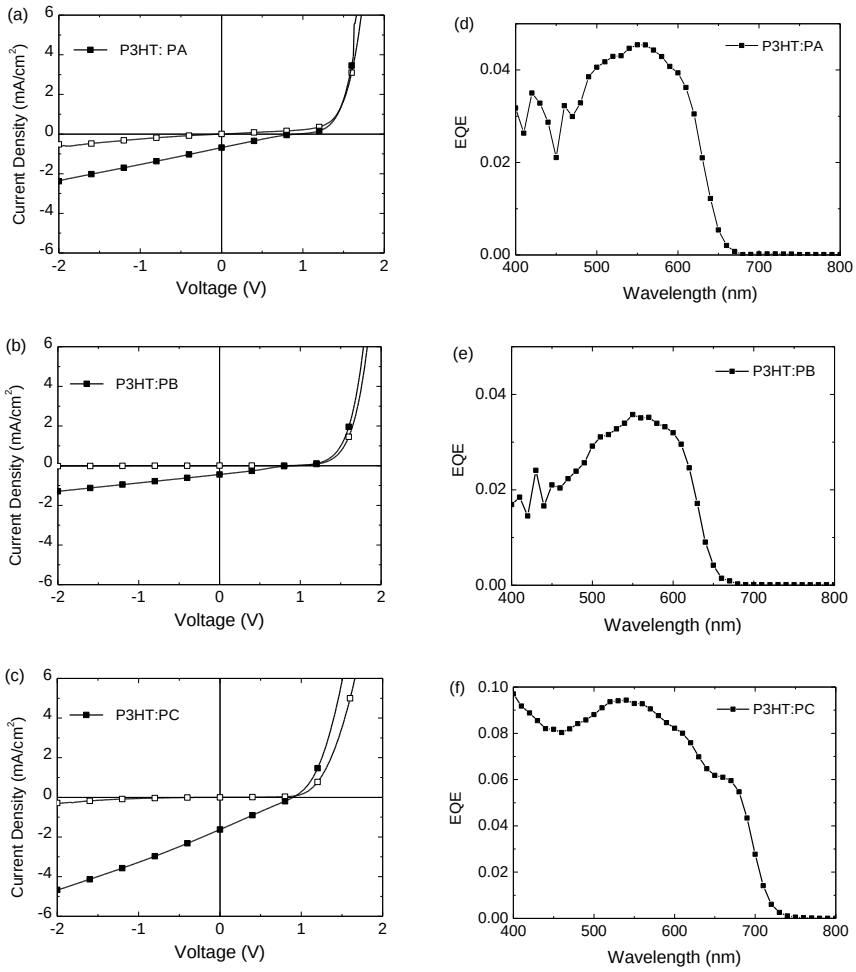

Figure 4.4: (a, b, c) Representative *J-V* curves for P3HT:**PA**, P3HT:**PB** and P3HT:**PC** solar cells in the dark (open markers) and under simulated AM1.5G conditions (closed markers). (d, e, f) EQE spectra of P3HT:**PA**, P3HT:**PB** and P3HT:**PC** solar cells under 1 Sun equivalent light bias illumination.

Atomic force microscopy. A key parameter for power conversion efficiency in solar cells is the morphology of the active layer. A nanoscale phase separation in the bulk heterojunction (BHJ) of ~10-20 nm is desirable to ensure the diffusion of the exciton to the interface where charge generation takes place.[25,26] On the other hand larger domains and percolating pathways will favour and improve the separation of the formed charges from the interface and their transport to the electrodes. It is thus important to find a good balance and make sure that the morphology of the active layer does not limit the performance. To assess the morphology, the thermally annealed layers used in the devices have been studied with AFM. As shown in Figure 4.5 the films are relatively smooth (5-15 nm) and the phase image presents bright and dark regions that can be associated with two different (not necessarily pure) materials, phase segregated at the surface. The smallest features that can be discerned in the phase images are on the order of ten nanometres, which would indicate relatively intimate mixing. If the mixing is too intimate, the reduced domain size could account for the reduced device performance.

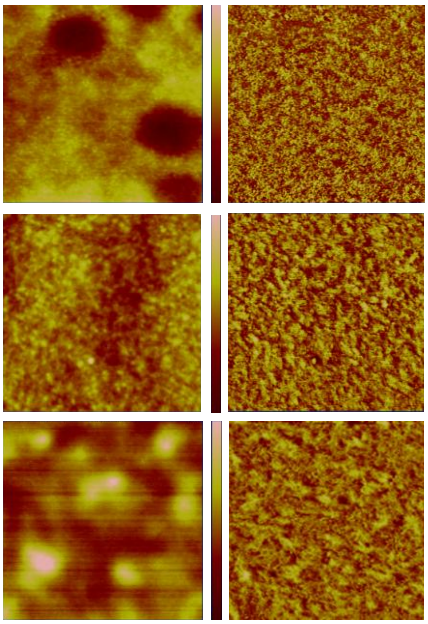

Figure 4.5: Height (left) and phase (right) AFM images of the surface of the P3HT:acceptor polymer blends (1 μm × 1 μm). Top: P3HT:**PA**, vertical scale 10 nm and 30°. Middle: P3HT:**PB** vertical scale 8 nm and 15°. Bottom P3HT:**PC**, vertical scale 15 nm and 40°.

Photoluminescence quenching. The extent of the interaction between the two materials on a nanoscale has been investigated by measuring the fluorescence quenching in a blend of P3HT with 50% of acceptor polymer after annealing. As shown in Figure 4.6, the experiment reveals that the fluorescence in the blends is quenched by approximately one order of magnitude compared to the pristine polymers. Figure 4.6 also shows that the fluorescence intensity of pristine **PC** is less than that of **PA** and **PB**. For **PA** and **PB** the optical gap is higher than that of P3HT and hence the fluorescence quenching can be due to energy or electron transfer. **PC**, however, shows a lower optical gap than P3HT and in this case quenching cannot be due to energy transfer. The spectrum of the P3HT:**PC** blend also shows some fluorescence of P3HT as a shoulder at ~630 nm which is due to direct excitation of P3HT. For all three blends the significant quenching of the fluorescence is consistent with the surface topography of the active layer as inferred from the AFM phase images where relatively small domains were observed. The remaining fluorescence can be ascribed to larger domains of pure polymer or to the rate of the quenching process being similar to the fluorescence rate constant.

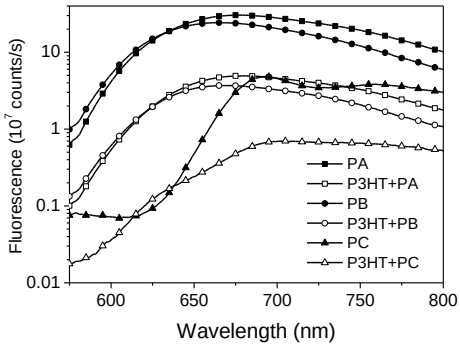

Figure 4.6: Fluorescence spectra recorded at room temperature of the pristine polymers (closed markers) and their 1:1 annealed blends with P3HT (open markers).

Photoinduced absorption. Photoinduced absorption (PIA) spectroscopy has been carried out in order to investigate the charge transfer and to probe the charge formation and recombination in these blends. Upon photoexcitation of the blend, P3HT is expected to transfer an electron to the acceptor polymer and -provided that the charge separated state has a significantly long lifetime- it can be detected with PIA spectroscopy. Figure 4.7a shows the PIA spectrum of pristine P3HT. The $T_n \leftarrow T_1$ absorption of the pure P3HT triplet state is at 1.06 eV and bleaching signals are at 1.97 and 2.13 eV.[17,27] A weak PIA signal is also observed at ~0.5 eV that is characteristic for the low-energy excitation of P3HT radical cations. This highlights that only very few long lived charges are formed in pure P3HT after photoexcitation. The PIA spectra of **PA** and the P3HT:**PA** blend are shown in Figure 4.7b, together with the signal of pure P3HT. The PIA spectrum of **PA** shows a bleaching signal at 2.25 eV and two bands at 1.28 and 1.64 eV, which we attribute to the $T_n \leftarrow T_1$ transitions of **PA**. The PIA spectrum of the P3HT:**PA** blend is a superposition of the PIA signals of P3HT and **PA**. In the blends also the bleaching signals of both P3HT and **PA** are present. Similar results can be observed for **PB** ($T_n \leftarrow T_1$ at 1.36 eV with shoulders at higher energies) and the P3HT:**PB** blend (Figure 4.7c). We note that the intensity of the PIA bands does not change drastically upon blending and that in both P3HT:**PA** and P3HT:**PB** blends no significant signal is observed at ~0.5 eV, indicating that no long lived charges are present after photoexcitation. Hence, PIA does not give evidence of photoinduced electron transfer from P3HT to either **PA** or **PB** and the luminescence quenching observed in the blends of either P3HT:**PA** or P3HT:**PB** is, therefore, most likely due to energy transfer from **PA** and **PB** to the weakly luminescent P3HT. The fact that the triplet signatures of both P3HT and **PA** or **PB** are observed in the blends is likely a consequence of triplet energy pooling and suggests that the triplet states of P3HT, **PA** and **PB** are almost isoenergetic. This is consistent with the result that the optical gaps (S_1 energies) of P3HT, **PA** and **PB** are similar and the fact that the T_1 energy (E_T) of conjugated polymers is often found about 0.7 eV below that of S_1.[28] The absence of clear signals due to charges can be rationalized in two ways. First, by considering that the energies of the charge transfer states (E_{CT}, Table 4.1) of P3HT:**PA** and P3HT:**PB** at 1.73 and 1.76 eV, respectively are close to the optical gap of P3HT at 1.91 eV, such that electron transfer from the P3HT S_1 state is only weakly exergonic and does not occur to a significant extent. Second, by realizing that charges formed at the interface do no separate and can effectively recombine into the triplet states of either P3HT, **PA** or **PB** at the interface because the T_1 energy estimated as $E_T = E_g - 0.7$ eV is well below the expected energy of the charge transfer state (E_{CT}, Table

4.1). Figure 4.7d shows the PIA spectra of **PC**, P3HT and the P3HT:**PC** blend. The PIA spectrum of **PC** shows a very weak PIA signal. Because the fluorescence signal of **PC** also has a low intensity (cf. Figure 4.6 where the fluorescence of **PC** is a factor of ~10 less compared to **PA** and **PB**), the low PIA signal is likely a consequence of rapid internal conversion of the S_1 state of **PC** that effectively reduces the fluorescence and intersystem crossing quantum yields. The PIA spectrum of the P3HT:**PC** blend is different from that of pristine **PC** and pristine P3HT. The main bleaching signal peaks at 1.79 eV and crosses zero at 1.72 eV. This position corresponds to the optical gap of **PC**, which suggests that the PIA spectrum predominantly originates from **PC**. The shape of PIA band of the P3HT:**PC** blend between 1.30 and 1.65 eV actually resembles the $T_n \leftarrow T_1$ PIA spectra of pure **PA** and **PB** in the same region. Based on these considerations we attribute the PIA signal of the P3HT:**PC** blend to the $T_n \leftarrow T_1$ transition of **PC**. This triplet state is then formed from the interfacial $P3HT^+$-$\mathbf{PC}^-$ charge transfer state via recombination. This assignment is consistent with the estimated T_1 energy of **PC** which is at about $E_g - 0.7$ eV = 1.02 eV[28] and much less than the expected E_{CT} = 1.65 eV for this blend (Table 4.1). The weak PIA signal present at ~0.5 eV indicates the presence of some long-lived free charges.

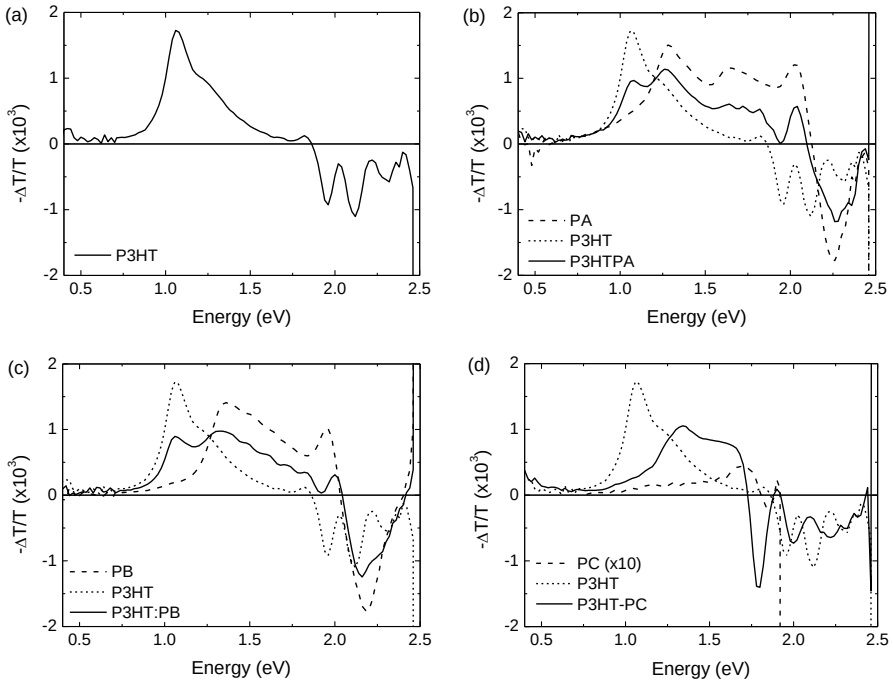

Figure 4.7: PIA spectra recorded at 80 K of (a) P3HT, (b) **PA** and P3HT:**PA**, (c) **PB** and P3HT:**PB** (d) **PC** and P3HT:**PC** (**PC** was exited at 633 nm while P3HT:**PC** blend was excited at 496 nm.).

Field-dependent photocurrent. The device performance is in each blend limited by a low short-circuit current and low fill factor. The inefficient generation of long-lived free charges as inferred from the PIA experiments accounts for this result but the collection and possibly formation of free charge carriers may be assisted by an electric field. Figure 4.8a shows the photocurrent, J_{ph}, recorded for the three blends on a double logarithmic scale as a function of the effective voltage, $V_0 - V$, applied to the device where V_0 is the compensation voltage corresponding to $J_{ph} = 0$. The results for the three blends are compared to that for a well performing solar cell using P3HT:[60]PCBM as active layer.[29] At small effective voltages ($V_0 - V$) < 0.1 V the photocurrent of the P3HT:[60]PCBM cell increases linearly with the effective voltage, $J_{ph} \propto (V_0 - V)$, because at higher electric fields the distance the charges travel increases and more charges can be collected.

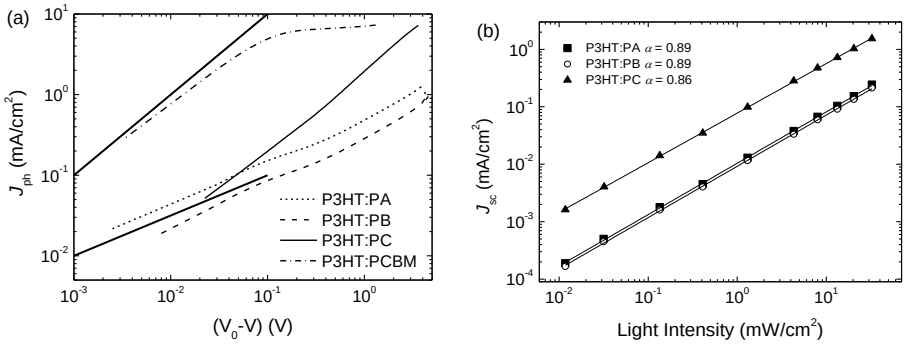

Figure 4.8: (a) Photocurrent versus the effective applied voltage for P3HT:**PA**, P3HT:**PB**, P3HT:**PC** and P3HT:PCBM devices. Thick lines represents represent slopes of ½ and 1 and serve as a guide to the eye. (b) Light intensity dependence of the short-circuit current density.

At higher effective voltages ($V_0 - V > 0.1$ V), where the field becomes large enough such that the mean carrier drift length ($\mu_{e,h}\tau_{e,h}E$, with τ the lifetime and E the field) exceeds the layer thickness, the photocurrent quickly saturates as the number of free carriers is limited by the amount of photons absorbed. For the blends with the DPP acceptor polymers under study here the behaviour is different. For P3HT:**PA** and P3HT:**PB** the photocurrent increases with the square root of the voltage ($J_{ph} \propto (V_0 - V)^{½}$). This behaviour has been observed before in organic solar cells [30,31] and has its origin in the fact that the mean drift length of at least one carrier is less than the thickness of layer such that recombination of charge carriers is significant.[32] The electron mobilities of μ_e = ~10^{-11} m^2/Vs measured for **PA** and **PB** are three orders of magnitude below the value of $\mu_h = 2\times10^{-8}$ m^2/Vs for pristine P3HT.[29] Under such conditions, where μ_h exceeds μ_e by three orders of magnitude, a build-up of electrons can occur under illumination.[30] This then creates a non-uniform electric field that enhances the extraction of electrons close to the negative electrode and reduces the extraction of holes at the positive electrode and gives rise to a square root dependent photocurrent on the effective voltage. For P3HT:**PA** and P3HT:**PB** there is a small sub-linearity of the short-circuit current with light intensity ($J_{sc} \propto I^{\alpha}$, with I the light intensity and $\alpha \approx 0.89$, Figure 4.8b) which shows that the photocurrent is not yet space charge limited, for which $\alpha = 0.75$ would have been expected.[30] For **PC**, which has a higher electron mobility ($\mu_e = 5 \times 10^{-10}$ m^2/Vs), J_{ph} is again linear with ($V_0 - V$), suggesting that the difference in mobility is not large enough to create substantial space charge. However, the effective voltage in the P3HT:**PC** blend required to reach a photocurrent of ~7 mA/cm^2 is 4 V compared to 0.2 V for the P3HT:PCBM blend and saturation has not yet occurred.

4.3 Conclusions

Three diketopyrrolopyrrole-based polymers have been synthesized. They have been combined with P3HT as the donor material in bulk heterojunction solar cells. The photovoltaic devices exhibit open-circuit voltages of 0.9 V but low short-circuit current densities and fill factors that limit the efficiency between 0.1 and 0.36%. For P3HT:**PA** and P3HT:**PB** PIA spectroscopy gives no evidence for charge transfer, consistent with the small short-circuit current density (0.68 and 0.44 mA/cm^2, respectively). For P3HT:**PC** a higher short-circuit current (1.63 mA/cm^2) was measured. PIA measurements indicated formation of free charges in the P3HT:**PC** blend that recombine to the triplet state. By applying a reverse electric field, charge recombination in P3HT:**PC** can be prevented and the photocurrent increases considerably under these conditions. We conclude that the low electron mobility of the acceptor materials combined with an inefficient generation of long-lived free charge carriers are the main reasons for the limited device performance. Further improvements of acceptor polymers can possibly be made by focusing on the design of materials with high electron mobility in blends with P3HT.

4.4 Experimental section

Materials and methods. Polymerization reactions were conducted under an argon atmosphere. Commercial chemicals were used as received. 2,5-bis[4,4,5,5-tetramethyl-1,3,2-dioxaborolan-2-yle]thiophene and 2,1,3-benzothiadiazole-4,7-bis(boronic acid pinacol ester) were obtained from Sigma-Aldrich and used as received. The P3HT used in this study had M_n = 30 kg/mol with a polydispersity of 2.1 and regioregularity higher than 98.5%. ^{1}H NMR and ^{13}C NMR spectra were recorded at 400 MHz on a VARIAN mercury spectrometer with $CDCl_3$ as the solvent and tetramethylsilane (TMS) as the internal standard. The peaks are given in ppm, relative to TMS (0 ppm). Molecular weights were determined with GPC on a Shimadzu LC-10AD using a Polymer Laboratories Resipore column (length 300 mm, diameter 7.5 mm), a Shimadzu SPD-M20A photodiode array detector from 250-700 nm and chloroform as the eluens with a flow rate of 1 mL/min. (T = 343 K). Polystyrene standards were used.

UV-vis-nearIR spectra were recorded on a Perkin-Elmer Lambda 900 spectrophotometer. Cyclic voltammetry was conducted under an inert atmosphere with a scan rate of 0.1 V/s, using 1 M tetrabutylammonium hexafluorophosphate in ODCB as the electrolyte. The working electrode was a platinum disk and the counter electrode was a silver rod electrode. Fc/Fc^+ was used as an internal standard. . Atomic force microscopy (AFM) was measured using a Veeco MultiMode with a Nanoscope III controller, in tapping mode. The used probes were PPP-NCH-50 from Nanosensors.

Photovoltaic devices were made by spin coating poly(ethylenedioxythiophene): poly(styrene sulfonate) (PEDOT:PSS) (Clevios P, VP Al4083) onto pre-cleaned, patterned indium tin oxide (ITO) substrates (14 Ω per square) (Naranjo Substrates). The counter electrode, consisting of LiF (1 nm) and Al (100 nm), was deposited by vacuum evaporation at ~3×10^{-7} mbar. The active area of the cells was 0.091 cm^2. *J-V* characteristics were measured under ~100 mW/cm^2 white light from a tungsten-halogen lamp filtered by a Schott GG385 UV filter and a Hoya LB120 daylight filter, using a Keithley 2400 source meter. Short-circuit currents under AM1.5G conditions were estimated from the spectral response and convolution with the solar spectrum. The spectral response was measured under simulated 1 Sun operation conditions using bias light from a 532 nm solid state laser (Edmund Optics). Monochromatic light from a 50 W tungsten halogen lamp (Philips focusline) in combination with monochromator (Oriel, Cornerstone 130) was modulated with a mechanical chopper. The response was recorded as the voltage over a 50 Ω

resistance, using a lock-in amplifier (Stanford Research Systems SR830). A calibrated Si cell was used as reference. The device was kept behind a quartz window in a nitrogen filled container. The thickness of the active layers in the photovoltaic devices was measured on a Veeco Dektak150 profilometer.

Photoinduced absorption (PIA) spectra were recorded by exciting with a mechanically modulated Ar-ion (496.5 nm) or Helium-Neon (633 nm) pump beam and monitoring the resulting change in transmission of a tungsten-halogen probe light through the sample (ΔT) with a phase-sensitive lock-in amplifier after dispersion by a grating monochromator and detection, using Si, InGaAs and cooled InSb detectors. The pump power incident on the sample was typically 50 mW with a beam diameter of 2 mm. The PIA ($\Delta T/T$) was corrected for the photoluminescence, which was recorded in a separate experiment. Photoinduced absorption spectra and photoluminescence spectra were recorded with the pump beam in a direction almost parallel to the direction of the probe beam. Temperature of the substrates was controlled by using an Oxford Optistat continuous flow cryostat.

Polymer PA. To an argon bubbled solution of 2,1,3-benzothiadiazole-4,7-bis(boronic acid pinacol ester) (85.4 mg, 0.22 mmol), 3,6-bis(4-bromophenyl)-2,5-bis(2'-hexyldecyl)pyrrolo[3,4-c]pyrrole-1,4(*2H,5H*)-dione[33] (200 mg, 0.22 mmol), Aliquat 336 (3 drops), K_2CO_3 (150 mg, 1 mmol) and PPh_3 (10 mg, 38 μmol) in 5 mL toluene, $Pd_2(dba)_3$ (7 mg, 7.6 μmol) were added. The reaction mixture was heated to 120 °C. After 10 hours water (10 mL) was added, followed by an extraction with $CHCl_3$ (200 mL). Ammonia (100 mL of 25% aq. sol.) was added to the organic phase and the mixture was refluxed for 2 h. The organic phase was concentrated under reduced pressure. The polymer was precipitated in methanol, filtered through a Soxhlet thimble and fractionated by Soxhlet extraction using methanol, acetone, hexane and $CHCl_3$, respectively. The polymer was obtained in 123 mg as a deep red solid (54% yield). GPC (PS): M_n = 16.6 kg/mol, PDI = 2.2. ^{1}H-NMR (400 MHz, $CDCl_3$): δ 7.79 (br, 8H), 6.90 (br, 2H), 4.1 (br, 4H), 1.55 (br, 6H), 1.12 (br, 40H), 0.80 (br, 14H).

Polymer PB. 2,5-Bis[4,4,5,5-tetramethyl-1,3,2-dioxaborolan-2-yle]thiophene (73.9 mg, 0.22 mmol) and 3,6-bis(4-bromophenyl)-2,5-bis(2'-hexyldecyl)pyrrolo[3,4-c]pyrrole-1,4(*2H,5H*)-dione[33] (200 mg, 0.22 mmol) were reacted according to the procedure described above and gave 90 mg of a deep red solid (50 %). GPC (PS): M_n = 11.8 kg/mol, PDI = 2.0. ^{1}H-NMR (400 MHz, $CDCl_3$) δ: 7.64 (br, 4H), 7.42 (br, 4H), 7.14 (br, 2H), 3.75 (br, 4H), 1.55 (br, 6H), 1.11 (br, 40H), 0.83 (br, 14H).

Polymer PC. The synthesis of **PC** has been described in Ref. 20. GPC (PS): M_n = 10.5 kg/mol, PDI = 2.2. ^{1}H-NMR (400 MHz, $CDCl_3$): δ 8.98 (br, 2H), 7.77 (d, 2H, J = 8.5Hz), 7.71 (d, 2H, J = 8.1Hz), 7.64 (br, 2H), 7.55 (br, 2H), 4.13 (br, 4H), 2.04 (br, 6H), 1.48-0.98 (m, 52H), 0.95-0.57 (m, 22H).

References

(1) Brabec, C.; Winder, C.; Sariciftci, N. S.; Hummelen, J. C.; Dhanabalan, A.; van Hal, P.A.; Janssen, R. A. J. *Adv. Funct. Mater.* **2002**, 12, 709.

(2) Svensson, M.; Zhang, F.; Veenstra, S. C.; Verhees, W. J. H.; Hummelen, J. C.; Kroon, J. M.; Inganäs, O.; Andersson, M. R. *Adv. Mater.* **2003**, 15, 988.

(3) Mühlbacher, D.; Scharber, M.; Morana, M.; Zhu, Z.; Waller, D.; Gaudiana, R.; Brabec, C. *Adv. Mater.* **2006**, 18, 2884.

(4) Blouin, N.; Michaud, A.; Gendron, D.; Wakim, S.; Blair, E.; Neagu-Plesu, R.; Belletete, M.; Durocher, G.; Tao, Y.; Leclerc, M. *J. Am. Chem. Soc.* **2008**, 130, 732.

(5) Hou, j.; Chen, H-Y.; Zhang, S.; Li, G.; Yang, Y. *J. Am. Chem. Soc.* **2008**, 130, 16144.

(6) Wienk, M. M.; Turbiez, M.; Gilot, J.; Janssen, R. A. J. *Adv. Mater*. **2008**, 20, 2556.

(7) Liang, Y.; Xu, Z.; Xia, J.; Tsai, S.-T.; Wu, Y.; Li, G.; Ray, C.; Yu, L. *Adv. Mater.* **2010**, 22, E135.

(8) Chen, H.-Y.; Hou, J.; Zhang, S.; Liang, Y.; Yang, G.; Yang, Y.; Yu, L.; Wu, Y.; Li, G. *Nat. Photon.* **2009**, 3, 649.

(9) Halls, J. J. M.; Walsh, C. A.; Greenham, N. C.; Marseglia, E. A.; Friend, R. H.; Moratti, S. C.; Holmes, A.B. *Nature* **1995**, 376, 498.

(10) Veenstra, S.C.; Verhees, W. J. H.; Kroon, J. M.; Koetse, M. M.; Sweelssen, J.; Bastiaansen, J. A. M.; Schoo, H. F. M.; Yang, X.; Alexeev, A.; Loos, J.; Schubert, U. S.; Wienk, M.M. *Chem. Mater.* **2004**, 16, 2503.

(11) McNeill, C. R.; Halls, J. J. M.; Wilson, R.; Whiting, G. L.; Berkebile, S.; Ramsey, M. G.; Friend, R. H.; Greenham, N. C. *Adv. Funct. Mater.* **2008**, 18, 2309.

(12) Halls, J. J. M.; Cornil, J.; dos Santos, D. A.; Silbey, R.; Hwang, D. H.; Holmes, A. B.; Brédas, J. L.; Friend, R. H. *Phys. Rev. B* **1998**, 60, 5721.

(13) Koster, L. J. A.; Mihailetchi, V. D.; Blom, P. M. W. *Appl. Phys. Lett.* **2006**, 88, 093511.

(14) Scharber, M. C.; Mühlbacher, D.; Koppe, M.; Denk, P.; Waldauf, C.; Heeger, A. J.; Brabec, C. J. *Adv. Mater.* **2006**, 18, 789.

(15) Bao, Z.; Dodabalapur, A.; Lovinger, A. J. *Appl. Phys. Lett.* **1996**, 69, 4108.

(16) Ma, W.; Yang, C.; Gong, X.; Lee, K.; Heeger, A. J. *Adv. Funct. Mater.* **2005**, 15, 1617.

(17) Veldman, D.; Meskers, S. C. J.; Janssen, R. A. J. *Adv. Funct. Mater.* **2009**, 19, 1939.

(18) Zou, Y.; Gendron, D.; Aïch, B.-R.; Najari, A.; Tao, Y.; Leclerc, M. *Macromolecules* **2009**, 42, 2891.

(19) Bijleveld, J. C.; Zoombelt, A. P.; Mathijssen, S. G. J.; Wienk, M. M.; Turbiez, M.; de Leeuw, D. M.; Janssen, R. A. J. *J. Am. Chem. Soc.* **2009**, 131, 16616.

(20) Zoombelt, A. P.; Mathijssen, S. G. J.; Turbiez, M. G. R.; Wienk, M. M.; Janssen, R. A. J. *J. Mater. Chem.* **2010**, 20, 2240.

(21) Using a potential value of 4.6±0.2 eV for NHE versus vacuum (ref. 22) and 0.63 eV (ref. 23) for Fc/Fc+ versus NHE.

(22) Bockris, J. O. M.; Khan, S. U. M. Surface Electrochemistry. A Molecular Level Approach, Kluwer Academic/Plenum Publishers, New York 1993.

(23) Pavlishchuk, V. V.; Addison, A. W. *Inorg. Chim. Acta* **2000**, 298, 97.

(24) Murgatroyd, P. N. *J. Phys. D: Appl. Phys.* **1970**, 3, 151.

(25) Halls, J. J. M.; Pichler, K.; Friend, R. H.; Moratti, S. C.; Holmes, A. B. *Appl. Phys. Lett.* **1996**, 68, 3120.

(26) Markov, D. E.; Amsterdam, E.; Blom, P. W. M.; Sieval, A. B.; Hummelen, J. C. *J. Phys. Chem. A* **2005**, 109, 5266.

(27) van Hal, P. A.; Christiaans, M. P. T.; Wienk, M. M.; Kroon, J. M.; Janssen, R. A. J. *J. Phys. Chem. B* **1999**, 103, 4352.

(28) A. Köhler and D. Beljonne, *Adv. Funct. Mater.* **2004**, 14, 11.

(29) Mihailetchi, V. D.; Xie, H. X.; de Boer, B.; Koster, L. J. A.; Blom, P. W. M. *Adv. Funct. Mater*. **2006**, 16, 699.
(30) Mihailetchi, V. D.; Wildeman, J.; Blom, P. W. M. *Phys. Rev. Lett.* **2005**, 94, 126602.
(31) Lenes, M.; Morana, M.; Brabec, C. J.; Blom, P. W. M. *Adv. Funct. Mater*. **2009**, 19, 1106.
(32) Goodman, A. M.; Rose, A. *J. Appl. Phys*. **1971**, 42, 2823.
(33) Zhang, K.; Tieke, B.; Forgie, J. C.; Skabara, P. J.; *Macromol. Rapid Commun.* **2009**, 30, 1834.

Chapter 5

Photoinduced charge transfer in P3HT/soluble indigo dye blends

Abstract. We explore new molecular acceptor materials for use in bulk heterojunction solar cells. Two molecules have been synthesized: soluble indigo and isoindigo dyes, both exhibiting reduction potentials at -1.25 V vs. Fc/Fc^{+}. We observed that blending of poly(3-hexylthiophene) with the dyes leads to the formation of long-lived free charges upon illumination. This observation suggests that the dyes are attractive as acceptor material for bulk heterojunction solar cells. However, field-effect transistor measurements revealed that these materials do not exhibit appreciable electron transport characteristics and the solar cell devices only showed a photocurrent but no photovoltaic effect.

5.1 Introduction

The global demand for low-cost renewable energy sources has intensified over the last few years. Organic solar cells are a promising approach towards the increasing demand for green and inexpensive energy. Until now, the most efficient solar cells are made of a blend of a conjugated polymer as the donor p-type material and a C_{60} or C_{70} fullerene derivative as the acceptor n-type material.[1,2] The good electron mobility and the easy processability of the fullerene derivatives make them ideal materials for these bulk heterojunction organic solar cells. Their only disadvantage is the low absorption coefficient in the visible and near IR region.[3] Finding alternatives to fullerenes that would lift this drawback remains a challenging, but possibly rewarding approach, in further improving the performance of polymer solar cells.

A number of n-type small molecules have been developed in the past. Perylene bisimides exhibit very high n-type mobility in field-effect transistors (FETs) thanks to their extended planar π-conjugated structure.[4-7] Their use in bulk-heterojunction solar cell has met with limited success however, mainly due to morphological problems.[8] The excellent π–π stacking of these molecules enhances crystallization and hampers intermixing with the donor material. Consequently, large phase separation is usually observed in blends with perylene bisimides. In 2007, a vinazene derivative was synthesized in a one-step Heck coupling between 2-vinyl-4,5-dicyanonimidazole and 4,7-dibromo-2,1,3-benzothiadiazole. This vinazene derivative possesses a low reduction potential and yielded a power conversion efficiency of 0.45% in a solar cell when used in a 1:1 blend with poly(3-hexylthiophene) (P3HT).[9] Lately, a diketopyrrolopyrrole-based molecule flanked with two benzotrifluoride end groups was synthesized and used as electron acceptor material in a bulk heterojunction cell. An efficiency of 1% was achieved when blending the molecule with P3HT as the donor material.[10] More recently, Wudl and co-workers developed a new class of acceptor molecules using a 9,9′-bifluorenylidene backbone.[11] The opto-electronic properties can be tuned by extension of the backbone or functionalization of the core. Efficiencies up to 1.7% were achieved in bulk-heterojunction solar cells when mixing with P3HT.

In the previous chapters, we described the synthesis and efficiency of new acceptor polymers. The relative high-lying LUMO level of these materials leads to a small driving force for electron transfer and to recombination processes. Therefore, in this chapter we focus on the use of acceptor molecules exhibiting a low-lying LUMO energy. We describe the synthesis and performance of a soluble indigo dye (**I**) and one of its isomers, the isoindigo (**II**), depicted in Scheme 5.1. Isoindigo has already been used as donor material in bulk heterojunction solar cells.[12-14] The performance of the isoindigo-based materials seems to be limited by low hole mobility[12] and charge trapping effects.[15]

5.2 Results and discussion

Synthesis. The synthetic pathway to indigo derivative **I** is depicted in Scheme 5.1. The iodination and *N*-alkylation of commercially available indole **1** were carried out in a one-pot procedure. First, the iodination was performed regioselectively at the 3-postion using a mixture of iodine and potassium *tert*-butoxide at room temperature in THF. The subsequent alkylation at the *N*-position was accomplished by addition of potassium *tert*-butoxide and ethylbromide at reflux to yield to compound **2**. Compound **3** is obtained by substitution of the iodine atom by an acetoxy group. The substitution involves the reaction of **2** with silver acetate in acetic acid at 90°C. The hydrolysis of **3** with ammonia in methanol at room temperature leads to the formation of **I**. Isoindigo derivative **II** was obtained in two steps starting from the commercially available isatin **4**. First, alkylation of **4** using NaH and n-octyl bromide in DMF at reflux yields intermediate **5**. Subsequent reductive dimerization by deoxygenation in the presence of tris(diethylamino)phosphine at low temperature yields compound **II**.

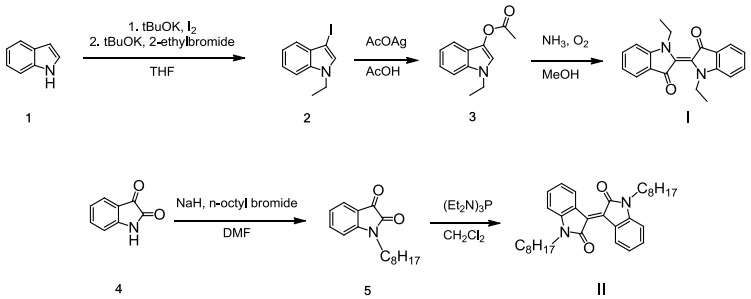

Scheme 5.1: Synthetic pathway to I and II.

Optical properties. The absorption spectra[1,2] of the dyes **I** and **II** dissolved in ODCB are shown in Figure 5.1. The optical gaps determined at the onset of absorption of **I** and **II** are 1.65 and 2.0 eV, respectively. The low band gap of **I** can be explained by its double donor (nitrogen) – acceptor (keto) motif connected via the central double bond that provides extended dipolar conjugated resonance structures (Scheme 5.2). It is interesting to note that compared to the parent N-H substituted indigo and isoindigo dyes that have absorption maxima of λ_{max} at 613 and 485 nm in tetrachloroethane ($\varepsilon_r = 8.2$[16,17]), the absorption spectra of the *N*-alkylated indigos in ODCB ($\varepsilon_r = 9.2$) is strongly red shifted for **I** to $\lambda_{max} = 684$ nm, but only slightly for **II** which has $\lambda_{max} = 493$ nm.

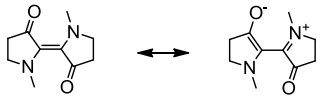

Scheme 5.2: Resonance structure of the double donor-acceptor motif.

Cyclic voltammetry was performed in ODCB for each dye (Figure 5.1). **I** and **II** both have a reduction potential onset at -1.25 V vs. Fc/Fc^+. The oxidation potential onset of **I** has been measured at +0.30 V vs. Fc/Fc^+ and the oxidation potential of **II** has been estimated from the reduction potential and the optical band gap at +0.75 V vs. Fc/Fc^+. For **I** the optical (1.65 eV) and electrochemical (1.55 eV) gaps in ODCB are similar.

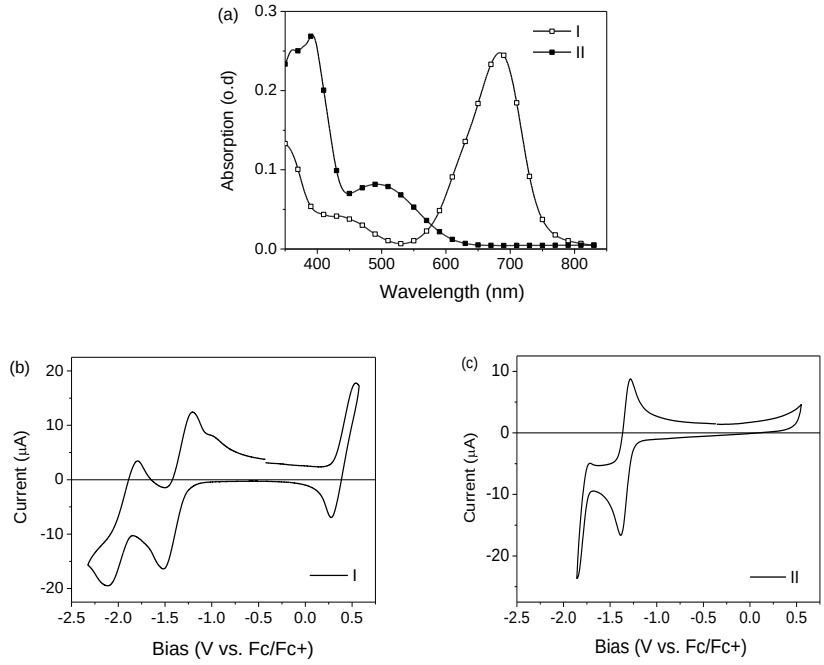

Figure 5.1: (a) Optical absorption spectra of **I** and **II** in solution in ODCB. (b,c) Cyclic voltamograms of **I** and **II** in solution in ODCB (0.1 M $TBAPF_6$).

Morphology. Blends of **I** and **II** with P3HT in a 1:1 weight ratio were spin coated from chloroform. The morphology of the resulting blends has been assessed by performing AFM. As shown in Figure 5.2, the phase images display distinct domains with large crystals segregating at the surface of the film. It seems that **I** and **II** do not intermix well with P3HT and crystallize during the spin-coating process. Crystal sizes of around 300 nm can be observed in a P3HT:**I** blend and the crystals are 10 times larger in P3HT:**II** blends.

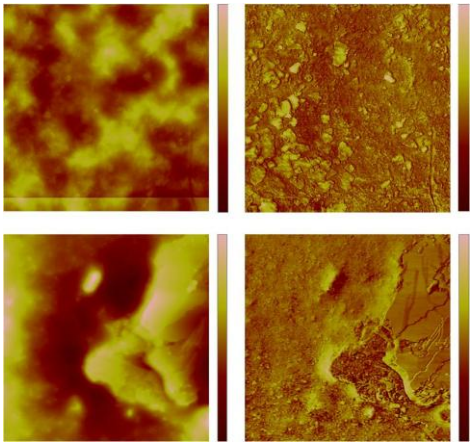

Figure 5.2: Height (left) and phase (right) AFM images of the surface of the P3HT:dye blends (3 µm × 3 µm). Top: P3HT:**I**, vertical scale 100 nm and 50°. Bottom P3HT:**II**, vertical scale 100 nm and 40°.

Photophysical processes in the blends. The reduction potentials of dyes **I** and **II** at -1.25 V vs. Fc/Fc^+ places their LUMO levels well below that of P3HT which has a reduction potential of -2.34 eV vs. Fc/Fc^+ (in solution). Also their HOMO levels are considerably lower as the oxidation potentials (+0.30 and +0.75 V vs. Fc/Fc^+) are higher than that of P3HT (+0.06 V vs. Fc/Fc^+). These LUMO-LUMO and HOMO-HOMO offsets should be large enough to allow photoinduced electron transfer from P3HT to **I** or **II**. To probe the charge transfer process, we compared the photoluminescence spectra of a pristine P3HT film and a dye-doped P3HT film. As can be seen in Figure 5.3, the luminescence of P3HT is quenched by a factor of 30 in the blends, providing a first indication of an efficient electron transfer process. We note that because the optical gap of **I** is smaller than that of P3HT, the luminescence quenching in the P3HT:**I** blend could also be due to energy transfer. The residual luminescence for both blends can be explained by the rather large phase segregation as observed by AFM.

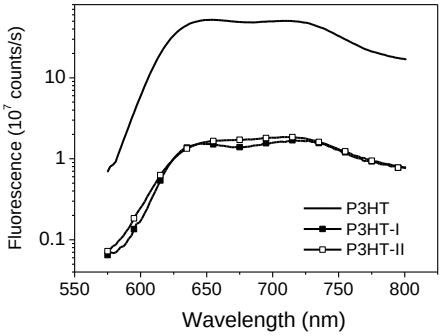

Figure 5.3: Fluorescence spectra recorded at room temperature of the pristine P3HT (black line), P3HT:**I** blend (closed squares) and P3HT:**II** blend (open squares).

To obtain more definite proof of the photoinduced charge transfer and to probe the formation of free charges, near-steady state PIA has been carried out. With this technique, long-lived free carriers can be detected.

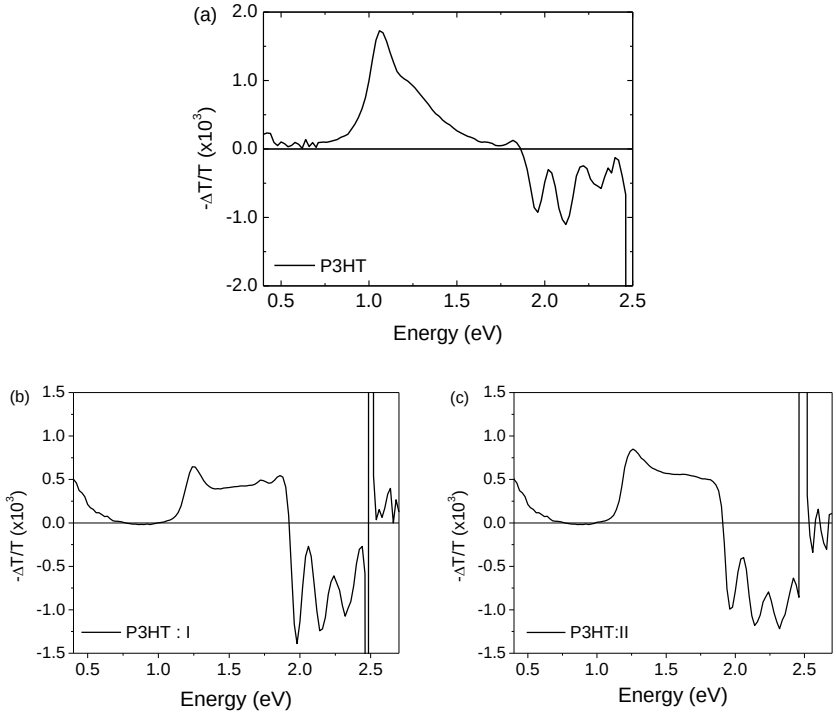

Figure 5.4: PIA spectra recorded at 80 K of (a) P3HT, (b) P3HT:**I** and (c) P3HT:**II**.

Figure 5.4a shows the PIA spectra of pristine P3HT. The $T_n \leftarrow T_1$ absorption of the pure P3HT triplet state is at 1.06 eV and bleaching signals are at 1.97 and 2.13 eV.[18,19] The weak PIA signal observed at ~0.5 eV is characteristic for the low-energy excitation of P3HT radical cations. The low intensity points out that only very few long-lived charges can be photogenerated in pristine P3HT. The PIA spectra of the dye-doped P3HT films are significantly different. The feature at 1.06 eV corresponding to the $T_n \leftarrow T_1$ transition has disappeared. Two signals with roughly the same intensity are observed, one broad plateau-like band at 1.25-1.85 eV and a signal at low energy (~0.5 eV). Both are characteristic of long-lived free charges. The band at 1.25-1.85 eV was already observed in blends of polythiophene with several acceptors and was assigned to the polymer radical cation.[20] This indicates efficient charge transfer and charge generation in P3HT:**I** and P3HT:**II** blends. These results make **I** and **II** attractive materials as alternative for fullerene in BHJ solar cells.

Solar cells. To investigate the charge transport properties of **I** and **II**, they were tested in a field-effect transistor (FET) employing a bottom gate - bottom contact configuration with Au source and drain electrodes and a passivated SiO_2 gate dielectric. In these FETs no appreciable source-drain current could be measured for both **I** and **II** and hence we conclude that their electron mobility is negligible.

Although the FET results indicate that **I** and **II** are not able to transport electrons, the dyes were applied in bulk heterojunction solar cell configurations with P3HT as the donor material. The active layers in 1:1 weight ratio were spin-coated from ODCB onto an indium tin oxide (ITO) covered glass substrate covered by a 50 nm film of PEDOT:PSS. LiF (1 nm) and Al (100 nm) were thermally evaporated as top electrode. For both dyes the device shows diode behaviour in the dark that is attributed to a hole current through the P3HT. Under illumination with simulated AM1.5G light a clear photocurrent is observed, but the absence of short-circuit current and open-circuit voltage demonstrates that there is no photovoltaic effect.

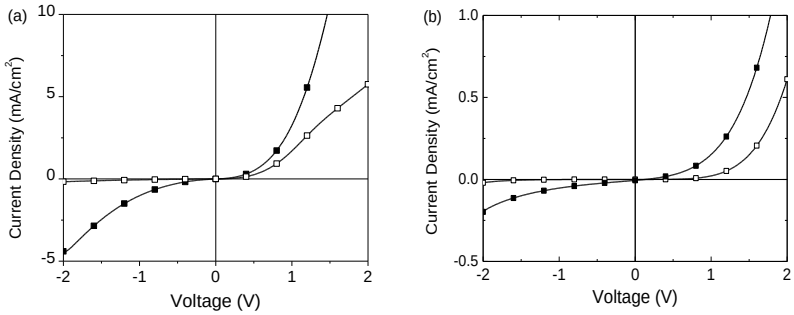

Figure 5.5: Representative *J-V* curves for P3HT:**I** and P3HT:**II** (weight ratio 1:1) solar cells in the dark (open markers) and under simulated AM1.5G conditions (closed markers).

5.3 Conclusions

The aim of this study was to synthesize electron-acceptor molecules with strong absorption in the visible and near IR regions combined with a low reduction potential in order to have a large driving force for photoinduced electron transfer from the P3HT donor material. Two dyes, **I** and **II**, have been successfully synthesized and present deep reduction potentials at -1.25 V vs. Fc/Fc^+, that are comparable with the common fullerene derivatives at -1.09 V vs. Fc/Fc^+. The optical band gaps of 1.65 and 2.00 eV and strong absorption bands make that **I** and **II** can both contribute to the optical absorption. Steady-state PIA measurements revealed the formation of long-lived free charges in thin films blends of dye **I** and **II** with P3HT. These results suggested that **I** and **II** can be attractive electron-acceptor materials in bulk-heterojunction solar cell, but this promise is not fulfilled because both dyes fail to have appreciable electron mobility. As a result, when blends of P3HT with dye **I** or **II** were sandwiched between transparent bottom and metal top electrodes only a photocurrent could be observed, but a photovoltaic effect was absent.

5.4 Experimental section

Materials and methods. Commercial chemicals were used as received. ^{1}H NMR and ^{13}C NMR spectra were recorded at 400 MHz on a VARIAN mercury spectrometer with $CDCl_3$ as the solvent and tetramethylsilane (TMS) as the internal standard. The peaks are given in ppm, relative to TMS (0 ppm). UV-vis-nearIR optical absorption spectra were recorded on a Perkin-Elmer Lambda 900 spectrophotometer. Cyclic voltammetry was conducted under an inert atmosphere with a scan rate of 0.1 V/s, using 1 M tetrabutylammonium hexafluorophosphate in ODCB as the electrolyte. The working electrode was a platinum disk and the counter electrode was a silver rod electrode. A silver wire coated with silver chloride (Ag/AgCl) was used as a quasi reference electrode in combination with Fc/Fc^{+} as an internal standard. Atomic force microscopy (AFM) was measured using a Veeco MultiMode with a Nanoscope III controller, in tapping mode. The used probes were PPP-NCH-50 from Nanosensors.

Photovoltaic devices were made by spin coating poly(ethylenedioxythiophene): poly(styrene sulfonate) (PEDOT:PSS) (Clevios P, VP Al4083) onto pre-cleaned, patterned indium tin oxide (ITO) substrates (14 Ω per square) (Naranjo Substrates). The top electrode, consisting of LiF (1 nm) and Al (100 nm), was deposited by vacuum evaporation at ~3×10^{-7} mbar. The active area of the cells was 0.091 cm^2. *J-V* characteristics were measured under ~100 mW/cm^2 white light from a tungsten-halogen lamp filtered by a Schott GG385 UV filter and a Hoya LB120 daylight filter, using a Keithley 2400 source meter. The thickness of the active layers in the photovoltaic devices was measured on a Veeco Dektak150 profilometer.

Field-effect transistors were fabricated using heavily doped silicon wafers as the common gate electrode with a 200 nm thermally oxidized SiO_2 layer as the gate dielectric. Using conventional photolithography, gold source and drain electrodes were defined in a bottom contact device configuration with channel width and length of 10000 μm and 10 μm, respectively. A 10 nm layer of titanium was used, acting as an adhesion layer for the gold on SiO_2. The SiO_2 layer was exposed to the vapor of the primer hexamethyldisilazane for 60 min. prior to semiconductor deposition in order to passivate the surface of the dielectric. Films of Dye **I** and Dye **II** were spun from a chloroform solution at 1000 rpm for 30 s. Freshly prepared devices were annealed in a dynamic vacuum of 10^{-5} mbar at 140 °C for 2 h to remove traces of solvent. All electrical measurements were performed in vacuum using an HP 4155C semiconductor parameter analyzer.

Photoinduced absorption (PIA) spectra were recorded by exciting with a mechanically modulated Ar-ion (496.5 nm) pump beam and monitoring the resulting change in transmission of a tungsten-halogen probe light through the sample (ΔT) with a phase-sensitive lock-in amplifier after dispersion by a grating monochromator and detection, using Si, InGaAs and cooled InSb detectors. The pump power incident on the sample was typically 25 mW with a beam diameter of 2 mm. The PIA ($\Delta T/T$) was corrected for the photoluminescence, which was recorded in a separate experiment. Photoinduced absorption spectra and photoluminescence spectra were recorded with the pump beam in a direction almost parallel to the direction of the probe beam. Temperature (80 K) of the samples was controlled by using an Oxford Optistat continuous flow cryostat.

***N*-Ethyl-3-iodoindole (2).** To a solution of indole **1** (5 g, 42.65 mmol) and potassium *tert*-butoxide (7.2 g, 64 mmol) in THF (200 mL), iodine (10.8 g, 42.65 mmol) was added in one portion. The reaction mixture was stirred at room temperature for 1 h. Potassium *tert*-butoxide (7.2 g, 64 mmol) and ethylbromide (3.8 mL, 51.2 mmol) were added and the reaction was stirred at reflux for 3 h. The solvent was evaporated under reduced pressure and the residue was extracted with ethyl acetate and water. The organic layers were combined, dried with Na_2SO_4 and concentrated to offer **2** (6.7 g, 24.6 mmol) in 56% yield. Compound **2** was used for the following reaction without purification because of its lability. ^{1}H NMR (400 MHz, $CDCl_3$) δ: 7.44 (d, J = 7.7 Hz, 1H), 7.31 (d, J = 8.15 Hz, 1H), 7.25 (m, 1H), 7.19 (s + m, 1H + 1H), 4.16 (q, J = 7.15, 2H), 1.45 (t, J = 7.15 Hz, 3H); ^{13}C NMR (100 MHz, $CDCl_3$) δ: 135.9, 131.1, 130.6, 122.6, 121.3, 120.3, 109.6, 55.0, 41.4, 15.6.

***N*-Ethyl-3-acetoxyindole (3).** Silver acetate (6.15 g, 36.9 mmol) was added to a solution of **2** (6.7 g, 24.6 mmol) in acetic acid (500 mL). After stirring for 1 h at 90 °C, the mixture was cooled to room temperature and filtered. The filtrate was evaporated to dryness under reduced pressure. The residue was chromatographed on silica gel with $CHCl_3$ to give **3** (1.0 g, 4.9 mmol) in 20 % yield. ^{1}H NMR (400 MHz, $CDCl_3$) δ: 7.55 (d, J = 8.05, 1H), 7.32 (s + m, 1H + 1H), 7.11 (t, J = 7.8 Hz, 1H), 7.23 (m, 1H), 4.14 (q, J = 7.3 Hz, 3H), 2.36 (s, 3H), 1.46 (t, J = 7.3 Hz, 3H); ^{13}C NMR (100 MHz, $CDCl_3$) δ: 168.7, 132.7, 129.3, 122.2, 120.2, 119.2, 117.6, 116.1, 109.3, 41.0, 21.0, 15.4.

***N,N'*-Diethylindigo (I).** Ammonia (25% wt., 6.5 mL, 88 mmol) was added to a solution of **3** (995 mg, 4.9 mmol) in methanol (20 mL). The resulting precipitate was collected by filtration, washed with water and dried. The residue was chromatographed on silica gel with $CHCl_3$ to give **I** (150 mg, 19 % yield). ^{1}H NMR (400 MHz, $CDCl_3$) δ: 7.71 (bd, *J* = 7.25 Hz, 2H), 7.52 (m, 2H), 7.14 (d, *J* = 8.15 Hz, 2H), 7.03 (t, *J* = 7.24 Hz, 2H), 4.26 (q, *J* = 7.18 Hz, 4H), 1.19 (t, *J* = 7.18 Hz, 6H). ^{13}C NMR (100 MHz, $CDCl_3$) δ: 186.1, 152.2, 134.9, 125.5, 124.1, 122.3, 121.1, 111.2, 42.8, 12.5.

***N*-Octylisatin (5).** Sodium hydride (526 mg, 13 mmol) was added portionwise to a solution of isatin (1.75 g, 12 mmol) in DMF (35 mL). The reaction mixture was stirred at room temperature for 2 h. A solution of *n*-octyl bromide (2.25 mL, 13 mmol) in DMF (3 mL) was added dropwise for 10 minutes and the reaction mixture was stirred at room temperature overnight. After extraction with ethyl acetate, the organic layer was washed with hydrochloric acid (0.4 N) and water. The organic fraction was dried over Na_2SO_4 and concentrated under vacuum. The resulting solid was recrystallized from hexane to offer **5** (2.3 g, 9 mmol) in 75% yield. ^{1}H NMR (400 MHz, $CDCl_3$) δ: 7.59 (m, 2H), 7.11 (t, *J* = 7.25 Hz, 1H), 6.90 (d, *J* = 7.25 Hz, 1H), 3.71 (t, *J* = 7.35 Hz, 2H), 1.70 (m, 2H), 1.29 (m, 10H), 0.87 (t, *J* = 6.54 Hz, 3H). ^{13}C NMR (100 MHz, $CDCl_3$) δ: 183.7, 158.1, 151.1, 138.3, 125.4, 123.6, 117.6, 110.2, 63.1, 40.3, 31.8, 29.4, 27.3, 25.8, 22.6, 14.1.

***N,N'*-Dioctylisoindigo (II).** A solution of **5** (650 mg, 2.5 mmol) in CH_2Cl_2 (10 mL) was cooled to –60 °C and tris(diethyl)phosphine (0.69 mL, 2.5 mmol) was added dropwise. The mixture was immediately allowed to warm to room temperature, the precipitate was filtered off and recrystallized from hexane to give the **II** (730 mg, 1.5 mmol) in 60% yield. ^{1}H NMR (400 MHz, $CDCl_3$) δ: 9.18 (dd, *J* = 7.96, 0.66 Hz, 2H), 7.34 (dt, *J* = 7.66, 1.13 Hz, 2H), 7.04 (dt, *J* = 8.13, 1.04 Hz, 2H), 6.78 (d, *J* = 7.74 Hz, 2H), 3.77 (t, *J* = 7.70 Hz, 4H), 1.70 (m, 4H), 1.34 (m, 20H), 0.87 (t, *J* = 7.12 Hz, 6H). ^{13}C NMR (100 MHz, $CDCl_3$) δ: 167.8, 144.7, 133.6, 132.3, 129.9, 122.1, 121.7, 107.9, 40.1, 31.8, 29.3, 29.2, 27.5, 27.1, 22.6, 14.1.

References

(1) Park, S. H. Roy, A. Beaupre, S. Cho, S. Coates, N. Moon, J. S. Moses, D. Leclerc, M. Lee, K.; Heeger, A. J. *Nat Photon* **2009**, *3*, 297.

(2) Liang, Y. Xu, Z. Xia, J. Tsai, S.-T. Wu, Y. Li, G. Ray, C.; Yu, L. *Adv. Mater.* **2010**, *22*, E135.

(3) Cook, S. Ohkita, H. Kim, Y. Benson-Smith, J. J. Bradley, D. D. C.; Durrant, J. R. *Chem. Phys. Lett.* **2007**, *445*, 276.

(4) Chesterfield, R. J. McKeen, J. C. Newman, C. R. Ewbank, P. C. da Silva Filho, D. A. Brédas, J.-L. Miller, L. L. Mann, K. R.; Frisbie, C. D. *J. Phys. Chem. B* **2004**, *108*, 19281.

(5) Gundlach, D. J. Pernstich, K. P. Wilckens, G. Grüter, M. Haas, S.; Batlogg, B. *J. Appl. Phys.* **2005**, *98*, 064502.

(6) Han, S. H. Lee, K. J. Lee, S. H.; Jang, J. *J. Non-Crystall. Solids* **2008**, *354*, 2870.

(7) Yoo, B. Jung, T. Basu, D. Dodabalapur, A. Jones, B. A. Facchetti, A. Wasielewski, M. R.; Marks, T. J. *Appl. Phys. Lett.* **2006**, *88*, 082104.

(8) Dittmer, J. J. Marseglia, E. A.; Friend, R. H. *Adv. Mater.* **2000**, *12*, 1270.

(9) Shin, R. Y. C. Kietzke, T. Sudhakar, S. Dodabalapur, A. Chen, Z.-K.; Sellinger, A. *Chem. Mater.* **2007**, *19*, 1892.

(10) Sonar, P. Ng, G.-M. Lin, T. T. Dodabalapur, A.; Chen, Z.-K. *J. Mater. Chem.* **2010**, *20*, 3626.

(11) Brunetti, F. G. Gong, X. Tong, M. Heeger, A. J.; Wudl, F. *Angew. Chem. Int. Ed.* **2009**, *48*, 532.

(12) Zhang, G. Fu, Y. Xie, Z.; Zhang, Q. *Macromolecules* **2011**, *44*, 1414.

(13) Stalder, R. Mei, J.; Reynolds, J. R. *Macromolecules* **2010**, *43*, 8348.

(14) Mei, J. Graham, K. R. Stalder, R.; Reynolds, J. R. *Org. Lett.* **2010**, *12*, 660.

(15) Xu, X. Li, L. Liu, B.; Zou, Y. *Appl. Phys. Lett.* **2011**, *98*, 063303.

(16) Serrano-Andrés, L.; Roos, B. O. *Chem. Eur. J.* **1997**, *3*, 717.

(17) Jacquemin, D. Preat, J. Wathelet, V.; Perpète, E. A. *J. Chem. Phys.* **2006**, *124*, 074104.

(18) van Hal, P. A. Christiaans, M. P. T. Wienk, M. M. Kroon, J. M.; Janssen, R. A. J. *J. Phys. Chem. B* **1999**, *103*, 4352.

(19) Veldman, D. Meskers, S. C. J.; Janssen, R. A. J. *Adv. Funct. Mater.* **2009**, *19*, 1939.

(20) Janssen, R. A. J. Christiaans, M. P. T. Hare, C. Martin, N. Sariciftci, N. S. Heeger, A. J.; Wudl, F. *J. Chem. Phys.* **1995**, *103*, 8840.

Chapter 6

Revisiting pyrrole as building block in small band gap polymers for solar cells

Abstract. By alternating diketopyrrolopyrrole units with aromatic segments involving pyrrole, three new small band gap (1.25-1.40 eV) polymers have been synthesized using a Stille cross-coupling polymerization. The three polymers exhibit excellent hole mobilities up to 0.57 cm^2/Vs. The materials were tested in bulk heterojunction solar cells with the acceptor [70]PCBM. The use of co-solvents had a strong effect on the active layer morphology and on the device performance. After optimization, power conversion efficiencies up to 3.3% have been reached with external quantum efficiencies up to 50% in the low energy region of the spectrum.

6.1 Introduction

In the 90's, two materials were developed to be used as donor materials in polymer solar cells: poly[2-methoxy-5-(3',7'-dimethyloctyloxy)-1,4-phenylene vinylene] (MDMO-PPV) and poly(3-hexylthiophene) (P3HT). When blended with [6,6]-phenyl-C_{61}-butyric acid methyl ester ([60]PCBM) these materials had power conversion efficiencies (PCEs) between 2.5 and 5%.[1-6] The major limiting parameter was the mismatch of the absorption spectrum of the active layer and the solar emission. The optical band gaps of MDMO-PPV and P3HT are 2.2 and 1.9 eV respectively, while the solar emission peaks around 1.75 eV. Accordingly, research focused on the development of new donor materials with smaller optical band gaps. Based on Havinga's work[7,8] on donor-acceptor polymers, Dhanabalan *et al.*[9-11] synthesized the first small band gap polymer (PTBTB) for use in organic solar cells involving an alternation of electron-rich *N*-dodecylpyrrole and electron-deficient 4,7-bis(2-thienyl)-2,1,3-benzothiadiazole units along the polymer chain (Scheme 6.1).

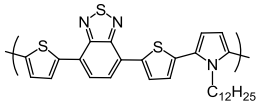

Scheme 6.1: Chemical structure of PTBTB, first small band gap polymer designed for use in polymer solar cells.

In recent years, a number of polymers based on the electron-deficient diketopyrrolopyrrole (DPP) unit have shown high performances in solar cells.[12-14] In most cases, DPP-based polymers need the use of 1,8-diiodooctane (DIO) or *o*-dichlorobenzene (ODCB) as additive in the processing solvent in order to create a favourable morphology and enhance their performance in bulk heterojunction solar cells.[14-19]

The aim of this chapter is to use a pyrrole unit as electron-rich unit and copolymerize it with three different DPP moieties: 3,6-bis(2-bromothieno[3,2-b]thiophen-5-yl)-2,5-bis(2'-octyldodecyl)pyrrolo[3,4-c]pyrrole-1,4(*2H,5H*)-dione, 3,6-bis(5-bromo-2-thienyl)-2,5-bis(2'-hexyldecyl)pyrrolo[3,4-c]pyrrole-1,4(*2H,5H*)-dione and 3,6-bis(5-bromo-2-selenyl)-2,5-bis(2'-octyldodecyl)pyrrolo[3,4-c]pyrrole-1,4(*2H,5H*)-dione (**2**, **3** and **4**, respectively in Scheme 6.2). The synthesis and optical properties of the three polymers are described. The new materials were tested in bulk heterojunctions with [70]PCBM. Their mobility was measured and morphological properties of the photoactive layers have been investigated in detail.

6.2 Results and discussion

Synthesis. The synthetic path to monomer **1** is depicted in Scheme 6.2. Treatment of *N*-methylpyrrole with TMEDA and *n*-buthyllithium in hexane at low temperature and subsequent quenching with excess of trimethyltinchloride gave 3,5-bis(trimethylstannyl)-*N*-methylpyrrole **1**. Monomers **2,**[19] **3**[14] and **4**[20] were synthesized according to literature methods. Stille polymerization of **1** with either **2**, **3**, or **4** using tetrakis(triphenylphosphine)palladium(0) in *o*-xylene offered polymers **PA**, **PB** and **PC**. The reactions were run under microwave conditions. The molecular weights (M_n) of **PA**, **PB** and **PC** are 25.5, 15.8 and 15.2 kg/mol respectively.

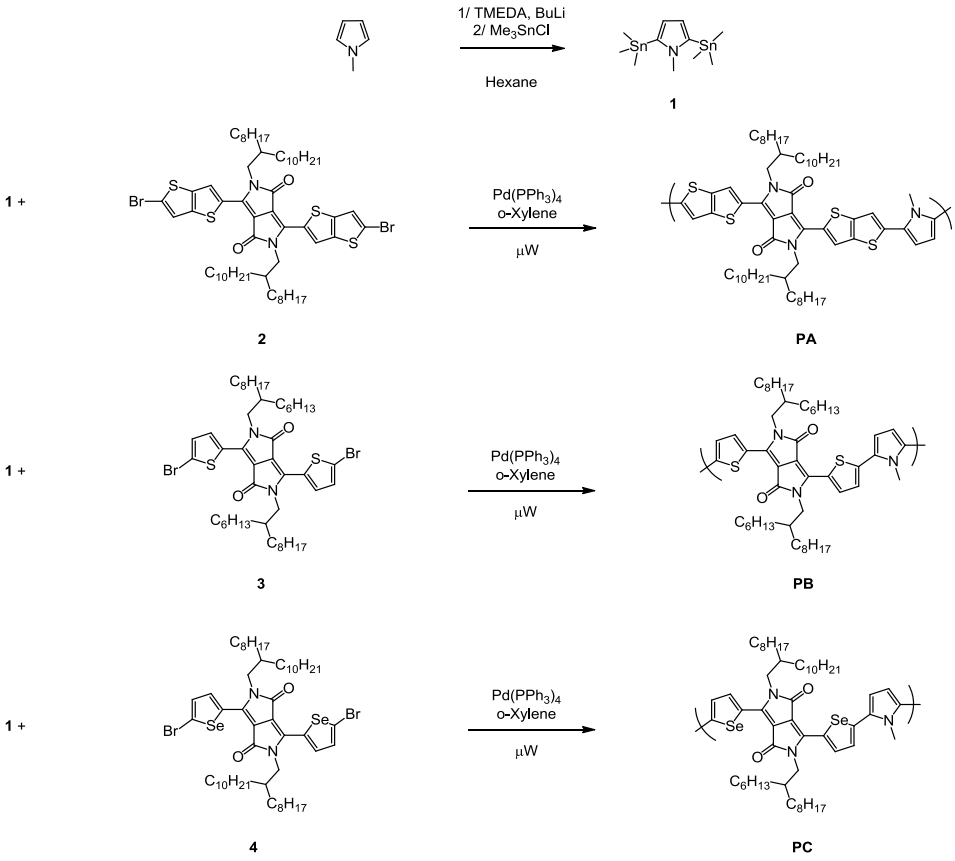

Scheme 6.2: Synthesis of monomer **1** and polymers **PA**, **PB** and **PC**.

Table 6.1: Molecular weights, optical and electrochemical properties of polymers **PA**, **PB** and **PC**.

	M_n (kg/mol)	M_w (kg/mol)	PDI	E_g^{sol} (eV)	E_g (eV)	E_{red} [a] (V)	E_{ox} [a] (V)	E_{cv}^{sol} (eV)
PA	25.5	50.2	1.97	1.47	1.40	-1.64	-0.14	1.50
PB	15.8	36.5	2.30	1.36	1.32	-1.53	-0.16	1.37
PC	15.2	27.8	1.82	1.32	1.24	-1.42	-0.10	1.32

[a] CV measurements in ODCB (0.1M TBAPF6) vs. Fc/Fc^+ as internal standard.

Optical and electrochemical properties. The room temperature absorption spectra of the polymers dissolved in ODCB and as thin film are shown in Figure 6.1 together with the cyclic voltammograms that were recorded for the polymers in ODCB. The results are collected in Table 6.1. The optical band gaps determined at the onset of absorption are 1.47, 1.35 and 1.29 eV for **PA**, **PB** and **PC**, respectively. Increasing the length of the aromatic segment between two DPP units as in **PA** increases the optical band gap by about 0.1 eV compared to **PB** and **PC**. The reduced optical band gap of **PC** compared to **PB** is analogous to the reduction of the optical band gap of poly(3-hexylselenophene) (P3HS) compared to P3HT.[21] In this case the reduction of the optical band gap is due to a lower energy of the LUMO level, which has been ascribed to a larger stabilization of the LUMO by selenium than by sulfur, because of its smaller ionization potential and the direct relation that exists between the LUMO energy and the ionization potential.[21,22] We note that the reduction potential of PCBM is -1.09 eV vs. Fc/Fc^+ and that the LUMO-LUMO offset between **PC** and PCBM is only 0.3 eV. It is believed that an energy difference of at least 0.35 eV is necessary to ensure efficient charge transfer.[23-25] Hence, the driving force for electron transfer might be on borderline in the case of **PC**:PCBM blends.

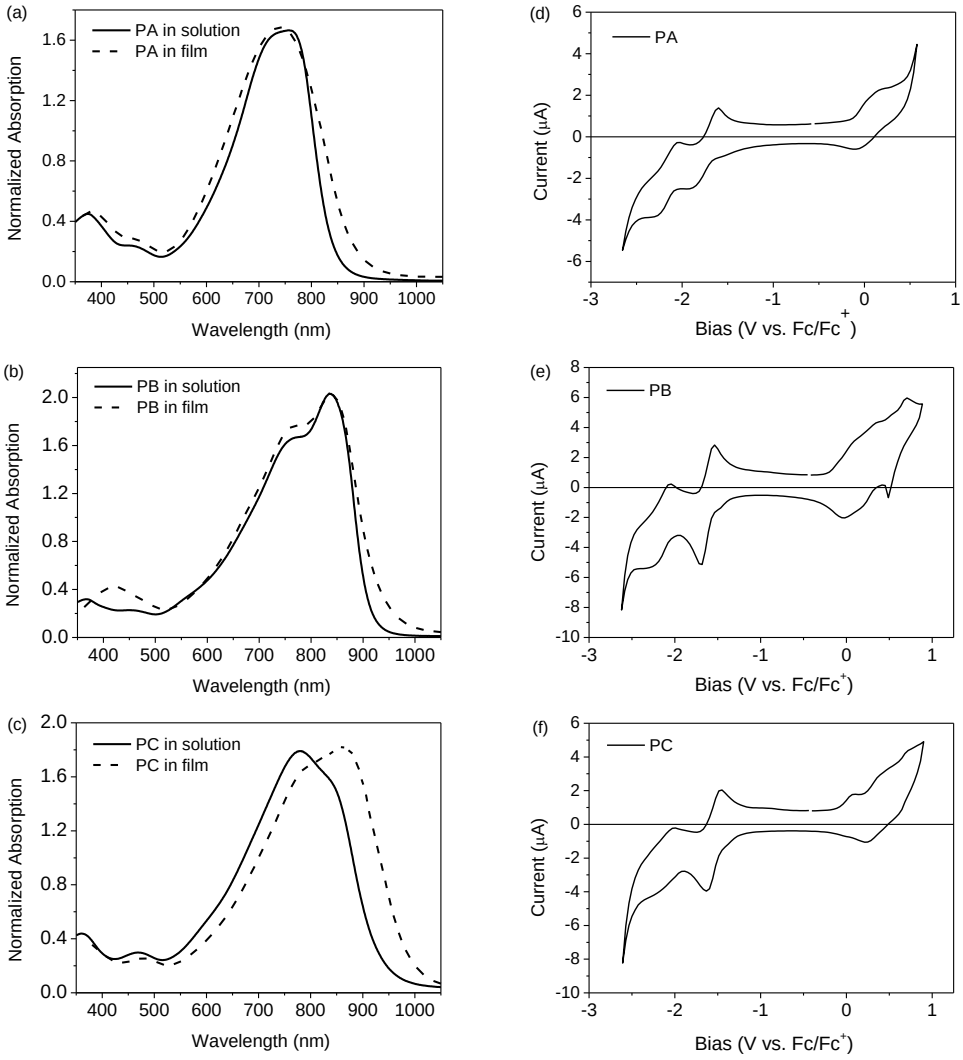

Figure 6.1: Optical absorption spectra of **PA** (a), **PB** (b) and **PC** (c). The solid lines represent the absorption of the polymers in solution in ODCB. The dashed lines represent the absorption of the polymers in thin films. Cyclic voltammograms of **PA** (d), **PB** (e) and **PC** (f) in ODCB solution with 0.1 M $TBAPF_6$.

Solar cells. The polymers were applied in bulk heterojunction solar cells with [70]PCBM. The active layers with thicknesses of about 100 nm, were spin coated onto an indium tin oxide (ITO) covered glass substrate covered by a 50 nm film of PEDOT:PSS. LiF (1 nm) and Al (100 nm) were thermally evaporated as top electrode. The composition of the active layer was optimized between polymer:[70]PCBM weight ratios of 1:1 and 1:3; the ratio 1:2 was found to give the highest power conversion efficiency (PCE). The active layers were spin coated from chloroform with different concentration of ODCB or DIO. The variation in performance as a function of the additive concentration is represented in Figure 6.2 for **PA**:[70]PCBM and Figure 6.3 for **PB**:[70]PCBM.

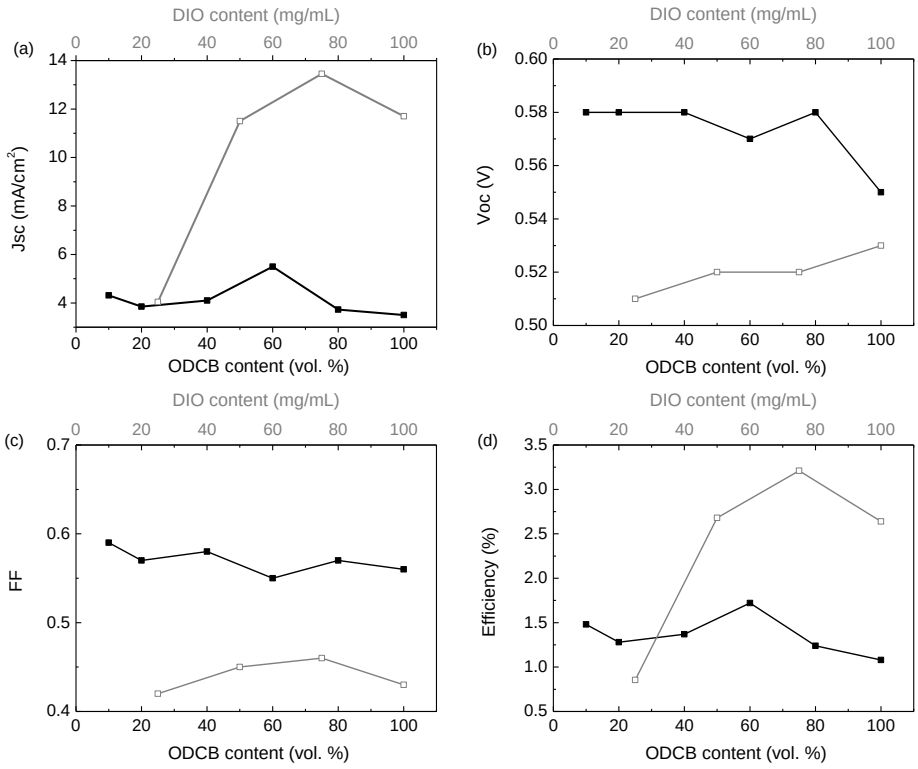

Figure 6.2: Variation of J_{sc} (a), V_{oc} (b), FF (c) and PCE (d) as a function of additive content for **PA**:[70]PCBM solar cells. The grey line with open symbols represents the performance of devices processed with DIO as processing additive in chloroform. The black line with closed symbols represents the performance of devices processed using ODCB as a co-solvent in chloroform.

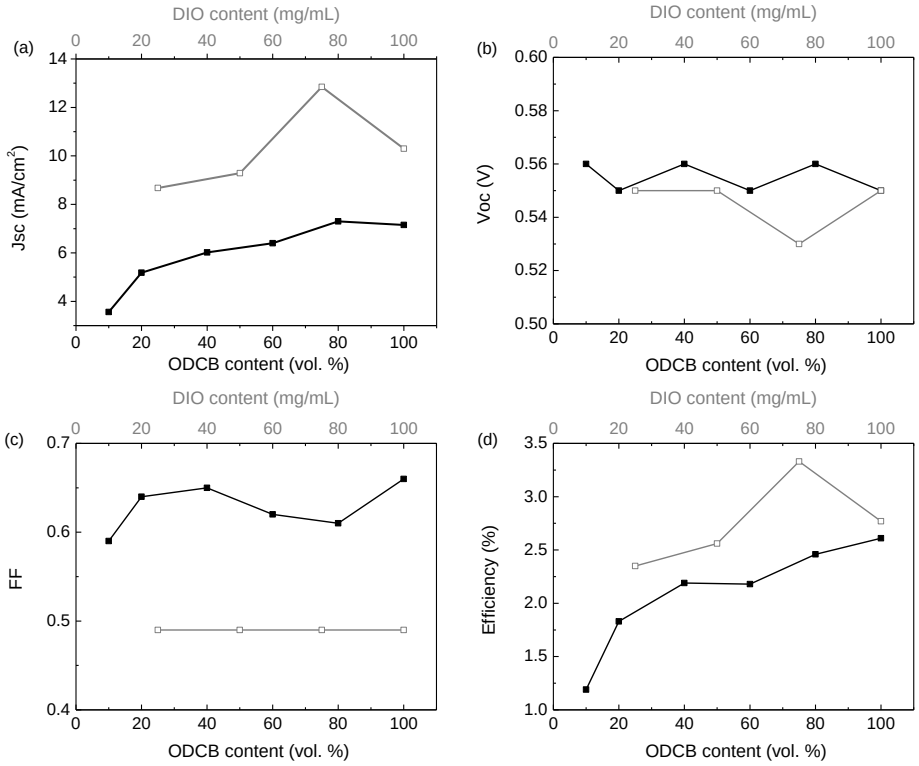

Figure 6.3: Variation of J_{sc} (a), V_{oc} (b), FF (c) and PCE (d) as a function of additive content for **PB**:[70]PCBM solar cells. The grey line with open symbols represents the performance of devices processed with DIO as processing additive in chloroform. The black line with closed symbols represents the performance of devices processed using ODCB as a co-solvent in chloroform.

PA:[70]PCBM blends were first processed from chloroform with different concentrations of ODCB as co-solvent. Almost no changes in fill factor (FF ≈ 0.58) and open circuit voltage (V_{oc} ≈ 0.58 V) are observed as the co-solvent concentration is increased. The short circuit current (J_{sc}) varies more; from J_{sc} = 4.31 mA/cm^2 for 10% ODCB to 5.5 mA/cm^2 for 60% ODCB, where the maximum in J_{sc} – and thus in PCE – is obtained. This improvement is attributed to a change in morphology. Representative AFM images are shown in Figures 6.4a and 6.4b. When using 10% ODCB large, irregularly shaped [70]PCBM domains protrude at the film surface. The mixing seems to increase significantly when the amount of ODCB as co-solvent in chloroform is increased to 60%. At this concentration the domain size becomes smaller and the layer smoother.

PA:[70]PCBM blends were also processed using chloroform solutions with different concentrations of DIO. An optimum in PCE is observed for a 75 mg/mL DIO concentration. The device exhibits a high J_{sc} of 13.45 mA/cm^2. While the use of DIO thus provides more than a doubling of J_{sc} compared to the best devices processed with ODCB, its use goes at the expense of the V_{oc} and FF which reduce to 0.52 V and 0.46, respectively. However, the PCE increases to 3.2%. The use of DIO as processing additive significantly changes the morphology of the films compared to ODCB as co-solvent. The AFM height image (Figure 6.4c) shows that the surface is corrugated, indicating phase separation.

Like for the **PA** blends, **PB**:[70]PCBM blends were first processed from chloroform with different concentration of ODCB. Similar to **PA**, almost no changes in FF (~0.62) and V_{oc} (~0.55 V) were observed with increasing concentration of the co-solvent. However, J_{sc} and PCE increase significantly with increasing amount of ODCB and reach their highest values when the active layer is processed from pure ODCB. The current rises from J_{sc} = 3.56 mA/cm^2 for 10% ODCB in chloroform to 7.15 mA/cm^2 for pure ODCB. Like for **PA**, this improvement is attributed to a change in morphology. As shown in Figure 6.4d irregularly shaped [70]PCBM domains are observed in the AFM height image when the layers are processed from 10% ODCB in chloroform. When pure ODCB is used as solvent, these domains disappear and the two materials become better intermixed (Figure 6.4e). When processing **PB**:[70]PCBM blends from chloroform with different concentrations of DIO, similar changes occur as for **PA**:[70]PCBM: J_{sc} increases dramatically up to 12.45 mA/cm^2 and FF drops to 0.49. In this case V_{oc} is reduced only slightly to 0.55 V. The PCE increases to 3.3%. The films appear to be somewhat rougher than the films processed from ODCB and the regions seem slightly smaller (Figure 6.4f).

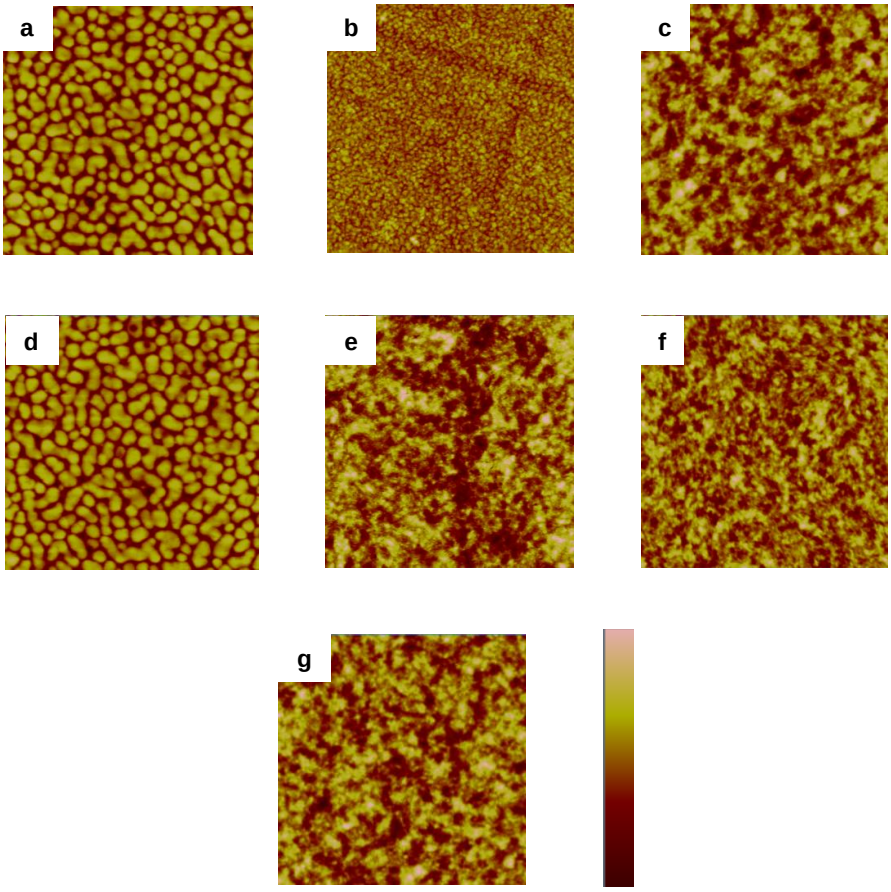

Figure 6.4: AFM height images of the surface of the **PA**:[70]PCBM blends processed from 10% ODCB in chloroform (a), 60% ODCB in chloroform (b) and 75 mg/mL DIO in chloroform (c); **PB**:[70]PCBM blends processed from 10% ODCB in chloroform (d), pure ODCB (e) and 75 mg/mL DIO in chloroform (f); **PC**:[70]PCBM blends processed from 100 mg/mL DIO in chloroform (g). All images show 5 µm × 5 µm areas with vertical scale: 40 nm (a,d); 30 nm (c, f, g); 20 nm (b,e).

The results show that for **PA** and **PB**, the effect of ODCB and DIO as co-solvent or processing additive to chloroform is quite different. This is opposite to what has been seen before for other DPP-based *p*-type polymers.[26] For **PA** and **PB**, the use of DIO induces a significant gain in current but also a large loss in FF. Looking carefully at the *J*-*V* curves depicted in Figure 6.5, the loss of FF for the devices processed with DIO is due to a less efficient charge collection close to open-circuit. On the other hand, for the devices processed with ODCB the photocurrent increases more strongly under reverse bias. For

PA:[70]PCBM the increase in photocurrent going from 0 to -2 V is about 80% when the blend processed with ODCB, but only 13% when processed with DIO. This field-assisted carrier collection for the ODCB processed cells shows that many more carriers are created than can be collected at short circuit. For **PB**:[70]PCBM the effect is also seen, but smaller (28% vs. 16%). Together with the higher FF the field-dependent photocurrent under reverse bias for **PA** and **PB** devices processed from ODCB indicates that some charges are easily collected but that for others a relatively strong reverse field is required for collection. For the DIO-processed cells the higher current, low FF and reduced field-dependence under reverse bias, suggest that only one mechanism for charge collection prevails. Clearly, the low FF indicates that separation and collection are not optimal. Of course, as more charges are created, the probability for them to meet and recombine – especially at low field – is enhanced.

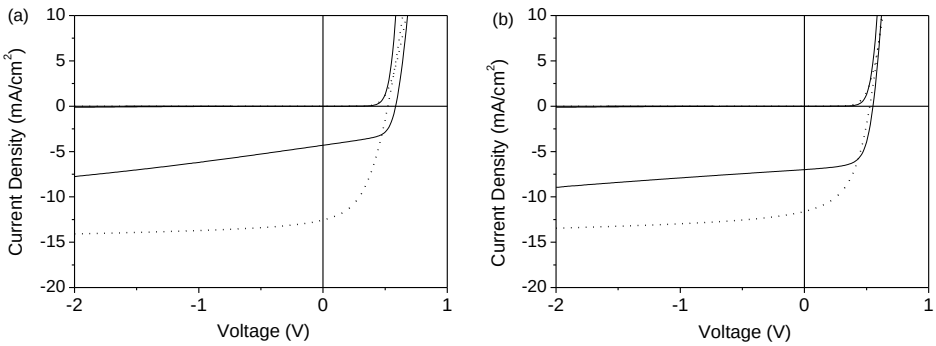

Figure 6.5: Representative *J-V* curves for **PA**:[70]PCBM (a) and **PB**:[70]PCBM (b) solar cells. The solid line represents the *J-V* curve of blends processed from ODCB and chloroform. The dotted line represents the *J-V* curve of blends processed from DIO and chloroform.

PC behaves differently in devices compared to **PA** and **PB**. Processing from a mixture of chloroform and ODCB does not give such a high PCE. This material needs to be processed from chloroform with 100 mg/mL DIO to give its best performance. The device exhibits J_{sc} = 9.81 mA/cm^2, V_{oc} = 0.47 V and FF = 0.59, resulting in a PCE of 2.49%. Compared to **PA** and **PB**, the cells made with **PC** stand out for their high FF, but the V_{oc} is somewhat less than expected considering that **PC** has the highest oxidation potential. The surface topology of the **PC**:[70]PCBM film processed from DIO/chloroform is similar to those obtained for **PA** and **PB** under similar conditions (compare panels c, f and g in Figure 6.5).

The performance of the best devices processed from DIO/chloroform is collected in Table 6.2. Figure 6.6 shows the corresponding *J-V* curves and the spectrally resolved external quantum efficiencies (EQE). For each of the three polymers the contribution of the polymer absorption to the EQE is evident, with onsets between 925 and 1025 nm. For **PA**:[70]PCBM and **PB**:[70]PCBM the maximum EQE in the low energy region reaches between 45% and 50%, but for **PC**:[70]PCBM the EQE is significantly lower (25%). As mentioned, the LUMO-LUMO offset between **PC** and PCBM is on the borderline for efficient charge transfer, which may rationalize the lower EQE in this case. A more refined estimate can be made using the expected energies of the charge transfer state (E_{CT}) in the three blends and comparing it to the optical band gaps. This CT energy can be estimated from the E_{HOMO}^{opt} and E_{LUMO}^{opt} energies via the empirical relation, as explained in Ref. 27.

$$E_{CT} = | E_{HOMO}^{opt}(D) - E_{LUMO}^{opt}(A) | + 0.29\,eV \quad (6.1)$$

This provides E_{CT} = 0.99, 0.98 and 1.02 eV as CT energies for the blends of **PA**, **PB** and **PC** with [70]PCBM respectively. As a consequence, the energy difference $E_g - E_{CT}$ decreases for the polymer:[70]PCBM blends from 0.42 eV for **PA**, via 0.34 eV for **PB**, to 0.22 eV for **PC**. In each case the energy difference is larger than the criterion of $E_g - E_{CT} \geq$ 0.08 (±0.02) eV that has been established empirically for electron transfer to occur,[27] but the lowering of the driving force for electron transfer (i.e. $E_g - E_{CT}$) going from **PA**, via **PB**, to **PC** coincides with a loss of EQE in the low energy region.

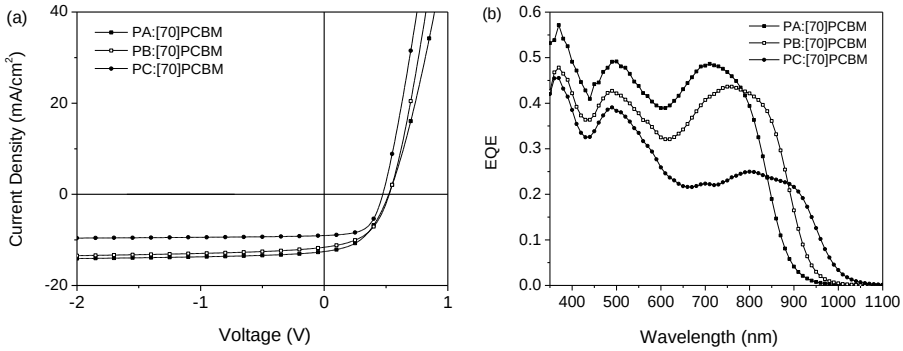

Figure 6.6: Representative *J-V* curves (a) for **PA**:[70]PCBM, **PB**:[70]PCBM and **PC**:[70]PCBM solar cells under simulated AM1.5G conditions. EQE spectra (b) of **PA**:[70]PCBM, **PB**:[70]PCBM and **PC**:[70]PCBM solar cells under 1 Sun equivalent light bias illumination.

Table 6.2: Characteristics of the best polymer:[70]PCBM devices under 100 mW/cm^2 white light illumination all processed from chloroform, using DIO as an additive.

	Ratio	*d* (nm)	J_{sc} (mA/cm^2)	V_{oc} (V)	FF	PCE (%)
PA:[70]PCBM	1:2	98	13.45	0.52	0.46	3.21
PB:[70]PCBM	1:2	102	12.85	0.53	0.49	3.33
PC:[70]PCBM	1:2	100	9.81	0.47	0.59	2.49

Field effect transistors. Hole mobilities of polymers, measured in a top gate bottom contact field-effect transistor, were determined from the slope of the square root of the source drain current versus the gate voltage in the saturation regime. **PA**, **PB** and **PC** exhibit excellent hole mobilities of 0.11, 0.36 and 0.57 cm^2/Vs respectively. The transfer and output characteristics are displayed in Figure 6.7.

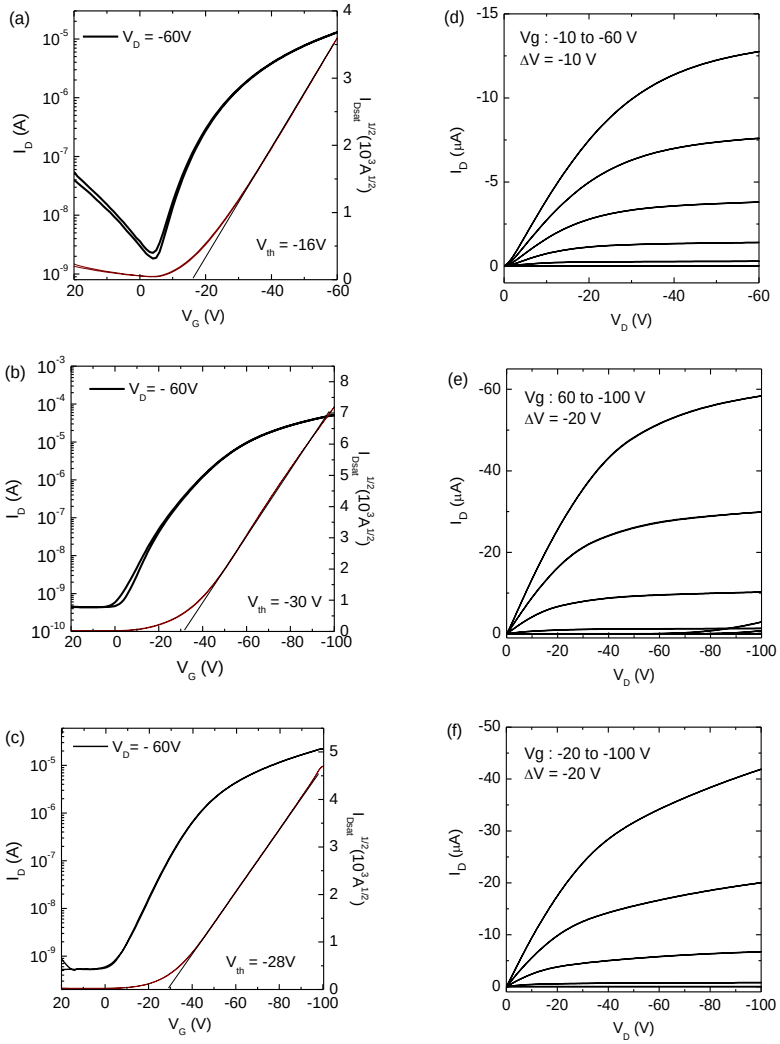

Figure 6.7: Transfer characteristics of **PA** (a), **PB** (b) and **PC** (c). Output characteristics of **PA** (d), **PB** (e) and **PC** (f).

6.3 Conclusions

Three new diketopyrrolopyrrole-based polymers with optical band gaps varying from 1.45 to 1.25 eV have been synthesized. All three polymers show excellent hole mobility between 0.1 and 0.6 cm^2/Vs. When applied in bulk heterojunction solar cells with [70]:PCBM, **PA** and **PB** show similar performances with high currents and a limiting fill factor of around 0.5. The power conversion efficiency is 3.2 and 3.3 % respectively with external quantum efficiency up to 50%. **PC** shows somewhat lower performance, characterized by a low EQE of 25%, probably due to a smaller driving force for photoinduced electron transfer.

6.4 Experimental section

Materials and methods. Polymerization reactions were conducted under an argon atmosphere. Commercial chemicals were used as received. ^{1}H NMR and ^{13}C NMR spectra were recorded at 400 MHz on a VARIAN mercury spectrometer with $CDCl_3$ as the solvent and tetramethylsilane (TMS) as the internal standard. The peaks are given in ppm, relative to TMS (0 ppm). Molecular weights were determined with GPC on a Shimadzu LC-10AD using a Polymer Laboratories Resipore column (length 300 mm, diameter 7.5 mm), a Shimadzu SPD-M20A photodiode array detector from 250-700 nm and ODCB as the eluent with a flow rate of 1 mg/min. (T = 293 K). Polystyrene standards were used.

UV-vis-nearIR spectra were recorded on a Perkin-Elmer Lambda 900 spectrophotometer. Cyclic voltammetry was conducted under an inert atmosphere with a scan rate of 0.1 V/s, using 1 M tetrabutylammonium hexafluorophosphate in ODCB as the electrolyte. The working electrode was a platinum disk and the counter electrode was a silver rod electrode. Fc/Fc^+ was used as an internal standard. Atomic force microscopy (AFM) was measured using a Veeco MultiMode with a Nanoscope III controller, in tapping mode. The used probes were PPP-NCH-50 from Nanosensors.

Photovoltaic devices were made by spin coating poly(ethylenedioxythiophene): poly(styrene sulfonate) (PEDOT:PSS) (Clevios P, VP Al4083) onto pre-cleaned, patterned indium tin oxide (ITO) substrates (14 Ω per square) (Naranjo Substrates). The counter electrode, consisting of LiF (1 nm) and Al (100 nm), was deposited by vacuum evaporation at ~3×10^{-7} mbar. The active area of the cells was 0.091 cm^2. *J-V* characteristics were measured under ~100 mW/cm^2 white light from a tungsten-halogen lamp filtered by a

Schott GG385 UV filter and a Hoya LB120 daylight filter, using a Keithley 2400 source meter. Short-circuit currents under AM1.5G conditions were estimated from the spectral response and convolution with the solar spectrum. The spectral response was measured under simulated 1 Sun operation conditions using bias light from a 532 nm solid state laser (Edmund Optics). Monochromatic light from a 50 W tungsten halogen lamp (Philips focusline) in combination with a monochromator (Oriel, Cornerstone 130) was modulated with a mechanical chopper. The response was recorded as the voltage over a 50 Ω resistance, using a lock-in amplifier (Stanford research Systems SR830). A calibrated Si cell was used as reference. The device was kept behind a quartz window in a nitrogen filled container. The thickness of the active layers in the photovoltaic devices was measured on a Veeco Dektak150 profilometer.

Top-gate, bottom-contact field-effect transistors were fabricated on glass with pentafluorobenzenethiol (PFBT) treated Au electrodes, a CYTOP dielectric and an Al gate. Polymer films were spin coated at 2000 rpm from chlorobenzene solution (5 mg/ml) and annealed for 10 min. at 300 °C for **PA** and at 200 °C for **PB** and **PC**.

2,5-Bis(trimethylstannyl)-*N*-methylpyrrole (1): To a solution of TMEDA (3.6 mL, 24.0 mmol) in hexane (50 mL), *n*-butyllithium (2.5 M in hexane, 9.6 mL, 24.0 mmol) was added over 15 min. at room temperature. N-methylpyrrole (10.3 mmol) was added and the mixture was refluxed for 9 h. After cooling to -30 °C a solution of $(CH_3)_3SnCl$ (5.86 g, 24.0 mmol) in hexane (10 mL) was added dropwise. The mixture was allowed to warm to room temperature and stirred for 15 h. Volatile compounds were removed under reduced pressure, the residue was dissolved in hexane and filtered. The filtrate was concentrated in vacuo and the colorless solid obtained was recrystallized from acetonitrile. Yield: 2.88 g (69%) colorless **1**. ^{1}H NMR ($CDCl_3$, 400 MHz): 0.22 [s, 18 H, ^2J(H,^{117}Sn) 53.4 Hz (7.1%), ^2J(H,^{119}Sn) 55.9 Hz (7.7%), SnCH_3], 3.41 (s, 3 H, ^4J(H,Sn) 2.4 Hz, NCH_3), 6.65 (s, 2 H, ^3J(H,Sn) 10.5 Hz, C*H*). ^{13}C NMR ($CDCl_3$, 100 MHz): 136.3, 120.1 (^2J(C,Sn) 50.5 Hz and 60.5 Hz, *C*H), 39.4 (NCH_3), 8.8 (^1J(C,Sn) 348.3 Hz and 364.3 Hz, SnCH_3).

Polymer PA. To a microwave vial were added 3,6-bis(2-bromothieno[3,2-*b*]thiophen-5-yl)-2,5-bis(2'-octyldodecyl)pyrrolo[3,4-*c*]pyrrole-1,4(2*H*,5*H*)-dione (**2**) (200 mg, 0.18 mmol), 2,5-bis(trimethylstannyl)-*N*-methylpyrrole (**1**) (71.9 mg, 0.18 mmol) and the solids were dissolved in *o*-Xylene (0.6 mL). The solution was then degassed before addition of $Pd(PPh_3)_4$ (20 mg, 0.018 mmol). The reaction mixture was further degassed and

subsequently sealed. The vial was heated in a microwave reactor at 100 °C (2 min.), 140 °C (2 min.), 170 °C (2 min.) and 200 °C (30 min.). After cooling to room temperature, the mixture was precipitated in methanol (200 mL), the precipitate was filtered and washed with methanol (2 × 25 mL). The solid polymer was purified by Soxhlet extraction with acetone (24 h), hexane (24 h) and finally chloroform (12 h). An aqueous solution of sodium diethyldithiocarbamate (~1 g/100 mL) was added to the chloroform layer and the mixture was heated to 60 °C with vigorous stirring for 2 h. After cooling to room temperature, the layers were separated and the organic fraction was extracted with water (4 × 250 mL) and concentrated under reduced pressure. The resulting residue was dissolved in a minimum amount of chloroform and added dropwise to vigorously stirred methanol (250 mL). The resulting precipitate was isolated by filtration and dried *in vacuo* to afford **PA** (80 mg, 43%). GPC(PS): M_n = 25.5 kg/mol, PDI = 1.97. ^{1}H (400 MHz, $CDCl_3$) δ: 9.22 (br, 2H), 7.47 (br, 2H), 6.97 (br, 2H), 3.98 (br, 4H), 1.90 (br, 2H) 1.20-1.00 (m, 64H), 0.80-0.70 (m, 12H).

Polymer PB. 3,6-bis(5-bromo-2-thienyl)-2,5-bis(2'-hexyldecyl)pyrrolo[3,4-c]pyrrole-1,4(*2H,5H*)-dione (200 mg, 0.22 mmol) (**3**), 2,5-bis(trimethylstannyl)-*N*-methylpyrrole (**1**) (89.7 mg, 0.22 mmol) and $Pd(PPh_3)_4$ (25 mg, 0.022 mmol) were reacted according to the procedure described above to give **PB** (60 mg, 33%). GPC(PS): M_n = 15.8 kg/mol, PDI = 2.3. ^{1}H (400 MHz, $CDCl_3$) δ: 8.89 (br, 2H), 7.34 (br, 2H), 6.98 (br, 2H), 4.01 (br, 4H), 1.90 (br, 2H) 1.22-1.00 (m, 48H), 0.80-0.70 (m, 12H).

Polymer PC. 3,6-bis(5-bromo-2-selenyl)-2,5-bis(2'-octyldodecyl)pyrrolo[3,4-c]pyrrole-1,4(*2H,5H*)-dione (**4**) (200 mg, 0.18 mmol), 2,5-bis(trimethylstannyl)-*N*-methylpyrrole (**1**) (73.1 mg, 0.18 mmol) and $Pd(PPh_3)_4$ (20 mg, 0.018 mmol) were reacted according to the procedure described above to give **PC** (50 mg, 30%). GPC(PS): M_n = 15.2 kg/mol, PDI = 1.82. ^{1}H (400 MHz, $CDCl_3$) δ: 8.82 (br, 2H), 7.29 (br, 2H), 6.93 (br, 2H), 3.95 (br, 4H), 1.90 (br, 2H) 1.20-1.00 (m, 64H), 0.80-0.70 (m, 12H).

6.5 References

(1) Wienk, M. M.; Kroon, J. M.; Verhees, W. J. H.; Knol, J.; Hummelen, J. C.; van Hal, P. A.; Janssen, R. A. J. *Angew. Chem. Int. Ed.* **2003**, *42*, 3371.

(2) Shaheen, S. E.; Brabec, C. J.; Sariciftci, N. S.; Padinger, F.; Fromherz, T.; Hummelen, J. C. *Appl. Phys. Lett.* **2001**, *78*, 841.

(3) Li, G.; Shrotriya, V.; Huang, J.; Yao, Y.; Moriarty, T.; Emery, K.; Yang, Y. *Nat Mater* **2005**, *4*, 864.

(4) Yu, G.; Gao, J.; Hummelen, J. C.; Wudl, F.; Heeger, A. J. *Science* **1995**, *270*, 1789.

(5) Schilinsky, P.; Waldauf, C.; Brabec, C. J. *Appl. Phys. Lett.* **2002**, *81*, 3885.

(6) Padinger, F.; Rittberger, R. S.; Sariciftci, N. S. *Adv. Funct. Mater.* **2003**, *13*, 85.

(7) Havinga, E. E.; Hoeve, W.; Wynberg, H. *Polym. Bull.* **1992**, *29*, 119.

(8) Havinga, E. E.; ten Hoeve, W.; Wynberg, H. *Synth. Met.* **1993**, *55*, 299.

(9) Dhanabalan, A.; van Duren, J. K. J.; van Hal, P. A.; van Dongen, J. L. J.; Janssen, R. A. J. *Adv. Funct. Mater.* **2001**, *11*, 255.

(10) Brabec, C. J.; Winder, C.; Sariciftci, N. S.; Hummelen, J. C.; Dhanabalan, A.; van Hal, P. A.; Janssen, R. A. J. *Adv. Funct. Mater.* **2002**, *12*, 709.

(11) Winder, C.; Mühlbacher, D.; Neugebauer, H.; Sariciftci, N. S.; Brabec, C.; Janssen, R. A. J.; Hummelen, J. K. *Mol. Cryst. Liq. Cryst.* **2002**, *385*, 93.

(12) Zou, Y.; Gendron, D.; Badrou-Aïch, R.; Najari, A.; Tao, Y.; Leclerc, M. *Macromolecules* **2009**, *42*, 2891.

(13) Zoombelt, A. P.; Mathijssen, S. G. J.; Turbiez, M. G. R.; Wienk, M. M.; Janssen, R. A. J. *J. Mater. Chem.* **2010**, *20*, 2240.

(14) Bijleveld, J. C.; Zoombelt, A. P.; Mathijssen, S. G. J.; Wienk, M. M.; Turbiez, M.; de Leeuw, D. M.; Janssen, R. A. J. *J. Am. Chem. Soc.* **2009**, *131*, 16616-16617.

(15) Bijleveld, J. C.; Gevaerts, V. S.; Di Nuzzo, D.; Turbiez, M.; Mathijssen, S. G. J.; de Leeuw, D. M.; Wienk, M. M.; Janssen, R. A. J. *Adv. Mater.* **2010**, *22*, E242-E246.

(16) Woo, C. H.; Beaujuge, P. M.; Holcombe, T. W.; Lee, O. P.; Fréchet, J. M. J. *J. Am. Chem. Soc.* **2010**, *132*, 15547.

(17) Bijleveld, J. C.; Karsten, B. P.; Mathijssen, S. G. J.; Wienk, M. M.; de Leeuw, D. M.; Janssen, R. A. J. *J. Mater. Chem.* **2011**, *21*, 1600.

(18) Bijleveld, J. C.; Verstrijden, R. A. M.; Wienk, M. M.; Janssen, R. A. J. *J. Mater. Chem.* **2011**, *21*, 9224.

(19) Bronstein, H.; Chen, Z.; Ashraf, R. S.; Zhang, W.; Du, J.; Durrant, J. R.; Shakya Tuladhar, P.; Song, K.; Watkins, S. E.; Geerts, Y.; Wienk, M. M.; Janssen, R. A. J.; Anthopoulos, T.; Sirringhaus, H.; Heeney, M.; McCulloch, I. *J. Am. Chem. Soc.* **2011**, *133*, 3272.

(20) Shahid, M. *to be published*.

(21) Heeney, M.; Zhang, W.; Crouch, D. J.; Chabinyc, M. L.; Gordeyev, S.; Hamilton, R.; Higgins, S. J.; McCulloch, I.; Skabara, P. J.; Sparrowe, D.; Tierney, S. *Chem. Commun.* **2007**, 5061.

(22) Villar, H. O.; Otto, P.; Dupuis, M.; Ladik, J. *Synth. Met.* **1993**, *59*, 97.

(23) Halls, J. J. M.; Cornil, J.; dos Santos, D. A.; Silbey, R.; Hwang, D. H.; Holmes, A. B.; Brédas, J. L.; Friend, R. H. *Phys. Rev. B* **1999**, *60*, 5721.

(24) Koster, L. J. A.; Mihailetchi, V. D.; Blom, P. W. M. *Appl. Phys. Lett.* **2006**, *88*, 093511.

(25) Scharber, M. C.; Mühlbacher, D.; Koppe, M.; Denk, P.; Waldauf, C.; Heeger, A. J.; Brabec, C. J. *Adv. Mater.* **2006**, *18*, 789.

(26) Bijleveld J. *PhD Thesis*, Eindhoven University of Technology **2010**.

(27) Veldman, D.; Meskers, S. C. J.; Janssen, R. A. J. *Adv. Funct. Mater.* **2009**, *19*, 1939.

Summary

Renewable energies are considered as the energies of the future because of their small impact on the environment. Among them, solar energy is probably the most promising one because it can be directly converted into electricity using photovoltaic modules. Organic photovoltaics, that is solar cells with an organic or polymer material as photoactive layer, represent an attractive future technology as large-scale and low-cost green energy source. In organic solar cells, donor and acceptor materials are combined in the active layer to convert light in to electrical power. While new donor materials have received considerable interest and have strongly improved the efficiency of organic solar cells in the last decade, much less attention has been given to new acceptor materials. This is the main topic of the research described in this thesis.

Chapters 2 and 3 aim at establishing design rules for the structure and the synthesis of acceptor polymers for organic solar cells. In a first attempt, three polymers using different combinations of electron-deficient aromatic heterocylcles (quinoxaline, benzothiadiazole and thienopyrazine) have been synthesized and characterized. The electrochemical properties of the materials reveal that it is not possible to use them as acceptor polymer. However, by correlating the frontier orbital energies to the chemical structure, a new perspective towards the design of acceptor polymers could be established. Based on the improved design, three new polymers were then synthesized by alternating one thiophene ring with one electron-deficient unit. This new design led to materials with suitable electrochemical properties. The new polymers were tested as acceptor material in solar cells with poly(3-hexylthiophene) (P3HT) as the donor, resulting in power conversion efficiencies up to 0.22% in simulated solar light. Near steady-state photoinduced absorption spectroscopy revealed that charge separation in these blends is in competition with charge recombination. In addition, the incomplete exciton dissociation prevents from achieving efficient charge generation and the low electron-mobility in the acceptor polymers hampers charge collection.

A number of polymers bearing diketopyrrolopyrrole (DPP) units in the main chain display high electron mobilities and, hence, the electron-deficient DPP unit is an interesting unit for acceptor polymers. In Chapter 4, the synthesis of three new DPP-based polymers (PA, PB and PC) were described and have been used as acceptor materials in solar cells. Among them, one shows higher electron mobility than the polymers described in Chapter 3. Photoinduced absorption spectroscopy shows that in blends of P3HT with PA or PB charge formation is limited, while for the P3HT:PC blend photogenerated charges

recombine into the PC triplet state before they can separate, unless assisted by a reverse electric field. The materials show power conversion efficiencies up to 0.36%.

In Chapter 3 and 4, the acceptor polymers we used had a relatively high reduction potential which caused an incomplete exciton quenching. To overcome this problem, the goal of the research described in Chapter 5 is to explore new molecular acceptor materials presenting low reduction potentials. Two molecules have been synthesized: a soluble indigo dye and an isoindigo dye, both exhibiting a reduction potential at -1.25 V vs. Fc/Fc^{+}. Near steady-state photoinduced absorption spectroscopy revealed the formation of long-lived free charges in thin films blends of both dyes with P3HT. These observations suggest that the dyes can be very attractive acceptor material for bulk heterojunction solar cell. However, this promise is not fulfilled because both dyes fail to have appreciable electron mobility.

In Chapter 6, three new DPP-based polymers with optical band gaps varying from 1.45 to 1.25 eV have been synthesized. All three polymers show excellent hole mobility, up to 0.57 cm^2/Vs. The materials were applied in bulk heterojunction solar cells with [70]PCBM as acceptor. Optimization involving the use of co-solvents has led to power conversion efficiencies up to 3.3% with external quantum efficiencies up to 50% in the low energy region of the spectrum.

Samenvattig

Duurzame vormen van energie worden gezien als de energie van de toekomst vanwege hun beperkte invloed op het milieu. Zonne-energie is van alle vormen waarschijnlijk de meest veelbelovende omdat het direct in elektriciteit kan worden omgezet met behulp van fotovoltaïsche modules. Organische fotovoltaïsche cellen, oftewel zonnecellen met een organisch molecuul of een polymeer als het fotoactieve materiaal, vormen een aantrekkelijke technologie voor de toekomst als grootschalige en goedkope groene energiebron. In organische zonnecellen worden elektrondonerende en elektronaccepterende materialen gecombineerd in de actieve laag om licht om te zetten in elektrisch vermogen. In het afgelopen decennium heeft de ontwikkeling van nieuwe donerende materialen volop in de aandacht heeft gestaan en is het rendement van organische zonnecellen daarmee sterk verbeterd. Daarentegen is er veel minder aandacht besteed aan nieuwe acceptormaterialen. Dit is het hoofdonderwerp van het onderzoek dat in dit proefschrift beschreven staat.

Hoofdstukken 2 en 3 zijn gericht op het formuleren ontwerpregels voor de structuur en synthese van elektronaccepterende polymeren voor organische zonnecellen. In een eerste aanzet zijn drie polymeren met verschillende elektronarme aromatische heterocyclische verbindingen (chinoxaline, benzothiodiazool en thienopyrazine) gesynthetiseerd en gekarakteriseerd. De elektrochemische eigenschappen van deze materialen laten zien dat het niet mogelijk is hen te gebruiken als accepterende polymeren. Door de energieën van grensorbitalen te correleren met de chemische structuur bleek het wel mogelijk een nieuw perspectief te bieden voor het ontwerp van accepterende polymeren. Gebaseerd op dit verbeterde ontwerp zijn drie nieuwe copolymeren gesynthetiseerd waarin alternerend één thiofeenring en één elektronarme heterocyclische eenheid in de keten zijn aangebracht. Dit nieuwe ontwerp leidde tot materialen met geschikte elektrochemische eigenschappen. De nieuwe polymeren zijn getest als accepterend materiaal in zonnecellen met poly(3-hexylthiofeen) (P3HT) als donor. Dit resulteerde in cellen met rendement tot 0.22% voor de omzetting van gesimuleerd zonlicht in elektrische energie. Fotogeïnduceerde absorptiespectroscopie liet zien dat ladingsscheiding in deze mengsels in competitie is met ladingsrecombinatie. Daar komt bij dat onvolledige dissociatie van de aangeslagen toestand voorkomt dat ladingen efficiënt worden gegenereerd en dat de lage elektronenmobiliteit in de polymeren collectie van ladingen bemoeilijkt.

Een aantal polymeren met elektronenarme diketopyrrolopyrrool (DPP) eenheden in de hoofdketen verwerkt is bezitten een hoge elektronenmobiliteit Dit maakt de DPP eenheid tot een interessante bouwsteen voor accepterende polymeren. In hoofdstuk 4 wordt de synthese van drie nieuwe, op DPP gebaseerde, polymeren (PA, PB en PC) beschreven. De nieuwe polymeren worden toegepast als accepterend materiaal in zonnecellen. Eén van deze materialen bezit een hogere elektronenmobiliteit dan de polymeren die in hoofdstuk 3 beschreven zijn. Fotogeïnduceerde absorptiespectroscopie laat zien dat in mengsels van

P3HT met PA en PB de ladingsscheiding beperkt is, terwijl voor het P3HT:PC mengsel de met licht gegenereerde ladingen terugvallen in de triplettoestand van PC voordat de ladingen gescheiden kunnen worden, tenzij geholpen door een omgekeerd elektrisch veld. De zonnecellen gemaakt met deze nieuwe acceptormaterialen hebben een rendement tot 0.36%.

De polymeren beschreven in hoofdstukken 3 en 4 hebben een relatief hoge reductiepotentiaal wat tot onvolledige ladingscheiding uit de aangeslagen toestand leidt. Om dit probleem te omzeilen is het doel van het onderzoek in hoofdstuk 5 het zoeken naar nieuwe moleculaire acceptoren met een lage reductiepotentiaal. Daartoe zijn twee moleculen gesynthetiseerd: een oplosbare indigo- en isoindigo kleurstof, die allebei een reductiepotentiaal van -1.25 V tegen Fc/Fc^{+} bezitten. Fotogeïnduceerde absorptiespectroscopie laat het ontstaan zien van langlevende vrije ladingen in dunne lagen van mengsels van beide kleurstoffen met P3HT. Deze waarnemingen suggereren dat deze kleurstoffen aantrekkelijke acceptormaterialen kunnen zijn voor bulk heterojunctie zonnecellen. Deze belofte wordt echter niet ingewilligd omdat met beide kleurstoffen geen acceptabele elektronenmobiliteiten bereikt konden worden.

In hoofdstuk 6 zijn drie nieuwe op DPP gebaseerde polymeren met optische band afstand van 1.45 tot 1.25 eV gesynthetiseerd. Alle drie de polymeren laten excellente gatenmobiliteiten zien, tot wel 0.57 cm^2/Vs. Deze materialen zijn toegepast in bulk heterojunctie zonnecellen met [70]PCBM als accepterend materiaal. Optimalisatie met behulp van co-oplosmiddelen leidde tot een rendement voor energieconversie tot 3.3% in zonlicht en met een externe kwantumefficiëntie tot 50% in het laagenergetische deel van het spectrum.

Curriculum Vitae

Marie-France Falzon was born on the 31st of December 1984 in Montreuil-sous-Bois, France. After obtaining her scientific baccalaureate in 2002, she entered the "Ecole Superieure de Chimie Physique et Electronique" in Lyon. During her last year, she has been an exchange student at Durham University (UK) working on supramolecular gels in the laboratory of Prof. J. W. Steed. After obtaining her Diplome d'Ingénieur in 2007, she started as a PhD student at the Eindhoven University of Technology under the supervision of Prof. R.A.J. Janssen. The main results of her PhD project are collected in this thesis.

List of Publications

Designing Acceptor Polymers for Organic Photovoltaic Devices
Falzon, M.; Wienk, M.M.; Janssen R.A.J. *J. Phys. Chem. C*, **2011**, *115* (7), pp 3178–3187

Diketopyrrolopyrrole-based acceptor polymers for photovoltaic application
Falzon, M.; Wienk, M.M.; Janssen R.A.J. *Phys. Chem. Chem. Phys*, *115*(7), 3178-3187.

Acknowledgement

It is difficult to believe that already 4 years have passed since I first entered STO 4.25, said my name to Martin and heard him saying 'Marie-France ... Oh, so you're French!'. Since I started at MST, I have been working around many people; I would like to address them a few words.

First, I want to thank René Janssen -my supervisor- for giving me the opportunity to do a PhD in his research group. Thanks for always finding time when I needed it, for checking, double-checking, even triple-checking my presentations until we were both happy. Thanks for your guidance and advices during the entire project. 2011 has been more complicated than expected, thanks for giving me the time necessary to put myself back on track. Martijn, thank you for your co-supervision, your help during the 4 years has been very valuable. Thanks also to Stefan; your door was always open when I had a question.

I am grateful to Prof. Serdar Sariciftci, Prof. Kees Hummelen and Dr. Jef Vekemans for being part of my reading committee and Prof. Dick Broer for the extended defense committee. A special thanks for Jef, it has been a real pleasure to discuss with you about any synthetic questions, your help has been extremely valuable ... merci!

I would also like to thank Lou, Ralf, Joost, Carine, Angela, Joke, Ingrid, Nora, Patricia, Nancy, Jolanda, Henk and Hans to make the life easier at MST.

Adrien, on sait tous les deux qu'on n'a pas tout à fait les mêmes goûts alors je tiens à saluer le courage que tu as eu de supporter mon sens de l'humour parfois un peu potache, de m'avoir fait confiance concernant le choix des pièces de théâtre et d'avoir essayé de m'initier aux boites de Jazz parisiennes. Rien ne dit qu'on aurait fait l'effort de se connaitre si on s'était rencontré en France, le hasard a donc plutôt bien fait les choses. Noémie, l'année et demi passée ensemble entre le Labo 1, le Drie Gezusters et le Thuys restera définitivement comme une très belle rencontre. Merci aussi pour toute l'aide que tu m'as apportée à la paillasse.

Bram and Daniele, I want to thank you for the help you gave me with my favourite set-up. As far as I remember I always had a problem with the detector, the lamp, the cooling ramp or the cryostat and you always came to rescue me, even during week-ends, so thanks! To all my office mates: Arantxa, Dirk, Bram, Daniele, Dominique, Drithiman, Gijs (thanks for the summary), Girish, Irén, Jan Anton, Martin, Ratheesh, Robert and Stefan; I hope I did not annoy you too much with all my swearings!

I still have several people to thank for the nice time I spent with them: the ‘retreat 2010 team’, Jolanda and the ‘MST beach volleyball crew’, and the ‘party people’. I spent some really good moments with you guys.

Thanks also to Martin, Carel and Michel for being there for me. Merci à Geraldine, Camille, Mathilde, Sophie et JB de m’avoir épaulé à certains moments.

La natation a surement bâti une partie de mon tempérament, alors j’ai une pensée pour tous mes entraineurs: Doudou, Olivier, Fabrice, Michel, Mio et Dom. Je me dois aussi de remercier les personnes qui ont d’une manière ou d’une autre marqué mon parcours. Anne-Laure Rouanet, M. Lacote, M. Traoré, Catherine Ponthus, Anthony Smith, Jean-Pierre Majoral, Anne-Marie Caminade, Cédric-Olivier Turrin et Olivier Rolland. Thanks also to Jonathan Steed.

Merci à mes parents de m’avoir permis de faire mes études sans que je n’ai à me soucier de quoique ce soit. Je sais à quel point j’ai de la chance de vous avoir à mes côtes.

Marie-France